The role of orexin neurons in the regulation of sleep and wakefulness

Sawako Tabuchi

The Graduate University for Advanced Studies

School of Life Science

Department of Physiological Sciences

Tables of Contents

1. Summary

Sleep is an essential phenomenon which occurs in the brain. It is important to maintain our lives since sleep deprivation for a few weeks leads mice to death. However, we are not still able to answer the question "why do we need to sleep?". Recently, sleep disorders such as insomnia, sleep apnea syndrome and circadian rhythm syndrome became national diseases. Thus, to reveal the mechanism of sleep/wakefulness regulation and also sleep disorders has profound significance. I focused on the orexin neurons which have a critical role in the regulation of sleep/wakefulness. I studied following three topics using mouse models; local orexin neural network (Chapter I), the negative feedback circuit between orexin neurons and serotonergic neurons (Chapter II) and the mechanism of one of sleep disorders called "narcolepsy" (Chapter III).

Chapter I: Orexin directly excites orexin neurons through orexin 2 receptor

Orexin neurons have an important role in the regulation of sleep/wakefulness, and especially in the maintenance of arousal. It has been reported that orexin neurons are activated by orexin not directly but indirectly (1). However, here I revealed that orexin neurons are directly and indirectly activated by orexin via orexin 2 receptor (OX2R). Both orexin A (1 μM) and orexin B (1 μM) induced depolarization in orexin neurons, which was still observed when neural networks were inhibited by tetrodotoxin (1 μM). Orexin B application induced depolarization in orexin neurons of orexin 1 receptor (OX1R) knockout mice at comparable levels to wild-type mice. Whereas orexin B failed to depolarize orexin neurons in the OX2R knockout mice. These results suggested that OX2R was a primary receptor for this response. Moreover, immunoelectron microscopic analyses revealed direct contacts among orexin neurons, which exhibited structural

similarities to the glutamatergic synapses. Taken together, these results suggest that orexin neurons form a positive feedback circuit through indirect and direct pathways, which results in the maintenance of the orexin neuron network at a high activity level and/or for a longer period. Therefore, the activation of orexin neurons through OX2R might have an important role in the maintenance of arousal.

Chapter II: Influence of inhibitory serotonergic inputs to orexin neurons on the diurnal rhythm of sleep and wakefulness

Serotonergic (5HT) neurons of the dorsal raphe nuclei receive excitatory input from orexin neurons and are activated by orexin through both OX1R and OX2R. On the other hand, orexin neurons are inhibited by 5HT through the 5HT1A receptor. Thus the existence of the negative feedback circuit between orexin neurons and 5HT neurons has been speculated. However, the physiological significance of this circuit for sleep/wakefulness regulation is little understood. To reveal this role, 5HT1A receptor expression level was specifically and reversibly controlled in the orexin neurons using the Tet-off system. Under the 5HT1A receptor overexpression condition, *orexin-tTA; TetO Htr1a* mice exhibited severe fragmentation of sleep/wakefulness during the first half of the dark period, the time of maximal activity in nocturnal rodents. On the other hand, sleep/wakefulness during the light period was unchanged. However, when the 5HT1A receptor in orexin neurons was reduced to basal expression levels, sleep/wakefulness patterns in *orexin-tTA; TetO Htr1a* mice were indistinguishable from those in littermate *TetO Htr1a* mice. These results strongly suggest that inhibitory serotonergic input functions as negative feedback to orexin neurons in the early dark period and to help stabilize wakefulness bouts, thereby contributing to the diurnal rhythm of sleep and

wakefulness.

Chapter III: Conditional ablation of orexin neurons: A new mouse model for the study of narcolepsy and orexin system function

It is reported that one in six hundred people develops narcolepsy in Japan. There are four main symptoms; excessive daytime sleepiness, fragmentation of sleep/ wakefulness, sleep paralysis and cataplexy. The pathoetiology of narcolepsy is a loss of orexin neurons in human. For the narcolepsy study, *prepro-orexin* knockout mice, orexin receptor knockout mice and *orexin/ataxin-3* mice were used as narcolepsy model mice. However, these mice were not perfect mouse models for narcolepsy since they lose orexin functions before or soon after birth not in adolescence or early adulthood. I introduced a novel narcolepsy mouse model "*orexin-tTA; TetO diphtheria toxin A fragment* (*DTA*) mice" to address this problem. In this mouse, we can control the DTA expression with or without doxycycline (DOX). About 86% and 95% of orexin neurons were ablated at 1 and 2 weeks of DOX removal, respectively. 86% loss of orexin neurons induced fragmentation of wakefulness during the dark period which is an active period for mice. 95% loss of orexin neurons induced much severe fragmentation of wakefulness and cataplexy. As further death of orexin neurons, each symptom became severer. These results suggest that the progress of symptoms is highly related with the number of orexin neurons.

2. Overall Introduction

Sleep is essential for creatures. Without sleep, we cannot keep homeostasis. We spend one-third of our lifetime in sleep. If our lifetime is 80 years, we will be in sleep state more than 26 years. Why do we sleep? Although a lot of scientists have tried to figure it out, we do not have a clear answer. Sleep/wakefulness architecture is not identical among animals. For instance, mice are nocturnal and multiphasic sleep. Dolphin shows unihemispheric sleep not to drown. Sleep duration also differs with animals or individuals. People sleep 6-8 hours per day in average. However, some people sleep for less than 5 hours and are classified into short sleeper. On the other hand, people who sleep more than 10 hours per day are long sleepers. By monitoring cortical activity and muscle tone we can measure the sleep/wakefulness state. Human has four stages of slow wave sleep, stage I-IV. It is classified by waveform of electroencephalogram (EEG). We repeat the 90 minutes cycle of stage I to IV following rapid eye movement (REM) sleep about 4 times in one night. When this sleep architecture is disturbed, it will lead sleep disorders such as insomnia or narcolepsy.

The neural circuit which regulates sleep/wakefulness is very complicated. Many scientists have been challenging to reveal it and integrate the new findings to clarify the whole picture of it. However, we still need more steps to accomplish it. Sleep/wakefulness state transitions are based on the flip-flop switching between wake active and sleep active neurons(2). Most of wake active neurons are located in the upper brainstem such as locus ceruleus (LC, noradrenergic), dorsal raphe nucleus (DR, serotonergic), ventral periaqueductal gray matter (vPAG, dopaminergic) and parabrachial nucleus (PB, glutamatergic). Tuberomammillary nucleus (TMN, histaminergic) in the lateral hypothalamus is also known as wake active neurons. On the other hand, sleep active

neurons are located in the ventrolateral preoptic nucleus (VLPO, GABAergic and galanin) and median preoptic nucleus (MnPO, GABAergic). Wake active neurons inhibit sleep active neruons and vice versa. There is another flip-flop switch for REM sleep regulation (2). REM sleep is a mysterious phenomenon which is generally known as dreaming stage. EEG wave form is similar to wake stage but silence in muscle tone. Cholonergic pedunculopontine (PPT) and laterodorsal tegmental nuclei (LDT) are located in the upper brainstem and project to basal forebrain. PPT and LDT are active during REM sleep as well as wakefulness. On the other hand, ventrolateral periaqueductal gray matter (vlPAG) and lateral pontine tegmentum (LPT) are GABAergic and fire during slow wave sleep not to enter REM sleep. Our daily rhythm is influenced by circadian rhythm. The core of circadian rhythm is suprachiasmatic nucleus (SCN) in the hypothalamus. However, the SCN direct innervation to sleep or wake promoting neurons is hardly seen(2).

In 1998, two distinct groups discovered a neuropeptide named orexin or hypocretin (3, 4). This neuropeptide is produced in the lateral hypothalamic area and has crucial role for wakefulness. Discovery of orexin uncovered missing part of sleep/wakefulness regulation system and advanced the research for it. However, we still need more studies to answer the question “Why do we sleep?” Since the number of patients suffering from sleep disorders is growing in the modern world, it is required to address this issue. Combining electrophysiological analyses with behavioral analyses I tried to add some new hints to solve the complex sleep/wakefulness neural circuit.

Chapter I

Orexin directly excites orexin neurons through orexin 2 receptor

Yamanaka A*, Tabuchi S*, Tsunematsu T, Fukazawa Y, Tominaga M.

The Journal of Neuroscience (2010) 30(38):12642-12652

*contributed equally

I-1. Introduction

The neuropeptide orexins has two types called orexin A and orexin B. Orexin producing neurons, orexin neurons, are located in the lateral hypothalamic area (LHA) (3, 4). Orexins are generated from same precursor peptide called prepro-orexin. Orexin A is a 33-amino-acid peptide with an N-terminal pyroglutamyl residue and C-terminal amidation. On the other hand, orexin B is a 28-amino-acid peptide with C-terminal amidated linear. The actions of the two orexins are mediated via two G protein-coupled receptors, namely the OX1R and OX2R (3). OX1R which is Gq coupling has an approximately 100-fold higher affinity for orexin A than for orexin B. On the other hand, OX2R which is Gq and Gi/Go coupling has almost an equal affinity for both peptides. Animals that lack the *prepro-orexin* gene, *OX2R* gene, *OX1R* and *OX2R* genes or orexin neurons showed narcolepsy-like behavior such as fragmentation of sleep/wakefulness, direct transitions from wake to REM sleep, and the sudden loss of muscle tone while still awake (cataplexy) (5-8). However, OX1R null mice showed mild or almost no abnormality in the sleep/wakefulness pattern, suggesting that the orexin signal through OX2R has a critical role in the regulation of sleep/wakefulness, especially in the maintenance of arousal. Orexin neurons project throughout the brain. At the terminals of these projections, orexin receptors are expressed. *OX2R* mRNA has been shown to be prominent in the cerebral cortex, septal nuclei, hippocampus, and hypothalamic nuclei including the histaminergic TMN (9). Among these brain regions, the TMN is thought to be the center for the site of action of orexin-induced arousal because histaminergic TMN neurons are implicated in arousal (10, 11). The TMN neurons fire tonically during wakefulness (12) and are activated by orexin via OX2R (13-15). Additionally, the effect of orexin on arousal was not observed in histamine 1 receptor knockout ($H1^{-/-}$) mice (16).

However, histidine decarboxylase knockout (*HDC*$^{-/-}$) mice, *H1*$^{-/-}$ mice, and *OX1R*$^{-/-}$; *H1*$^{-/-}$ double knockout mice did not show severe abnormalities in the sleep/wakefulness (17, 18), suggesting that downstream pathways of OX2R, other than the histaminergic system, are critical for sleep/wakefulness regulation.

In this study, I revealed that orexin neurons are directly and indirectly activated by orexin via the OX2R. I showed that orexin neurons are directly innervated by orexin neurons using an immunoelectron microscope. In addition, orexin indirectly activates orexin neurons by increasing spontaneously excitatory post synaptic currents (sEPSCs) in orexin neurons. This indirect activation was also primarily mediated through the OX2R. Although orexin neurons in the *OX1R*$^{-/-}$ mice showed comparable activation with wild-type orexin neurons by orexin B application, the orexin neurons in the *OX2R*$^{-/-}$ mice completely failed to respond to orexin B. These results suggest that orexin neurons form a positive feedback circuit between orexin neurons. This circuitry might have a role in maintaining a high level of activity of orexin neurons while animals are awake.

I-2. Experimental Procedures

I-2-1. Animal usage

All experimental procedures involving animals were approved by the Institutional Animal Care and Use Committee of the National Institutes of Natural Sciences and were in accordance with NIH guidelines. All efforts were made to minimize animal suffering or discomfort and to reduce the number of animals used.

I-2-2. Animals

Transgenic mice, which express enhanced green fluorescent protein (EGFP) in orexin neurons (*orexin/EGFP* mice) under the control of human *prepro-orexin* promoter, were used for the experiments (19-21). *Orexin/EGFP* mice (BDF1; C57BL/6J:DBA=50:50) were bred with *OX1R*$^{-/-}$ (C57BL/6J) or *OX2R*$^{-/-}$ (C57BL/6J) mice to generate *orexin/EGFP; OX1R*$^{-/-}$ or *orexin/EGFP; OX2R*$^{-/-}$ mice. *OX1R*$^{-/-}$ mice and *OX2R*$^{-/-}$ mice were kindly gifted from Dr. Yanagisawa at the University of Texas Southwestern. The mouse, which have the *orexin/EGFP* transgene and alternative orexin receptor gene allele is hetero, was bred with each other to generate *orexin/EGFP; OX1R*$^{-/-}$ (*OE-OX1R*$^{-/-}$; C57BL/6J:DBA=75:25) or *orexin/EGFP; OX2R*$^{-/-}$ (*OE-OX2R*$^{-/-}$; C57BL/6J:DBA=75:25) mice. These mice express EGFP in orexin neurons and systemically lack the alternative orexin receptor gene (OX1R or OX2R).

I used transgenic mice, whose orexin neurons expressed a light-activated chloride pump halorhodopsin (haloR) fused with GFP (*orexin/haloR* mice) (22), for immunoelectron microscopic analyses. *Orexin/haloR* mice were bred with *orexin/EGFP* mice to obtain *orexin/EGFP; orexin/haloR* double transgenic mice. Both EGFP and haloR::GFP were expressed in the orexin neurons of these transgenic mice.

I-2-3. Brain slice preparation

Male and female *orexin/EGFP*, *orexin/EGFP; OX1R*$^{-/-}$ (*OE-OX1R*$^{-/-}$) and *orexin/EGFP; OX2R*$^{-/-}$ (*OE-OX2R*$^{-/-}$) mice (2-3 weeks old) were used for whole cell recordings. The mice were deeply anesthetized with isoflurane (Abbot Japan, Tokyo, Japan) and decapitated. Brains were quickly isolated and placed in ice-cold oxygenated cutting solution containing (in mM): 280 sucrose, 2 KCl, 10 HEPES, 0.5 $CaCl_2$, 10 $MgCl_2$, 10 glucose, pH 7.4 with NaOH, bubbled with 100% O_2. Brains were sliced in 350 μm coronal sections containing the lateral hypothalamic area with a microtome (VTA-1200S, Leica, Wetzlar, Germany). Then slices were transferred to an incubation chamber filled with physiological solution containing (in mM): 135 NaCl, 5 KCl, 1 $CaCl_2$, 1 $MgCl_2$, 10 HEPES, 10 glucose, pH 7.4 with NaOH, bubbled with 100% O_2 and incubated for at least 1 hour at room temperature (RT; 24-26℃).

I-2-4. Electrophysiological recordings

The slices were transferred to a recording chamber (RC-27L, Warner Instrument Corp., CT) on a fluorescence microscope stage (BX51WI, Olympus, Tokyo, Japan). Neurons which had EGFP fluorescence were identified as orexin neurons and were subjected to electrophysiological recording. The fluorescence microscope was equipped with an infrared camera (C2741-79, Hamamatsu Photonics, Hamamatsu, Japan) for infrared differential interference contrast (IR-DIC) imaging and a CCD camera (IK-TU51CU, Olympus) for fluorescent imaging. Recordings were carried out with an Axopatch 200B amplifier (Axon Instruments, Foster City, CA) using a borosilicate pipette (GC150-10, Harvard Apparatus, Holliston, MA) prepared by a micropipette puller (P-97, Sutter Instruments, Novato, CA) filled with intracellular solution (4-10 MΩ) containing (in mM): 138 K-gluconate, 8 NaCl, 10 HEPES, 0.2 EGTA-Na_3, 2 MgATP, 0.5 Na_2GTP, pH 7.3 with KOH. The osmolarity of the solutions were checked by a vapor

pressure osmometer (model 5520, Wescor, Logan, UT) and found to be 280-290 and 320-330 mOsm/L for the internal and external solutions, respectively. The liquid junction potential of the patch pipette and perfused extracellular solution was estimated to be 3.9 mV and was applied to the data. Recording pipettes were under positive pressure while advancing toward individual cells in the slice. Tight seals on the order of 1.0-1.5 GΩ were made by negative pressure. The membrane patch was then ruptured by suction. The series resistance during recording was 10-25 MΩ. The reference electrode was an Ag-AgCl pellet immersed in bath solution. During recordings, cells were superfused with extracellular solution at a rate of 1.6 mL/min using a peristaltic pump (Dynamax, Rainin, Oakland, CA). Spontaneous excitatory post synaptic currents (sEPSCs) and spontaneous inhibitory post synaptic currents (sIPSCs) were recorded in orexin neurons under whole cell voltage clamp mode at a holding potential of -20 mV and -60 mV, respectively. sEPSCs were recorded using a K-gluconate-based pipette solution containing the sodium channel blocker QX-314 (1 mM) to inhibit action potentials in the recording neuron and with picrotoxin (400 μM) in the bath solution. sIPSCs were recorded using a K-gluconate-based pipette solution containing QX-314 (1 mM) in the presence of AP5 (50 μM) and CNQX (20 μM) in the bath solution. The frequency and amplitude of sEPSCs or sIPSCs were measured using Minianalysis software (ver. 6.0.3, Synaptosoft Inc., NJ), and only those events with amplitudes > 10 pA were used in the analysis.

The output signal was low pass filtered at 5 kHz and digitized at 10 kHz. Data were recorded on a computer through a Digidata 1322A A/D converter using p-Clamp software (ver. 10, Axon Instruments). Traces were processed for presentation using Origin 8.1 (Origin Lab Corporation, Northampton, MA) and Canvas X (ACD systems, British Columbia, Canada) software.

I-2-5. Microscopic investigation of associations among orexin neurons

Six weeks old *orexin/EGFP; orexin/HaloR* double transgenic mice (male) were deeply anaesthetized with sodium pentobarbital (ip, 50 mg/kg body weight). They were perfused with 25 mM phosphate buffered saline (PBS) for 1 min followed by a fixative containing 4% paraformaldehyde (TAAB, Aldermaston, UK), 0.05% glutaraldehyde (Nacalai Tesque, Kyoto, Japan), and 15% saturated picric acid in 0.1 M phosphate buffer (PB, pH 7.4) for 12 min. Coronal sections containing the lateral hypothalamic area were cut from the fixed brain by a slicer (VT-1000S, Leica) at a thickness of 50 μm. These sections were washed twice in PB, cryoprotected in a solution containing 25% sucrose and 10% glycerol in 20 mM PB and freeze-thawed with liquid nitrogen. After several washes in PB and 50 mM Tris-HCl buffered saline (TBS, pH 7.4), the sections were incubated with blocking solution containing 20% normal goat serum (NGS) in TBS for 30 min and then for two nights at 4°C with an anti-EGFP rabbit polyclonal antibody (1:800, Invitrogen, Carlsbad, CA) and/or an anti-orexin rabbit antibody 1:2000 (23) in 50 mM TBS containing 1% NGS. After several washes in TBS, the sections were incubated overnight with biotinylated goat anti-rabbit IgG antibody (1:100, Vector laboratories, Burlingame, CA) diluted in 1% NGS in TBS at 4°C. The sections were washed with TBS and reacted with avidin-biotin peroxidase complex (1:100 ABC-Elite; Vector laboratories,) diluted in TBS for 2 h at room temperature. After washing three times in TBS, the sections were washed once in 50 mM Tris-HCl buffer (pH 7.4) and then incubated in 0.05% 3,3’-diamino benzidine tetrahydrochloride (DAB, Dojindo, Kumamoto, Japan) solution (containing 50 mM Tris-HCl buffer and 0.003% hydrogen peroxide) at room temperature until the appropriate signal was achieved. The DAB reaction was terminated by several incubations in PB, and then the sections were fixed

with 0.5% OsO_4 for 40 min, stained with uranyl acetate (1% in distilled water) for 35 min, dehydrated and flat-embedded in Durcupan resin (ACM, Fluka, Sigma-Aldrich, Gillingham, UK). We observed the flat-mounted sections with light microscopy using a BX50 microscope (Olympus) equipped with DP70 CCD camera (Olympus). Section areas containing immunopositive cells were trimmed out from the sections and re-embedded in Durcupan resin brocks. Ultrathin sections at thickness of 70 nm were prepared with an ultramicrotome (Ultracut T, Leica) and observed by a transmission electron microscope (Tecnai10, FEI, Eindhoven, The Netherlands). Digital images were captured by a MegaView III CCD camera (Olympus-SIS GmbH, Germany) and processed with iTEM software (Olympus-SIS) and Illustrator CS3 (Adobe, San Jose, CA) for image analysis and the preparation of figures, respectively. Three-dimensional reconstructions of the neuronal profiles were carried out with serially sectioned ultrathin sections by using Reconstruct (freeware) provided through the synapse web (24).

I-2-6. Drugs

Orexin A (Bachem, Bubendorf, Switzerland), orexin B (Peptide Institute, Osaka, Japan), [Ala^{11}, D-Leu^{15}]-orexin B ([Ala^{11}]-orexin B) (Tocris, MO) were dissolved in extracellular solution and applied by local application through a fine tube (100 μm diameter) positioned near the recording neurons. 6-cyano-7-nitroquinoxaline-2, 3-dione (CNQX), DL-2-amino-5-phosphono-pentanoic acid (AP5) (Sigma, St Louis, MO), picrotoxin (PTX), and tetrodotoxin (TTX) (Wako, Osaka, Japan) were dissolved in extracellular solution and applied by bath application. 1,2-Bis(2-aminophenoxy)ethane-N,N,N',N'-tetraacetic acid (BAPTA) (Dojindo) was dissolved in the pipette solution.

I-2-6. Statistical Analyses

Data were analyzed by one-way ANOVA followed by Fisher's Protected Least

Significant Difference test using the Stat View 4.5 software package (Abacus Concepts, Berkeley, CA). The Kolmogorov–Smirnoff statistical test was used to measure cumulative probability of synaptic events. Probability (p)-values less than 0.05 were considered statistically significant.

I-3. Results

I-3-1. Orexin neurons are activated by orexin

I studied the effect of orexin on the activity of orexin neurons using transgenic mouse models. Under current clamp mode, the local application of orexin B (1 μM) significantly depolarized the membrane potential and increased firing frequency (Figure 1A). The local application of vehicle (extracellular solution) induced depolarization (0.2 ± 0.2 mV, used as a vehicle control, n=7). Orexin A and B induced depolarization in a concentration-dependent manner in the presence of TTX, suggesting that orexin directly activates orexin neurons (Figure 1B, 1D, 1F). Orexin B (1 μM) and orexin A (1 μM) induced depolarization in the presence of TTX was 9.3 ± 1.5 mV (n=15, $p<0.0001$ vs. control) and 8.8 ± 1.2 mV (n=22, $p=0.001$, vs. control), respectively (Figure 1F). Orexin B induced depolarization of orexin neurons in *orexin/EGFP* mice was not inhibited by chelating intracellular Ca^{2+} ions. Orexin B (1 μM) induced depolarization in the presence of BAPTA (10 mM) in the pipette solution was 5.8 ± 0.8 mV (n=6, $p=0.14$, not significantly different vs. in the presence of TTX). Approximately 77% of orexin neurons tested were depolarized by orexin (112 out of 146) in the *orexin/EGFP* mice. A small number of orexin neurons showed no response or faint depolarization (23%, 34 out of 146). The EC_{50} of orexin A- and B-induced depolarizations were 352.7 nM (n=6-22) and 100.9 nM (n=6-15), respectively. Under voltage clamp mode at a holding potential of -60 mV, orexin B induced inward currents in orexin neurons (Figure 1C). Orexin B (1 μM) induced 30.9 ± 4.6 pA (n=6) inward currents. To further confirm the direct effect induced by orexin B, I used the glutamate receptor antagonists AP5 and CNQX. In the presence of TTX, AP5, and CNQX, orexin B (1 μM) still induced significant depolarization (5.8 ± 0.8 mV, n=7, $p=0.017$ vs. control; Figure 1G). These

results strongly suggest that orexin directly activates orexin neurons. The orexin B induced depolarization was comparable to orexin A, suggesting the involvement of OX2R in orexin induced activation of orexin neurons since OX2R has equal affinity for orexin A and B (3). Additionally, [Ala^{11}]-orexin B, an OX2R selective agonist (25), induced depolarization in the presence of TTX (8.25 ± 1.6 mV, n=6, p=0.0001 vs. control), suggesting that OX2R is involved in orexin induced depolarization in orexin neurons (Figure 1E).

I-3-2. Orexin indirectly activates orexin neurons through the activation of glutamatergic neurons

The previous report (1) showed that orexin neurons are indirectly activated by orexin through the activation of glutamatergic neurons. To confirm this indirect activation, sEPSCs were recorded from orexin neurons in the presence of PTX (400 μM) at a holding potential of -60 mV. In this recording condition, sEPSCs are recorded as an inward current. This inward current was completely abolished by adding AP5 (50 μM) and CNQX (20 μM) in the extracellular solution (data not shown). Both orexin A and B application increased sEPSC frequency in a concentration-dependent manner (Figure 2A, 2G and 2B, 2H, respectively). Although the inter-event interval was shortened by orexin A (1 μM) or orexin B (1 μM) application, the amplitude was not affected (Klomogorov-Smirnov test: amplitude, orexin A (p=0.9), orexin B (p=0.2); inter-event interval, orexin A (p<0.001), orexin B (p=0.001); Figure 2C and 2E or Figure 2D and 2F). Orexin A application of 100, 300 and 1000 nM induced 205.8 ± 50.4% (n=7, p=0.33), 508 ± 157.4% (n=9, p=0.0002) and 450.1 ± 98.4% (n=9, p=0.001) increases of the control value in sEPSC frequency, respectively (Figure 2G). On the other hand, 100, 300 and 1000 nM of orexin B

application increased sEPSC frequency to 219.7 ± 66.4% (n=9, p=0.35), 574.0 ± 177.1% (n=9, p=0.0006) and 728.2 ± 161.0% (n=9, p<0.0001) of the control value, respectively (Figure 2H). [Ala^{11}]-orexin B (1 μM), an OX2R selective agonist, also significantly increased sEPSCs in orexin neurons. Although the inter-event interval was shortened by [Ala^{11}]-orexin B (1 μM) application, the amplitude was not affected (Klomogorov-Smirnov test: amplitude, [Ala^{11}]-orexin B (1 μM) (p=0.9); inter-event interval, [Ala^{11}]-orexin B (1 μM) (p<0.001). [Ala^{11}]-orexin B (1 μM) increased sEPSC frequency in orexin neurons by 253.0 ± 38.9% (n=12, p<0.0001). Orexin B induced comparable increases in sEPSCs to orexin A. Additionally, an OX2R selective agonist also increased sEPSCs. These results might suggest an involvement of OX2R in orexin-induced increases in sEPSC frequency in orexin neurons.

I-3-3. Orexin application had little effect on sIPSC frequency in orexin neurons

The effect of orexin on sIPSCs in orexin neuons was studied as well. sIPSCs were recorded in the presence of AP5 (50 μM) and CNQX (20 μM) at a holding potential of -20 mV. In this recording condition, sIPSCs were recorded as an outward current since the reversal potential of the chloride ion in this recording condition is -74 mV. The outward current was completely abolished by adding PTX (400 μM) in the extracellular solution (data not shown). Orexin B application did not affect sIPSCs in the orexin neurons (Figure 3A). sIPSCs frequency after orexin B 100, 300 and 1000 nM application was 144.4 ± 15.9% (n=8, p=0.8), 93.0 ± 18.4% (n=8, P=0.9) and 168.4 ± 16.9% (n=8, p=0.6; Figure 3B) of the control value, respectively. These results suggest that orexin had little effect on GABAergic neurons which directly innervate orexin neurons in the slice preparation.

I-3-4. Orexin-induced activation of orexin neurons is mediated through OX2R

To determine the receptor subtype involved in orexin-induced depolarization of orexin neurons, we used OX1R and OX2R knockout mice. These orexin receptor knockout mice were bred with *orexin/EGFP* mice to obtain *orexin/EGFP; OX1R$^{-/-}$ (OE-OX1R$^{-/-}$)* mice and *orexin/EGFP; OX2R$^{-/-}$ (OE-OX2R$^{-/-}$)* mice in which orexin neurons express EGFP and alternative orexin receptor gene (OX1R or OX2R) is knocked out systemically. The basic membrane properties of orexin neurons in *OE-OX1R$^{-/-}$ and OE-OX2R$^{-/-}$* mice were not significantly different (Table 1) and corroborated our previous reports (20, 26). The input resistance was calculated from the slope of the current-voltage relationship obtained by step current injection in current clamp mode. On the other hand, spontaneous firing was determined by using loose cell-attached recordings. We found that orexin neurons in *OE-OX1R$^{-/-}$* mice showed comparable depolarization with orexin neurons in *orexin/EGFP* mice by orexin B (1 μM) application (6.5 ± 1.1 mV, n=9, p=0.11 vs. *orexin/EGFP* mice, Figure 4A and 4B). The percentage of orexin-responsive orexin neurons in the *OE-OX1R$^{-/-}$* mice was not different from those in *orexin/EGFP* mice. Twenty-one out of 29 orexin neurons in the *OE-OX1R$^{-/-}$* mice showed depolarization or inward current by orexin B (1 μM) application in the presence of TTX (72.4%). However, orexin neurons in *OE-OX2R$^{-/-}$* mice completely failed to depolarize with orexin B (1 μM) application (0.27 ± 0.6 mV, n=11, p<0.0001 vs. *orexin/EGFP* mice, Figure 4A and 4B). I used serotonin (5-HT) as a positive control because of previous results demonstrated that 5-HT hyperpolarized all orexin neurons by the activation of G protein-coupled inwardly-rectifying potassium (GIRK) channel via the 5HT1A receptor (26). All orexin neurons hyperpolarized by 5-HT (10 μM) application failed to respond to orexin B (1 μM)

application. These results strongly suggest that OX2R is the primary receptor that is involved in both orexin A- and B-induced depolarization in orexin neurons.

I-3-5. An increase in sEPSCs were mediated through the OX2R

To identify which orexin receptor subtype is involved in orexin-induced increases in sEPSCs in orexin neurons, *OE-OX1R*$^{-/-}$ and *OE-OX2R*$^{-/-}$ mice were used. Basal sEPSC frequency and amplitude in orexin neurons in *OE-OX1R*$^{-/-}$ and *OE-OX2R*$^{-/-}$ mice were slightly lower than those in *orexin/EGFP* mice but were not significantly different (Table 1). Orexin B (1 μM) application significantly increased sEPSC frequency in the *OE-OX1R*$^{-/-}$ mice to 483.2 ± 73.0% of the control value (n=12, $p<0.0001$ vs. control; Figure 5A, 5E and 5G). This value was not significantly different from that in *orexin/EGFP* mice ($p=0.4$ vs. *orexin/EGFP*; Figure 5G). Although inter-event interval of sEPSCs was significantly shortened, amplitude was not affected by orexin B (1 μM) application (Klomogorov-Smirnov test: amplitude, orexin B ($p=0.9$); inter-event interval, orexin B ($p<0.001$); Figure 5C and 5E). However, orexin B (1 μM) failed to increase sEPSCs in the *OE-OX2R*$^{-/-}$ mice 129.3 ± 17.5% (Figure 5B, n=13, $p=0.07$ vs. control). Neither amplitude nor frequency was significantly increased in these mice (Klomogorov-Smirnov test: amplitude, orexin B ($p=0.9$); inter-event interval, orexin B ($p=0.7$); Figure 5D and 5F). These results strongly suggest that orexin-induced increases in both sEPSCs were primarily mediated through OX2R.

I-3-6. Activation of non-selective cation channel is involved in orexin-induced activation of orexin neurons

Membrane resistance was decreased after orexin application which indicated

opening channels downstream of OX2R (Figure 1A and 1B). Additionally, orexin B induced inward currents in orexin neurons in the presence of TTX (Figure 1C). To examine the properties of orexin-induced currents in more detail, further electrophysiological experiments were performed. First, I removed calcium from the extracellular solution, because it is previously reported that cholecystokinin (CCK)-, arginine vasopressin (AVP)- and oxytocin-induced inward currents in orexin neurons are significantly increased in calcium-free extracellular solution. The removal of extracellular calcium ions markedly potentiated the orexin-induced inward currents (Figure 6A and 6B). In the presence and absence of calcium ions in the extracellular solution, orexin B (1 μM)-induced inward currents were 30.9 ± 4.6 pA (n=6) and 99.0 ± 25.9 pA (n=8, $p<0.03$ vs. in the presence of calcium ion, unpaired t-test), respectively. The orexin B-induced inward currents increased approximately 3.2-fold in calcium-free solution, suggesting that the orexin B-induced inward currents were suppressed by extracellular calcium ions. The reversal potential of the orexin B-induced currents in the calcium-free extracellular solution (in mM: 140 NaCl, 2 CsCl, 1 $MgCl_2$, 1 EGTA, 10 HEPES, 10 glucose and 10 tetraethyl ammonium chloride) was near 0 mV (0.93 ± 1.4 mV, n=6) when measured using a CsCl pipette solution (in mM: 145 CsCl, 1 $MgCl_2$, 10 HEPES, 1.1 EGTA and 0.5 Na_2GTP; Figure 6C). This reversal potential is consistent with the activation of non-selective cation channels in orexin B-induced depolarization of orexin neurons. Several recent reports suggest that the transient receptor potential (TRP) channels play an important role in the receptor-operated influx of cations (27, 28). In addition, the current through TRP channels has been shown to be suppressed by the presence of extracellular calcium ions (29). Thus, the activation of the TRP channel downstream of OX2R activation might be involved.

I-3-7. Orexin neurons make a synapse-like contact structure directly on orexin neurons

Orexin neurons are sparsely distributed in the lateral hypothalamic area, and it is unclear whether they make direct connections among orexin neurons. The observations that orexin neurons express functional OX2Rs; their activity is positively modulated by orexin; and they also release glutamate as a neurotransmitter lead us to suppose that they might establish a contact structure similar to that of other chemical synapses to form a positive feedback circuitry between orexin neurons. To explore this possibility, I took advantage of *orexin/EGFP; orexin/haloR::GFP* double transgenic mice, in which GFP-tagged haloR and EGFP is selectively expressed in orexin neurons; thus, their entire cell morphology can be visualized by immunolabeling for GFP. It should be noted that almost all orexin-immunoreactive (orexin-ir) neurons specifically expressed both haloR::GFP and EGFP and that there was no ectopic expression of GFP other than orexin-ir neurons. I found that the immunoreactivity for orexin (Figure 7A and 7B) or EGFP (GFP-ir, Figure 7C and 7D) allowed the successful visualization of orexin neurons and revealed a close apposition between immunopositive axons and dendrites or somata in the lateral hypothalamus (arrows in Figure 7A, 7B, 7C and 7D). The visualization of EGFP-ir axons was much clearer than orexin-ir axons; this may be due to the homogeneous distribution of haloR and EGFP in the plasma membrane and in the cytoplasm of orexin neurons, respectively. For this reason, an anti-GFP antibody was used for the following electron microscopic observations. At the electron microscopic level, GFP-ir was identified by the presence of electron-dense DAB reaction end-products. GFP-ir axon fibers were found to form synapse-like contacting structures on GFP-ir cell bodies and dendritic processes where the plasma membrane of cell body/dendrite was accompanied by electron-dense

matrix just beneath the contact (Figure 7E, 7F, 7G and 7H). At the contacting site, the GFP-ir axon fibers showed an enlargement in diameter, making a varicosity-like structure (Fig. 7F, 7G, 7I and 7J). I observed a few large vesicles (~100 nm in diameter) and some small clear vesicles (~50 nm in diameter) within the varicosity (Fig. 7F). An example of the contact between a GFP-ir axon and a GFP-ir dendrite was illustrated in a three-dimensional reconstruction obtained from serial sections including Figure 7G and 7H (Figure 7I and 7J). These electron microscopic observations suggest that orexin neurons communicate with each other, at least in part, at the close apposition site.

I-3-8. Orexin neurons in *OE-OX2R*$^{-/-}$ mice completely failed to respond to orexin

To further investigate the physiological role of orexin-induced activation of orexin neurons, the spontaneous activity of orexin neurons was recorded using a loose cell-attached recording in the brain slice preparation. Loose cell-attached recordings revealed that spontaneous firing rate of orexin neurons is not significantly different between *orexin/EGFP*, *OE-OX1R*$^{-/-}$, and *OE-OX2R*$^{-/-}$ mice (Table 1). Spontaneous firing is not affected in the presence of PTX (2.64 ± 0.40 Hz, n=8) or AP5, CNQX, and PTX (2.47 ± 0.37 Hz, n=9). The local application of orexin B (1 μM) significantly increased firing rate to 223.2 ± 39.3% (n=10, p=0.0002) of the control value in the orexin neurons in *orexin/EGFP* mice (Figure 8A, 8B and 8C). After orexin B local application, the firing rate gradually increased and reached a maximum response approximately 1 min after application. Furthermore, the increase in firing lasted for few minutes (3-6 min) after washout. Orexin-induced increases in firing rate were not inhibited in the presence of PTX alone or AP5, CNQX, and PTX. In the presence of PTX alone or AP5, CNQX, and PTX, orexin B (1 μM) application increased firing rate to 216.4 ± 43.0% (n=8, p=0.004

vs. control) or 153.5 ± 14.7% (n=9, p=0.006 vs. control) of the control value, respectively (Figure 8C). Orexin neurons in the *OE-OX1R*$^{-/-}$ mice showed equally potent increases in firing by orexin B (1 μM) application compared to *orexin/EGFP* mice, 257 ± 42.4% (n=21, p<0.001 vs. control). However, orexin neurons in the *OE-OX2R*$^{-/-}$ mice completely failed to respond to orexin B (1 μM, 101.3 ± 2.3%, n=21, p=0.29 vs. control). These results suggest that orexin signaling through OX2R has a crucial role in the regulation of the activity of orexin neurons.

I-4. Discussion

In this study, I demonstrated that orexin neurons are directly and indirectly activated by orexin. Slice patch clamp recordings from orexin neurons in orexin receptor knockout mice revealed that both direct and indirect activations of orexin neurons are mediated through OX2R. Immunoelectron microscopic analyses showed direct interaction between orexin neurons.

I-4-1. OX2R is involved in both direct and indirect activation of orexin neurons

The previous study reported that orexins indirectly activated orexin neurons through increasing sEPSCs in orexin neurons, but not direct activation (1). However, in the present study, orexin B (1 μM)-induced activation was still observed not only in the presence of TTX (1 μM), but also in the presence of TTX (1 μM), AP5 (50 μM) and CNQX (20 μM) (Figures 1G). Additionally, orexin B-induced inward currents in the presence of TTX (Figure 1C). These results strongly suggest that orexin directly activates orexin neurons. The discordance in the studies may be procedural in terms of the number of experiments conducted and the application of orexin. I studied large numbers of orexin neurons (149 neurons). However, some orexin neurons in *orexin/EGFP* mice failed to respond to orexin (23%, 34 out of 149), and the effect of orexin was obviously diminished in the second application. For these reasons, I replaced the brain slice preparation in each experiment.

The present study suggests that OX2R is involved in orexin activation of orexin neurons since both orexin A and B induced comparable depolarization and an OX2R specific agonist, [Ala^{11}]-orexin B, induced depolarization. Furthermore, orexin neurons in the *OE-OX2R*$^{-/-}$ mice completely failed to respond to orexin B. These observations

suggest that orexin neurons express functional OX2Rs, and orexin activates orexin neurons through the OX2R. Orexin B-saporin injection into the lateral hypothalamic area decreased the number of orexin neurons and histaminergic neurons (30), corroborating these results. Combined these results, it is speculated that orexin B-saporin injection ablated orexin neurons via the OX2R expressed in orexin neurons. The reversal potential of the orexin-induced current was near 0 mV (0.93 ± 1.4 mV, n=6). This suggests the activation of non-selective cation channels downstream of OX2R. The activation of phospholipase C by the βγ subunit of the G protein might be involved since OX2R is believed to couple with the Gq and Gi/o type of G proteins (31). It was previously reported that orexin neurons are activated by CCK and AVP via the G protein-coupled receptors (Gq), CCK_A receptor, and the V1a receptor (32, 33). Both CCK- and AVP-induced inward currents were robustly enhanced by removing the calcium ions from the extracellular solution. The orexin-induced inward current was also enhanced in the calcium-free solution (Figure 6), suggesting the involvement of the same type of non-selective cation channels, which are likely TRP channels, because the CCK- and AVP-induced currents were inhibited by the TRP channel blocker SKF96365 (32, 33). It has been reported that orexin-induced depolarization is mediated through the Na^+/Ca^{2+} exchanger in arcuate and TMN neurons (13, 34). To study the involvement of this exchanger in orexin-induced depolarization in orexin neurons, one of Ca^{2+} chelators BAPTA (10 mM) was added to the pipette solution. However, orexin-induced depolarization of orexin neurons was not inhibited by adding BAPTA to the pipette solution, suggesting that the Na^+/Ca^{2+} exchanger is not involved in orexin-induced depolarization of orexin neurons via the OX2R.

I-4-2. Physiological significance of orexin-induced activation of orexin neurons via OX2R

Prepro-orexin and OX2R knockout mice in addition to OX2R-mutated dogs have been shown to display various phenotypes: fragmentation of sleep/wakefulness cycle, direct transition from awake to REM sleep, and suddenly triggered behavioral arrest (cataplexy) (7, 8). These are strikingly similar to the symptoms observed in narcolepsy. However, OX1R knockout mice showed mild or almost no abnormality in sleep/wakefulness which suggests that OX2R has a critical role in the regulation of sleep/wakefulness. What is the cause of this different phenotype? The differential expression patterns of OX1R and OX2R might be a clue to answering this question. OX1R is densely expressed in the locus coerulus, bed nucleus of the stria terminalis, and paraventricular nucleus. On the other hand, OX2R is densely expressed in the septal nuclei, hippocampus, and hypothalamic nuclei including the histaminergic TMN (9). Among these brain regions, the TMN is thought to be the center for the site of action of orexin-induced arousal. Because histaminergic TMN neurons are implicated in arousal (10, 11), they fire tonically during wakefulness (12) and are activated by orexin via the OX2R (13-15). Histaminergic neurons inhibit the VLPO which is the sleep active neurons via the GABAergic interneurons. By suppressing the activity of VLPO histaminergic TMN keeps its activity (35). Additionally, the effect of orexin on arousal was not observed in *H1*$^{-/-}$ mice (16). However, *HDC*$^{-/-}$ mice, *H1*$^{-/-}$ mice, and *OX1R*$^{-/-}$*; H1*$^{-/-}$ double knockout mice did not show severe narcoleptic phenotypes (17, 18), suggesting that downstream pathways of OX2R, other than the histaminergic system, are critical for the regulation of sleep/wakefulness.

Here I revealed that orexin neurons are directly and indirectly activated by

orexin through the OX2R. Immunoelectron microscopic analyses revealed that orexin neurons are directly innervated by orexin neurons. These results suggest that connections between orexin neurons form a positive feedback circuit (Figure 9) summarizes schematic model for orexin-induced activation of orexin neurons via the OX2R. This positive feedback circuitry might function to keep the activity of orexin neurons at a high level while the animals are waking. In current clamp recording, we found that some orexin neurons showed burst type firing, and this type of neuron has been shown to fire in clusters or episodes of repetitive bursts (21). This rhythmic firing might work as a pacemaker to maintain orexin neural activity. Orexin-induced increases in sEPSCs were also mediated via OX2R. sEPSC increases in orexin neurons might include input from other orexin neurons since orexin neurons are believed to be glutamatergic. Additionally, they are activated by orexin via OX2R. Interestingly, PTX, AP5, and CNQX had little effect on the basal firing rates of orexin neurons; however, these inhibitors significantly inhibited orexin B-induced increases in firing (p=0.014 vs. orexin B alone). This result suggests that orexin neurons have spontaneous firing ability independent from excitatory inputs. This does not deny the contribution of sEPSCs and sIPSCs on the activity of orexin neurons. sEPSCs or sIPSCs additively modulate the activity of orexin neurons at relatively higher firing rates. The orexin neurons in the *OE-OX2R*$^{-/-}$ mice that completely failed to respond to orexin might suggest that the activity of orexin neurons *in vivo* is decreased in *OX2R*$^{-/-}$ mice. This results in a significant decrease in orexin release as orexin is stored in dense-core vesicles and is released at higher firing frequency (36). This might be one reason that the phenotype of *OX2R*$^{-/-}$ mice was similar to that of *prepro-orexin*$^{-/-}$ mice with regard to sleep/wakefulness regulation. In any case, these results help to clarify how the activity of orexin neurons is regulated *in vivo* and how arousal is maintained by

orexin neurons.

Loss of function of OX2R induces not only fragmentation of wakefulness, but also fragmentation of non-REM sleep. It is likely that the OX2R-mediated positive feedback is not directly involved in the fragmentation of non-REM sleep because orexin neurons are thought to be almost silent during non-REM sleep (37). However, the positive feedback between orexin neurons might indirectly affect non-REM sleep by increasing orexin release during wakefulness. An increase in orexin concentration in the cerebrospinal fluid (CSF) might contribute to consolidating wakefulness as well as non-REM sleep because orexin also activates GABAergic neurons that are implicated in initiation and maintenance of non-REM sleep (34, 38, 39). After silencing orexin neurons in non-REM sleep, orexin in the CSF might activate GABAergic neurons and increase IPSCs in neurons that are responsible for arousal, such as the TMN neurons (38).

The present study suggests that orexin neurons form a positive feedback circuit between orexin neurons. This circuitry might be important to maintain the activity of orexin neurons at a high level and/or for lasting long time. I found that not only the direct activation of orexin neurons but also indirect activation through an increase in excitatory input to orexin neurons (by activating glutamatergic neurons) is mediated through the OX2R. This synergistic activation of neurons might be important in amplifying signals for arousal from the brain stem and in the maintenance of arousal. Most recently, it has been reported that orexin neurons release orexins and glutamates in different time course (40); Glutamate release rapidly increase and decay in the early phase of activation of orexin neurons. On the other hand, release of orexin is gradual and long-lasting compared with glutamate. Thus, direct activation of orexin neurons by orexin is important for the stable firing of orexin neurons. Future experiments using transgenic mice in which the

OX2R is specifically knocked out in the orexin neurons may reveal the physiological importance of orexin-induced activation of orexin neurons through the OX2R.

I-5. Figures and Table

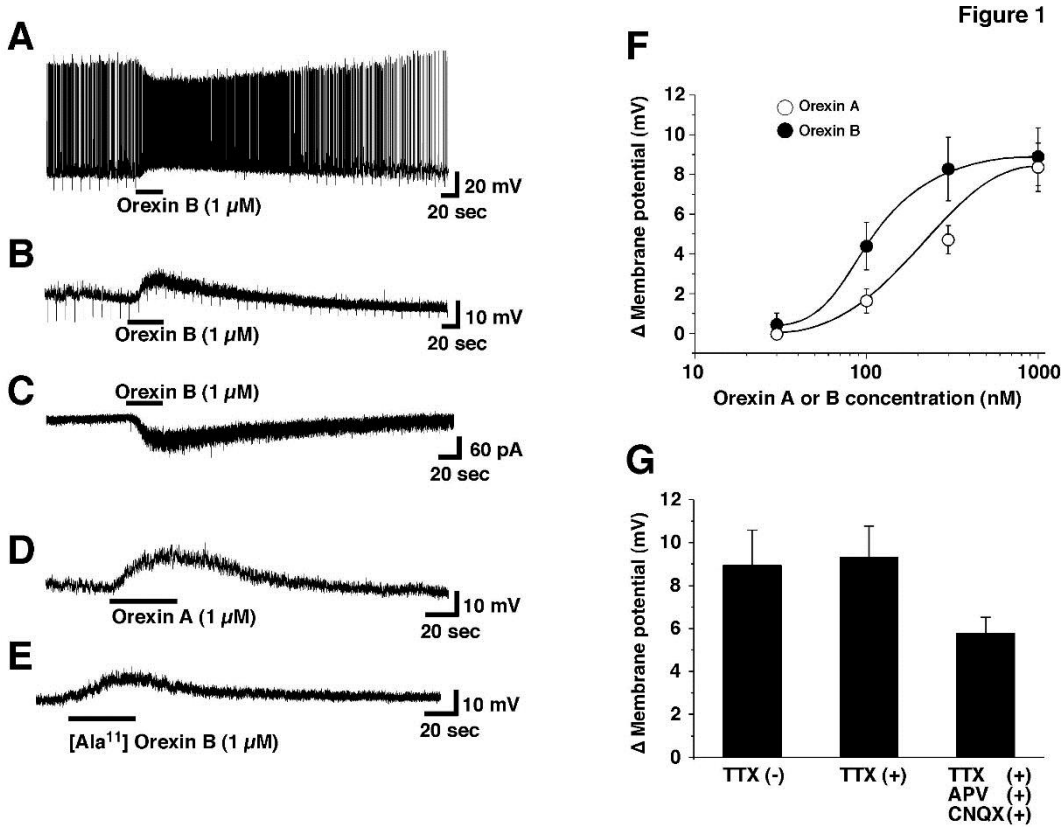

Figure 1

Orexin neurons are directly activated by orexins. A, Under current clamp mode, orexin B (1 μM) application induced depolarization and an increase in firing in orexin neurons. B, In the presence of TTX (1 μM), orexin B (1 μM) induced depolarization in orexin neurons. C, Under voltage clamp mode holding at -60 mV, orexin B (1 μM) application induced an inward current in orexin neurons in the presence of TTX (1 μM). Orexin A (1 μM) (D) or [Ala^{11}]-orexin B (1 μM) (E) application induced depolarization in the presence of TTX. F, Orexin A (EC_{50}=352 nM, n=6-22) and B (EC_{50}=101 nM (n=6-15) induced responses were concentration dependent. G, Bar graph shows orexin B induced depolarization in the presence of TTX (1 μM), AP5 (50 μM) and CNQX (20 μM) (n=7-15). Orexin A, B and [Ala^{11}]-orexin B were locally applied during the period represented by the bars. In A and B, input resistance was monitored by the amplitude of electrotonic potentials generated by the injection of a rectangular wave current pulse (-20 pA, 500 msec, 0.1 Hz). Values are mean ± S.E.M. (n=6-22).

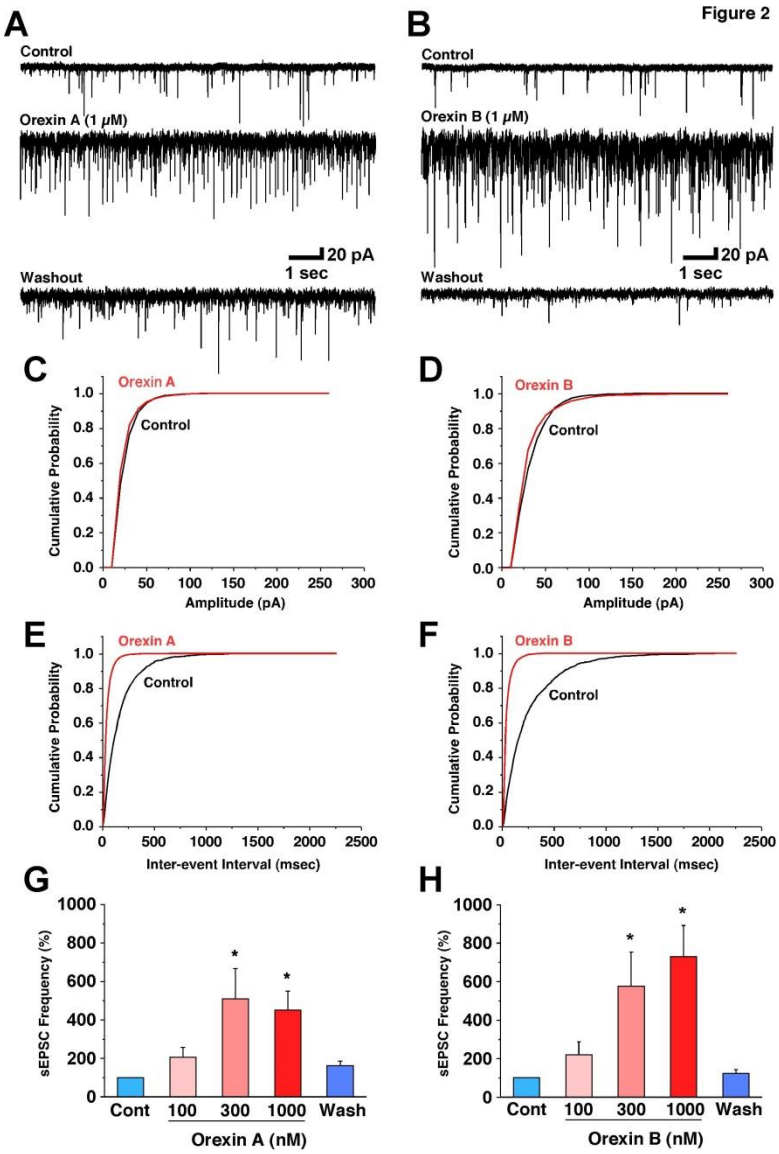

Figure 2

Both orexin A and B increased the sEPSCs in orexin neurons. A and B, sEPSCs were recorded in the presence of PTX (400 μM) at a holding potential of -60 mV. Orexin A and B (1 μM) increased sEPSCs. C and D, Orexin A and B (1 μM) did not change the sEPSC amplitude. E and F, Orexin A and B (1 μM) shortened the inter-event interval. G and H, Bar graphs show that orexin A and B increased sEPSCs in a concentration-dependent manner. Cont, control. Wash, washout. *, $p<0.05$ vs. control. Values are mean ± S.E.M. (n=7-12).

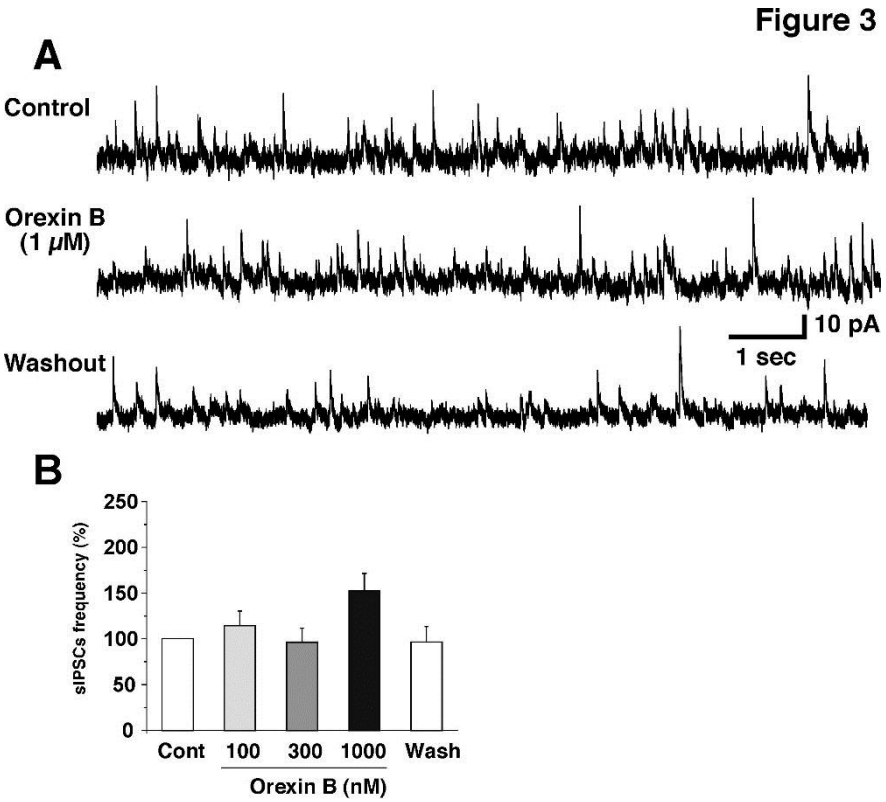

Figure 3

The effect of orexin B on the sIPSCs in orexin neurons. sIPSCs were recorded in the presence of AP5 (50 μM) and CNQX (20 μM) at a holding potential of -10 mV. A, Orexin B (1 μM) showed little effect on sIPSCs. B, Bar graph summarizes sIPSCs frequency data from Figure 3A. Cont, control. Wash, washout. *, $p<0.05$ vs. control. Values are mean ± S.E.M. (n=7-8).

Figure 4

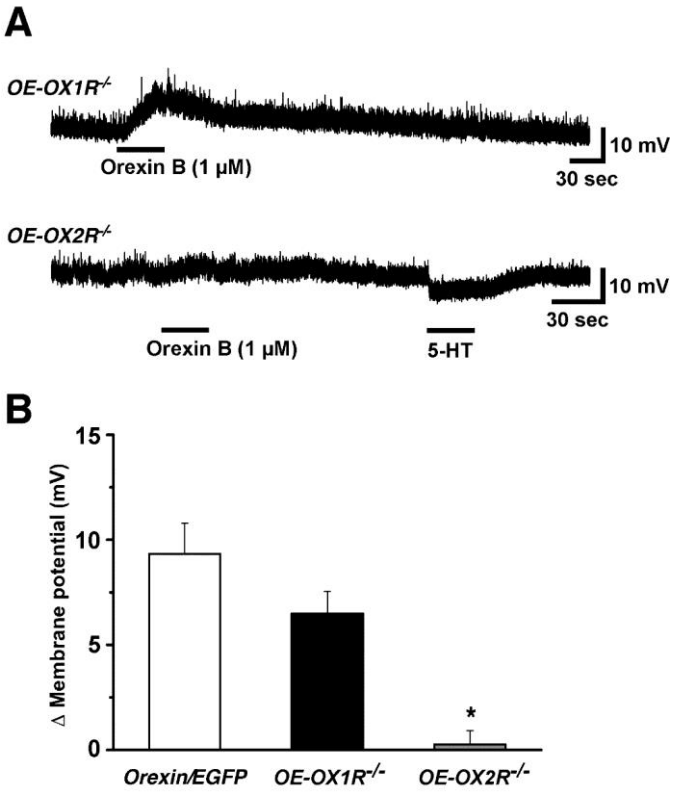

Figure 4

Orexin-induced depolarization of orexin neurons is mediated through OX2R. Orexin neurons in the *OE-OX1R*$^{-/-}$ mice were significantly depolarized by orexin B (1 μM) application (A, upper trace). However, orexin B failed to depolarize orexin neurons in the *OE-OX2R*$^{-/-}$ mice (A, lower trace). Orexin B and 5-HT (10 μM) were locally applied during the period represented by the bars. B, Bar graph summarizes the result from Figure 4A. *, $p<0.05$ vs *orexin/EGFP*. Values are mean ± S.E.M. (n= 9-10).

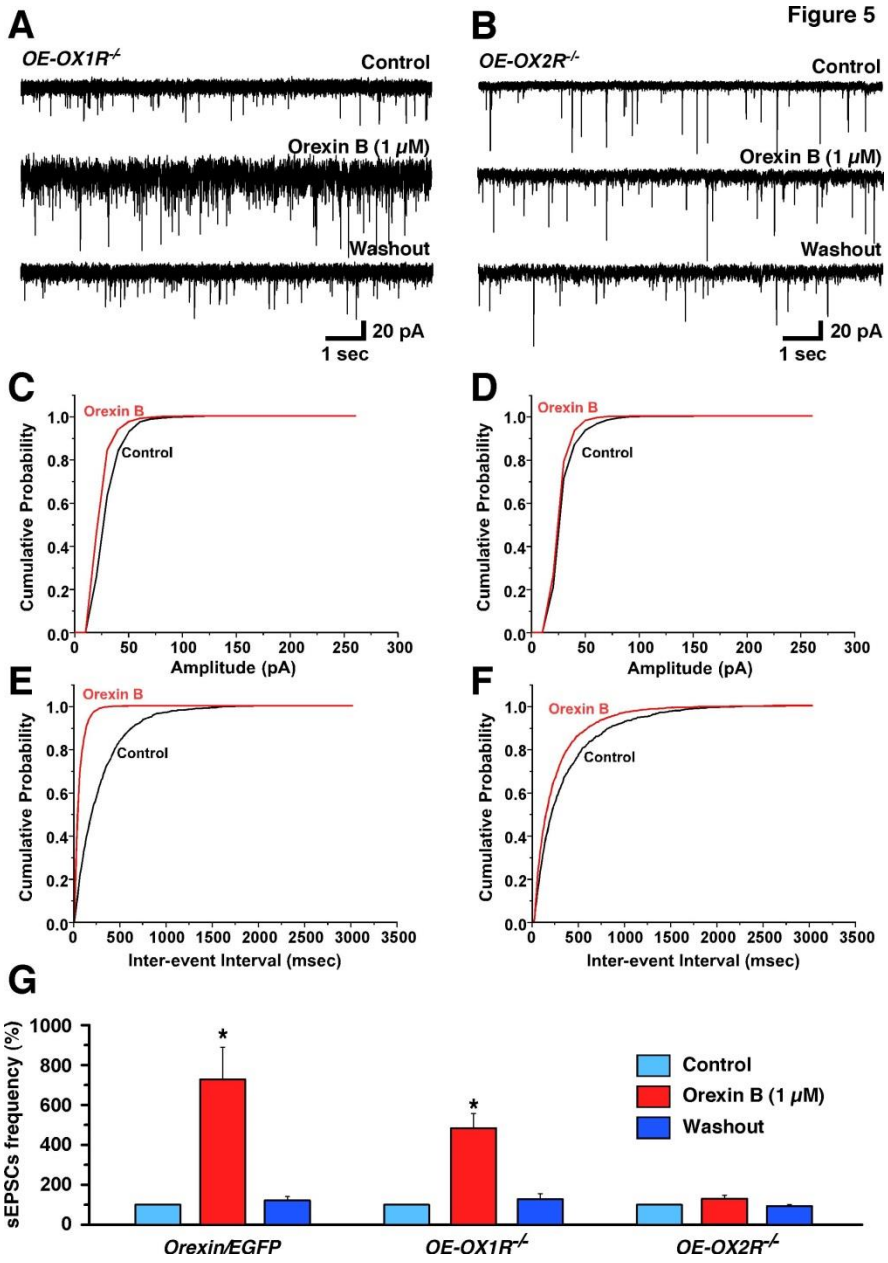

Figure 5

Orexin induced increases in sEPSCs were mediated through OX2R. sEPSCs were recorded in the presence of PTX (400 μM) at a holding potential of -60 mV. A, Orexin B (1 μM) increased sEPSC frequency in orexin neurons in the *OE-OX1R*$^{-/-}$ mice. B, Orexin B (1 μM) failed to increase sEPSCs in orexin neurons in the *OE-OX2R*$^{-/-}$ mice. C and D, Orexin B (1 μM) did not change sEPSC amplitude in *OE-OX1R*$^{-/-}$ and *OE-OX2R*$^{-/-}$ mice. E and F, Orexin B (1 μM) shortened the inter-event interval in *OE-OX1R*$^{-/-}$ but not *OE-OX2R*$^{-/-}$ mice. G, Bar graph summarizes the results from Figure 5A and 5B. *, $p<0.05$ vs. control. Values are mean ± S.E.M. (n=9-13).

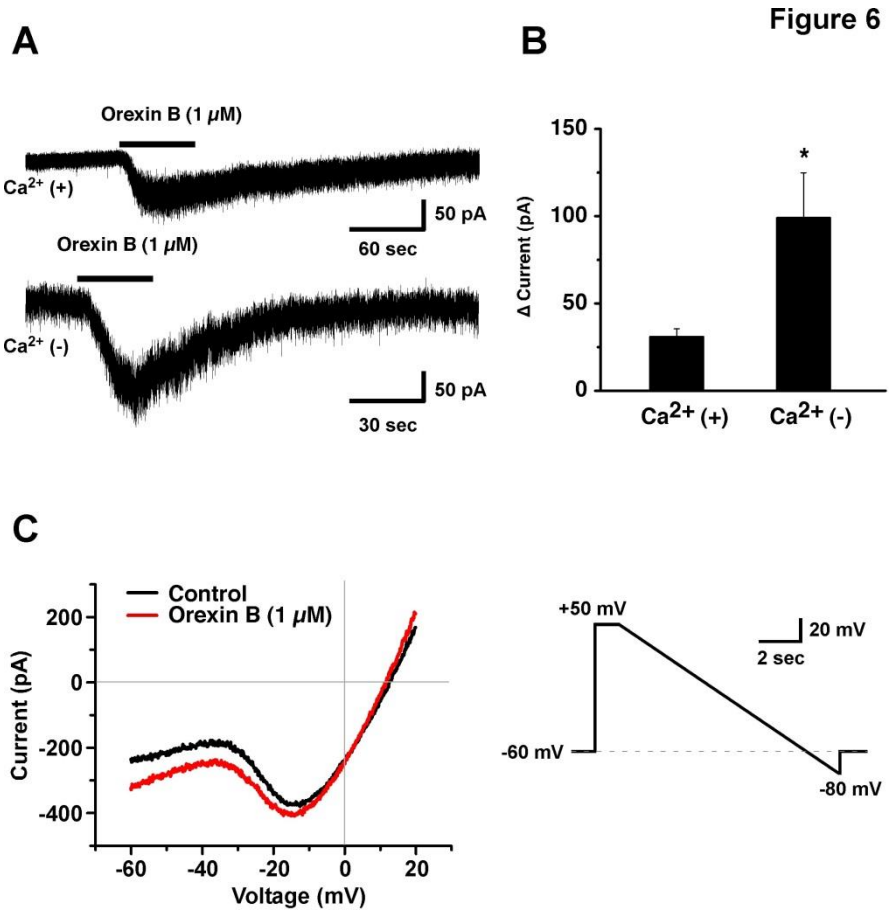

Figure 6

Orexin activated orexin neurons by opening non-selective cation channels in orexin neurons. A, The effect of extracellular Ca^{2+} on the orexin B (1 μM)-induced inward currents. Orexin B induced weak inward currents in the presence of extracellular calcium (Ca^{2+})(upper trace). This inward current was dramatically increased in the Ca^{2+} free solution (lower trace). B, The Ca^{2+}-free solution caused three-fold increases in inward current. C, The current-voltage relationship obtained by voltage ramp protocol using a CsCl pipette in the Ca^{2+} free extracellular solution is shown. The I-V curve shows that the reversal potential of the orexin B (1 μM)-induced currents was 0.93 ± 1.4 mV (n=6). Neurons were voltage-clamped at –60 mV, and the membrane potential was stepped to 50 mV (1 sec), and then ramped to -80 mV at duration of 10 sec (C, right panel). Orexin B was locally applied during the period represented by the bars. *, $p<0.05$ vs. Ca^{2+}(+). Values are mean ± S.E.M. (n=6-8).

Figure 7

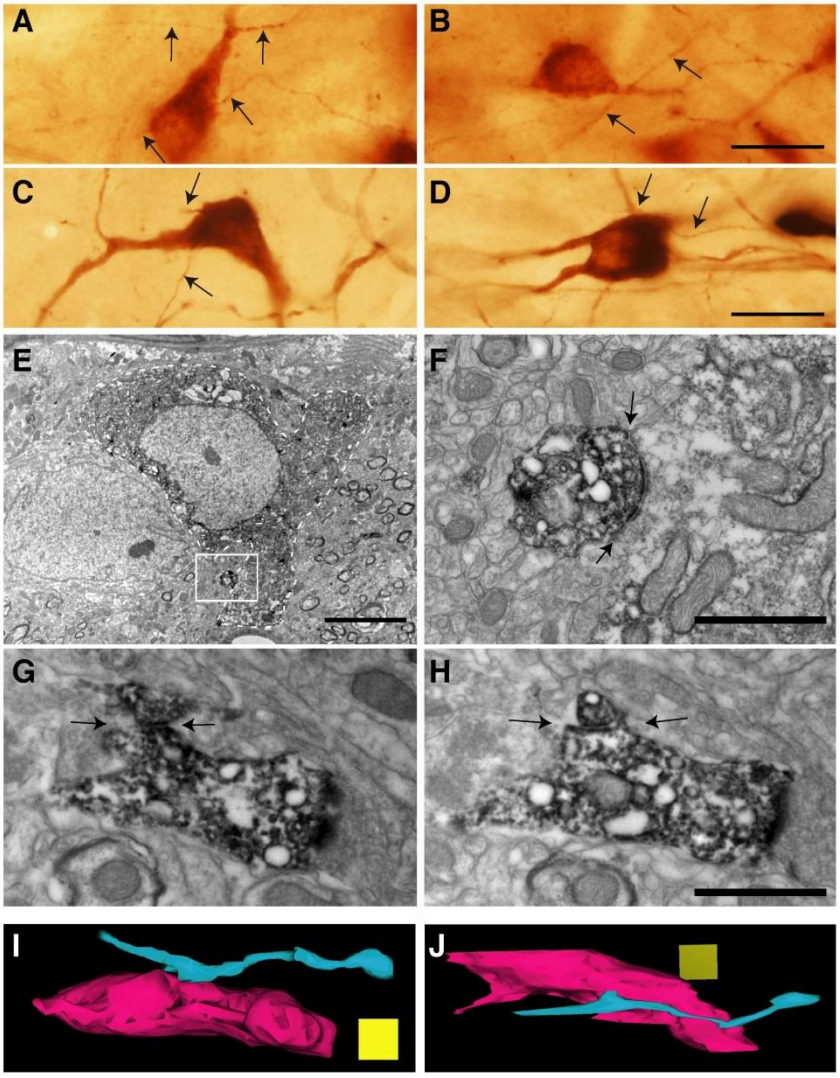

Figure 7

Immunoelectron microscopic observation revealed synapse-like close appositions between the axon and the dendrite of orexin neurons. A, B, C and D, Light microscopic images of DAB-labeled orexin neurons. Orexin neurons were labeled with anti-orexin antibody (A, B) or anti-GFP antibody (C and D) in *orexin/EGFP*; *orexin/haloR::GFP* double transgenic mice in which orexin neurons specifically express EGFP and haloR::GFP. The axons of orexin neurons were in close apposition with a dendrite or soma from other orexin neurons in many regions in the hypothalamus (arrows in A, B, C and D). E, F, G and H, Immuno-electron microscopy of the apposition sites between GFP-ir axons and a GFP-ir soma or dendrite (orexin neuron). F, Magnification of the square region in E. Arrows indicate a contacting zone of

two GFP-ir positive profiles, where two plasma membranes are aligning parallelly (F, G and H). Note that the plasma membranes of GFP-ir profiles shows thickening of the plasma membrane selectively at the contacting site. I and J, 3D reconstruction of two GFP-ir profiles from serial sections including G and H. A bulge structure appeared at where an axon of an orexin neuron contacted a dendrite of another orexin neuron. Scale bars 20 μm (A-D), 5 μm (E), 1 μm (F, G and H). Scale cube 0.7^3 μm^3 (I and J).

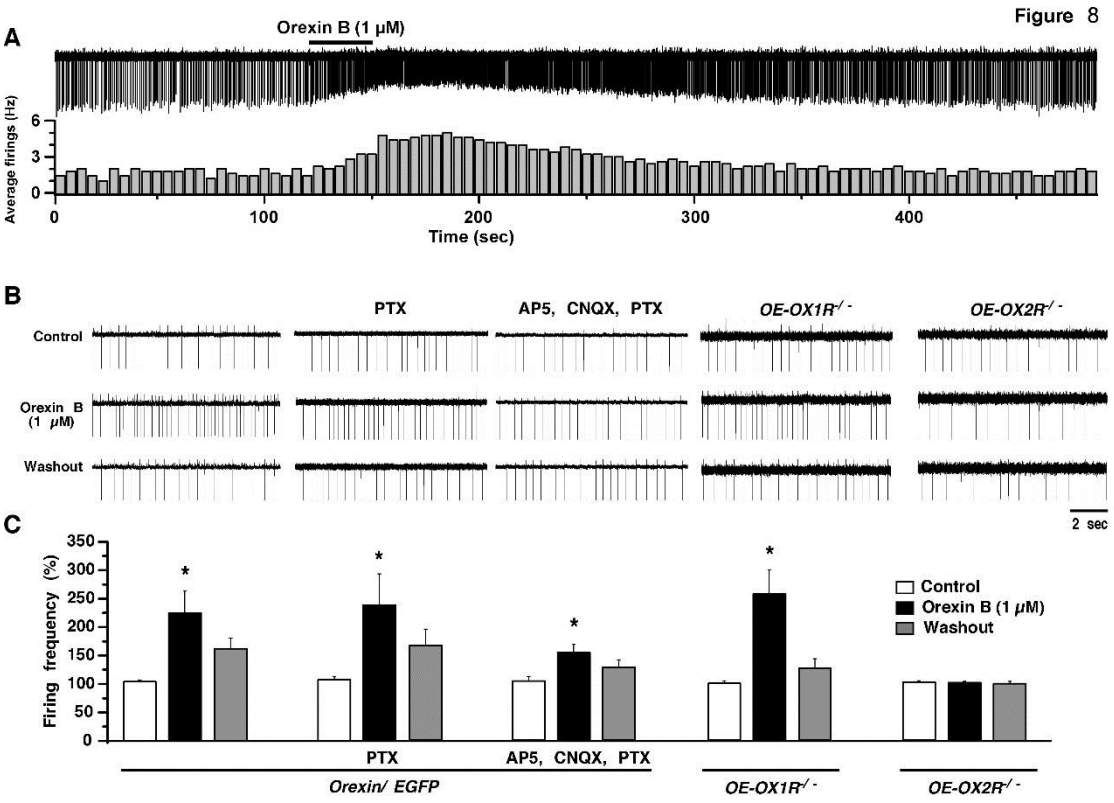

Figure 8

Loose cell-attached recordings revealed that orexin neurons in the *OE-OX2R*$^{-/-}$ mice completely failed to respond to orexin. A, Representative trace (upper trace) shows that orexin B application increased firing in orexin neurons in the *orexin/EGFP* mice. Bar graph shows an average firing for every 5 sec. B, Orexin B (1 μM) application increased firing in orexin neurons in the *orexin/EGFP* and *OE-OX1R*$^{-/-}$ mice. However, orexin B (1 μM) application completely failed to increase the firing rates of orexin neurons in the *OE-OX2R*$^{-/-}$ mice. C, Bar graph summarizes the results from Figure 8B. Orexin B was locally applied during the period represented by the bars. The firing increase is indicated as a percent increase from the basal firing rate (i.e., the average firing for 3 min before the start of the experiment). "Control" represents the average firing for 1 min before orexin B application. AP5 (50 μM), CNQX (20 μM), and PTX (400 μM) were applied by bath application. *, $p<0.05$ vs. control. Values are mean ± S.E.M. (n=5-21).

Figure 9

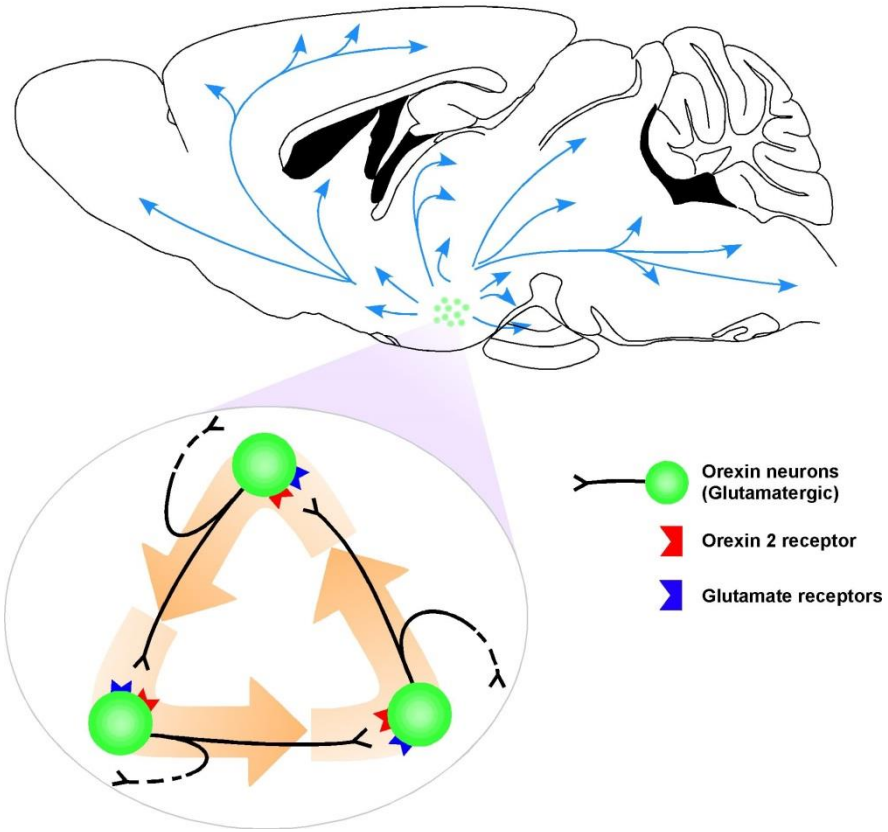

Figure 9

Schematic summarize of the mechanism underlying orexin–induced activation of orexin neurons through OX2R. Orexin neurons directly innervate orexin neurons and activate orexin neurons through OX2R. This might form a positive feedback circuit, and the circuitry might function to preserve the activity of orexin neurons and subsequently to maintain arousal. Glutamate receptors includes AMPA, NMDA receptors and metabotropic glutamate receptors (mGluR).

Table 1

Basic membrane properties of orexin neurons in the *orexin/EGFP*, *OE-OX1R*$^{-/-}$ and *OE-OX2R*$^{-/-}$ mice.

All parameters were determined by whole cell slice patch clamp recordings from orexin neurons with the exception of the number of orexin-ir neurons and spontaneous firing frequency. The number of orexin-ir neurons was counted in every fourth coronal brain section (40 μm) throughout the entire brain. The spontaneous firing frequency was determined by loose cell-attached recordings.

	Orexin/EGFP(n=10-20)	*OE-OX1R*$^{-/-}$ (n=10-24)	*OE-OX2R*$^{-/-}$ (n=13-35)
Number of orexin-ir neurons	620 ± 148 (n=4)	682 ± 88 (n=4)	583 ± 78 (n=4)
Capacitance (pF)	24.0 ± 2.5	27.6 ± 2.1	24.0 ± 1.0
Resting membrane potential (mV)	-60.1 ± 1.0	-59.8 ± 1.1	-59.2 ± 2.2
Membrane resistance (MΩ)	579.3 ± 28.0	592.5 ± 34.8	546.0 ± 27.8
Spontaneous firing frequency (Hz)	2.3 ± 0.3	2.3 ± 0.3	2.6 ± 0.2
Action potential peak	29.0 ± 2.4	28.6 ± 3.2	29.3 ± 2.2
Action potential amplitude	61.2 ± 3.2	61.8 ± 3.5	62.8 ± 2.9
Half-width (ms)	4.0 ± 0.4	3.5 ± 0.4	3.3 ± 0.3
sEPSC frequency (Hz)	4.5 ± 0.8	4.1 ± 0.8	3.5 ± 0.5
sEPSC amplitude (pA)	28.9 ± 1.4	27.1 ± 1.2	32.5 ± 3.1
sIPSC frequency (Hz)	1.7 ± 0.3	1.1 ± 0.3	1.1 ± 0.2
sIPSC amplitude (pA)	17.3 ± 0.9	21.5 ± 1.5	18.5 ± 1.6

Chapter II: Influence of inhibitory serotonergic inputs to orexin neurons on the diurnal rhythm of sleep and wakefulness

Tabuchi S, Tsunematsu T, Kilduff TS, Sugio S, Xu M, Tanaka KF, Takahashi S, Tominaga M, Yamanaka A.

SLEEP (2013) 1;36(9):1391-404.

II-1. Introduction

The neural circuit which regulates sleep and wakefulness is very complex. Various neurons are involved in the switching or maintenance of sleep or wakefulness. One of the players is orexin neuron which is located in the lateral hypothalamic area. Orexin neurons innervate throughout the brain. At the site of innervation, OX1R and/or OX2R are expressed and signal transduction occur the downstream of Gq and Gi/Go.

Neuronal serotonin contributes to many physiological functions such as cognition, feeding, thermoregulation, aggressive behavior and sleep/wakefulness regulation. Serotonergic neurons in the raphe nuclei are also known to be involved in sleep/wakefulness regulation. Destruction of serotonergic neurons in the raphe nuclei or inhibition of 5HT synthesis with p-chlorophenylalanine (PCPA) produces severe but transient insomnia that can be reversed by restoring 5HT synthesis (41, 42). On the other hand, the firing rate of serotonergic neurons in the DR nucleus is highest in waking (3 Hz), low in slow wave sleep (SWS) (1Hz) and almost quiescent in REM sleep (43). Consistent with its likely role in promoting wakefulness, blockade of 5HT neurotransmission through 5HT2A antagonists reduces wakefulness and enhances SWS (44). The DR sends inhibitory projections to sleep-active neurons in the VLPO (45) and also innervates the cerebral cortex, thereby influencing cortical arousal. The VLPO

neurons project to the TMN and inhibit wake-active neurons. However, the pharmacology underlying the involvement of the serotonergic system in sleep/wakefulness regulation is complicated by the fact that there are at least 14 different 5HT receptor subtypes distributed throughout the brain. 5HT3 receptors are the ionotropic receptors. Whereas 5HT1A-F, 5HT2A-C and 5HT4-7 are metabotropic receptors. 5HT1A is the widely expressed subtype among serotonin receptor subtypes. The signal transduction pathway is not identical among 5HT receptor family. 5HT1 and 5HT5 receptors negatively regulate adenylate cyclase. On the other hand, 5HT4, 5HT6 and 5HT7 receptors positively regulate adenylate cyclase. Furthermore, it is reported that there are subpopulations of serotontergic neurons in DR which coexpress different types of neurotransmitters such as GABA, glutamate, dopamine and substance P. The sophisticated approach is required to reveal this complicated 5HT function.

Previous studies have revealed a functional relationship between orexin and serotonergic neurons. Serotonergic neurons are innervated by orexin neurons and are directly and indirectly activated by orexin through the OX1R and OX2R (46, 47). Conversely, orexin neurons are densely innervated by serotonergic inputs from the DR (26, 32). Orexin neurons are inhibited by 5HT *in vitro* via activation of the 5HT1A receptor (26). 5HT1A receptor is the Gi coupled GPCR so that the βγ subunits open the

GIRK channels. These observations suggest negative feedback circuitry between orexin and serotonergic neurons. However, the functional significance of serotonergic inhibition of orexin neurons is little understood.

To address this, 5HT1A receptor expression level was specifically and reversibly controlled in the orexin neurons using the Tet-off system. Overexpression of 5HT1A receptor in the orexin neurons enhanced serotonergic inhibition and resulted in severe fragmentation of wakefulness, specifically early in the dark (active) period. Normalization of 5HT1A expression in the orexin neurons in the presence of DOX eliminated this fragmentation. These results suggest that serotonergic inhibition of orexin neurons may function as a negative feedback circuit early in the active period and could thereby contribute to the diurnal rhythms of sleep and wakefulness.

II-2. Experimental Procedures

II-2-1. Animal usage

All experimental procedures involving animals were approved by the Institutional Animal Care and Use Committee of the National Institutes of Natural Sciences was in accordance with NIH guidelines. All efforts were made to minimize animal suffering or discomfort and to reduce the number of animals used.

II-2-2. Generation of multiple *orexin-tTA* transgenic mouse strains

The characteristics of the 7 transgenic mouse strains used in the present study are summarized in Table 1. The transgenic construct to generate *orexin-tTA* transgenic mice was made by substituting the *nLacZ* gene (SalI-BamHI fragment) of the *orexin/nLacZ* transgenic construct (19) with 0.7 kb of the mammalianized tetracycline-controlled transcriptional activator (*tTA)* fragment (48). The transgene was excised and microinjected into pronuclei of fertilized mouse eggs (C57BL/6 mice) to generate transgenic founders. Founders were bred with C57BL/6J mice (Clea-Japan Inc., Tokyo, Japan) to produce stable *orexin-tTA* transgenic lines. A total of 9 *orexin-tTA* transgene-positive founders were obtained. *In situ* hybridization analysis of the N1 generation revealed that lines 29, C5 and G5 showed the highest *tTA* mRNA expression.

To confirm tTA function, each line was bred with the tetracycline operator (*TetO*) mCherry red fluorescent protein (RFP)-expressing mouse to generate *orexin-tTA; TetO RFP* mice (Table 1). Among these, line G5 showed the highest penetrance of RFP expression: 85% of orexin neurons expressed RFP. Thus, line G5 was used for further experiments.

To manipulate 5HT1A receptor expression in orexin neurons, *orexin-tTA* (line G5) mice were bred with *TetO Htr1a* mice (49) to generate *orexin-tTA; TetO Htr1a* mice

(Table 1). The *TetO Htr1a* mice had been backcrossed 7 times with C57BL/6J mice (Clea-Japan Inc., N=7). In this implementation of the "Tet-off" system, *orexin/tTA; Tet-O Htr1a* mice have very high *htr1a* mRNA expression in the orexin neurons. However, in the presence of DOX in the chow, *htr1a* mRNA levels in the orexin neurons decline to the basal levels observed in *TetO Htr1a* mice. Upon subsequent removal of DOX, *htr1a* mRNA expression returns to the high level observed in orexin neurons before DOX (see Results), demonstrating reversible *htr1a* gene expression in orexin neurons using the Tet-off system. Doxycycline-containing chow (DOX chow) was made by adding 10% DOX powder (Kyoritsu Seiyaku Corporation, Tokyo, Japan) to normal chow (Labo MR Stock, Nosan Corporation, Yokohama, Japan) at a final concentration of 100 mg/kg.

II-2-3. *In situ* hybridization

The *in situ* hybridization method using tissue sections has been described previously (50). Briefly, digoxigenin-labeled *prepro-orexin* (584bp, NM_010410.1) or *tTA* (coding region) cRNA probes were hybridized to tissue sections of mouse hypothalamus, NBT/BCIP compounds (Roche) were used for color development, and Nuclear Fast Red (Vector Lab, Burlingame, CA) was used for counterstaining.

For double fluorescence *in situ* hybridization, FITC-labeled *prepro-orexin* cRNA probes and DIG-labeled *tTA* cRNA probes were hybridized. After stringent washing, a peroxidase-conjugated anti-DIG antibody (Roche, Indianapolis, IN)) was applied and probes were visualized with Cy3 (TSA Plus Cyanine 3 & Fluorescein System, Perkin Elmer, Foster City, CA). After quenching the conjugated peroxidase of the anti-DIG antibody with hydrogen peroxide, peroxidase-conjugated anti-FITC antibody (Perkin Elmer) was applied and probes were visualized with FITC (TSA Plus Cyanine 3 & Fluorescein System, Perkin Elmer).

II-2-4. Brain slice preparation

Triple transgenic *orexin-tTA; orexin- EGFP; TetO Htr1a* mice were generated by breeding o*rexin-EGFP* mice (20) with *orexin-tTA; TetO Htr1a* mice (Table 1). *Orexin-tTA; orexin-EGFP; TetO Htr1a* mice (3-4 weeks old male and female mice) were used for whole cell slice patch recordings. The mice were deeply anesthetized with isoflurane (Abbot Japan) and decapitated. Brains were quickly isolated and placed in ice-cold oxygenated cutting solution containing (in mM): 280 sucrose, 2 KCl, 10 HEPES, 0.5 $CaCl_2$, 10 $MgCl_2$, 10 glucose, pH 7.4 with NaOH, bubbled with 100% O_2. Brains were sliced in 350 μm coronal sections containing the lateral hypothalamic area with a microtome (VTA-1200S, Leica). Then slices were transferred to an incubation chamber filled with physiological solution containing (in mM): 135 NaCl, 5 KCl, 1 $CaCl_2$, 1 $MgCl_2$, 10 HEPES, 10 glucose, pH 7.4 with NaOH, bubbled with 100% O_2 and incubated for at least 1 hour at RT; 24-26℃.

II-2-5. Electrophysiological recordings

The slices were transferred to a recording chamber (RC-27L, Warner Instrument Corp.) on a fluorescence microscope stage (BX51WI, Olympus). Neurons with EGFP fluorescence were subjected to electrophysiological recording. The fluorescence microscope was equipped with an infrared camera (C2741-79, Hamamatsu Photonics) for infrared differential interference contrast (IR-DIC) imaging and a CCD camera (IK-TU51CU, Olympus) for fluorescent imaging. Each image was displayed separately on a monitor (Gawin, EIZO, Tokyo, Japan) and was saved on a computer through a graphic converter (PIX-MPTV, Pixcela, Osaka, Japan).

Recordings were carried out with an Axopatch 200B amplifier (Axon Instruments) using borosilicate pipettes (GC150-10, Harvard Apparatus) prepared by a

micropipette puller (P-97, Sutter Instruments) filled with intracellular solution (4-10 MΩ) consisting of (in mM): 145 KCl, 1 $MgCl_2$, 10 HEPES, 1.1 EGTA-Na_3, 2 MgATP, 0.5 Na_2GTP, pH 7.3 with KOH. The osmolarity of the solutions were checked by a vapor pressure osmometer (model 5520, Wescor) and found to be 280-290 and 320-330 mOsm/L for the internal and external solutions, respectively. The liquid junction potential of the patch pipette and perfused extracellular solution was estimated to be 4.3 mV and applied to the data. Recording pipettes were under positive pressure while advancing toward individual cells in the slice. Tight seals on the order of 1.0-1.5 GΩ were made by negative pressure. The membrane patch was then ruptured by suction. The series resistance during recording was 10-25 MΩ. The reference electrode was an Ag-AgCl pellet immersed in bath solution. During recordings, cells were superfused with extracellular solution at a rate of 1.6 mL/min using a peristaltic pump (Dynamax, Rainin). In current clamp recordings, the membrane potential was set at -60 mV by current injection before the experiments. 5HT (Sigma) was dissolved in the extracellular solution and applied by local application through a fine tube (100 μm diameter) positioned near the neuron being recorded. TTX (Wako) was dissolved in extracellular solution and applied by bath application.

Output signals were low pass filtered at 5 kHz and digitized at 10 kHz. Data were recorded on a computer through a Digidata 1322A A/D converter using pClamp software (ver. 10, Axon Instruments). Traces were processed for presentation using Origin 8.1 (Origin Lab Corporation) and Canvas X (ACD systems) software.

II-2-6. Immunohistochemical studies

Male and female *orexin-tTA; TetO RFP* double transgenic mice (10 weeks old) were deeply anesthetized with isoflurane and perfused sequentially with 20 mL of chilled

saline and 20 mL of chilled 10% formalin solution (Wako). The brains were removed and immersed in the above fixative solution for 24 h at 4°C, and then immersed in a 30% sucrose solution for at least 2 d. The brains were quickly frozen in embedding solution (Sakura Finetechnical Co., Ltd., Tokyo, Japan). For orexin and RFP double-staining, coronal sections (40 μm) of *orexin-tTA; TetO RFP* mouse brains were incubated with rabbit polyclonal anti-RFP antiserum (1/1000, Cat. #632496, Clontech, CA, USA) for 24 h at 4°C. These sections were incubated with Alexa 594-labeled goat anti-rabbit IgG (1/800, Cat. #A-11037, Invitrogen) for 1 h at RT. The sections were then incubated with a guinea pig anti-orexin-A antiserum (1/500) for 24 h at 4°C. The antiserum was produced in our laboratory by immunizing guinea pigs with the same antigen reported in Nambu et al.(23). The antiserum was affinity purified using an affinity column. Sections were then incubated with Alexa 488-labeled goat anti-guinea pig IgG (1/800, Cat.# A-11073, Invitrogen) for 1 h at RT. The sections were mounted and examined with a fluorescence microscope (BZ-9000, Keyence, Osaka, Japan). This orexin antiserum did not produce any labeling on brain sections from orexin knockout mice.

II-2-7. EEG/EMG recording and analyses

Male mice (12 weeks old at the time of surgery) were anesthetized with pentobarbital (50 mg/kg, i.p.) and implanted with EEG and electromyogram (EMG) electrodes for polysomnographic recording. EEG signals were recorded using gold-coated pins placed on the dura mater (4 pins located ± 1.5 mm lateral of the bregma, ± 1.25 mm anterior or posterior to bregma). The EMG signal was acquired through a pair of multi-stranded stainless-steel wires inserted into the neck extensor muscles. Mice were then housed separately for a recovery period ≥7 d before recording. Continuous EEG and EMG recordings were carried out through a slip ring (Air Precision, Le Pressis Robinson,

France) designed so that the movement of the mouse was unrestricted. EEG and EMG signals were amplified (AB-610J, Nihon Koden, Tokyo, Japan), filtered (EEG 1.5-30 Hz; EMG 15-300 Hz), digitized at a sampling rate of 128 Hz, and recorded using SleepSign version 3 (Kissei Comtec, Nagano, Japan). The animal's behavior was monitored through a CCD video camera and recorded on a computer synchronized with EEG and EMG recordings using the SleepSign video option system (Kissei Comtec).

EEG and EMG records were automatically scored in 4 sec epochs and classified as wakefulness, SWS or REM sleep by SleepSign software according to standard criteria (14, 51). All vigilance state classifications assigned by SleepSign were examined visually and corrected. The same individual, blinded to genotype and experimental condition, scored all EEG/EMG recordings. Spectral analysis of the EEG was performed by fast Fourier transform (FFT). This analysis yielded a power spectra profile over a 0-40 Hz window with a 1 Hz resolution divided into delta (1-5 Hz), theta (6-10 Hz), alpha (10-13 Hz) and beta (13-25 Hz) bandwidths.

II-2-8. Statistical analyses

Data were analyzed by one-way ANOVA followed by Fisher's Protected Least Significant Difference test using the Stat View 4.5 software package (Abacus Concepts). Probability (*p*)-values less than 0.05 were considered statistically significant.

II-3. Results

II-3-1. *tTA* mRNA is specifically expressed in the orexin neurons

To control gene expression specifically in the orexin neurons using the tetracycline gene expression system, transgenic mice were generated in which orexin neurons specifically express tTA. To confirm that *tTA* mRNA was expressed in the orexin neurons, *in situ* hybridization was performed on brain slices from *orexin-tTA* transgenic mice brains. Figure 1A and 1C show that *prepro-orexin* mRNA was expressed in the lateral hypothalamic area. Figure 1B and 1D show that *tTA* mRNA was specifically expressed in the same area. Next, *tTA* mRNA expression in the orexin neurons was confirmed using double fluorescent *in situ* hybridization. The merged picture in Figure 1E shows that *tTA* mRNA (Cy3, red, middle panel) was expressed in the same neurons that expressed *prepro-orexin* mRNA (FITC, green, left panel). These results confirmed that tTA was expressed in the orexin neurons in the *orexin-tTA* mouse brain.

II-3-2. tTA-induced gene activity in orexin neurons

Next, tTA-induced gene activity was confirmed by breeding *orexin-tTA* mice with *TetO RFP* mice (which express RFP in the presence of tTA) to generate double transgenic *orexin-tTA; TetO RFP* mice (Figure 2A; Table 1). In the double transgenic mouse brain, RFP was specifically expressed in the orexin neurons (Figure 2B) since RFP-ir (Alexa594, red) was observed only in orexin-ir neurons (Alexa488, green) and no RFP expression was found elsewhere in the brain. Furthermore, 85% of orexin-ir neurons expressed RFP (n=4). These results indicate that tTA was expressed in the orexin neurons and correctly induced gene activity in the orexin neurons in the brains of these transgenic mice.

II-3-3. Reversible control of *Htr1a mRNA* expression in the orexin neurons

It is previously reported that orexin neurons were densely innervated by serotonergic neurons and were significantly inhibited through the 5HT1A receptor expressed in orexin neurons (26). The 5HT1A receptor is coupled with the Gi/o subtype of Gα subunit and subsequently βγ subunits activate GIRK channels (52). To evaluate the physiological significance of this inhibitory serotonergic input to orexin neurons, *orexin-tTA* transgenic mice were bred with *TetO Htr1a* mice in which the TetO sequence was knocked into the promoter region of the 5HT1A receptor gene allele to generate *orexin-tTA; TetO Htr1a* mice (49) (Table 1; Figure 3A). Since tTA binds to the TetO sequence, *Htr1a* mRNA transcription should be elevated above the basal *Htr1a* promoter activity, resulting in overexpression of 5HT1A receptor in tTA-expressing cells (49). Although the TetO sequence was inserted into endogenous 5HT1A receptor promoter region, this insertion does not interfere with endogenous 5HT1A receptor promoter activity. Thus, the 5HT1A receptor expression pattern in these knock-in mice was comparable to wild type mice (53). However, in the presence of DOX, tTA loses its ability to bind to the TetO sequence (Figure 3B), which should result in the return of *Htr1a* mRNA expression level in orexin neurons to the basal level (Figure 3C).

Htr1a mRNA overexpression in orexin neurons of *orexin-tTA; TetO Htr1a* mice was confirmed by fluorescent *in situ* hybridization in the absence of DOX. Figure 3D demonstrates that *Htr1a* mRNA (red, Cy3) was indeed expressed in *prepro-orexin* mRNA-expressing neurons (green, FITC).

Next, we used the "ABA" experimental design illustrated in the upper panel of Figure 3E to determine whether *Htr1a mRNA* expression could be reversibly controlled

in the orexin neurons of the *orexin-tTA; TetO Htr1a* mice by applying or removing DOX in the chow. *Htr1a* mRNA expression level was visualized by *in situ* hybridization. *Orexin/tTA; TetO Htr1a* mice were fed normal chow until 14 weeks of age. Panel b of Figure 3E illustrates that, at 13 weeks of age, *Htr1a* mRNA was overexpressed in the orexin neurons in these mice ("preDOX" condition). The chow was then replaced with chow containing DOX (100 mg/kg) for 7 d, from 14 to 15 weeks of age. After 5 d of DOX chow consumption, *Htr1a* mRNA expression in the orexin neurons returned to basal level (DOX(+), Figure 3E, Panel c). This expression level did not differ from that of *TetO Htr1a* control mice that lack the *orexin-tTA* transgene (Fig. 3E, Panel a). The *Htr1a* mRNA expression pattern and levels in the hypothalamus of *TetO Htr1a* mice did not differ from that of wild type mice (data not shown). When DOX chow was replaced with normal chow for two weeks from 15 to 17 weeks of age, *Htr1a* mRNA was overexpressed again ("postDOX", Figure 3E, Panel d). *Prepro-orexin* mRNA in the hypothalamus and *Htr1a* mRNA in the hippocampus were unaffected by the presence or absence of DOX (*prepro-orexin* mRNA: Figure 3E, Panels e, f, g and h; hippocampal *Htr1a* mRNA: Figure 3E, Panels i, j, k and l). These results confirm that *Htr1a* mRNA expression level was reversibly controlled by the presence or absence of DOX in the chow.

II-3-4. Patch clamp electrophysiological studies reveal the effects of 5HT1A receptor overexpression in orexin neurons

To determine the physiological effect of 5HT1A receptor overexpression in orexin neurons, slice patch clamp recording was performed. Since orexin neurons are sparsely distributed in the lateral hypothalamic area and there are no morphological features to distinguish them from other neurons, I generated triple transgenic mice,

orexin-EGFP; orexin-tTA; TetO Htr1a mice, by crossbreeding *orexin-EGFP* mice with *orexin-tTA; TetO Htr1a* mice (Table 1). In these mice, EGFP was expressed and the 5HT1A receptor was overexpressed in the orexin neurons in the absence of DOX in the chow. In contrast, in the presence of DOX in the chow, 5HT1A receptor expression level in the orexin neurons was normal (not overexpressed). Thus, orexin neurons of *orexin-EGFP; orexin-tTA; TetO Htr1a* mice in the presence of DOX were used as control and compared to orexin neurons from *orexin-EGFP; orexin-tTA; TetO Htr1a* mice in the absence of DOX.

First, I tested whether the basic membrane properties of orexin neurons were affected by overexpression of 5HT1A receptor in orexin neurons. Electrical properties of 5HT1A receptor-overexpressing orexin neurons were compared to those of control mice that were fed with DOX-containing chow until the day of experiment. There were no significant differences in the resting membrane potential, peak amplitude of action potentials, spontaneous firing, input resistance or membrane capacitance of orexin neurons between the overexpressing mice and control mice (Table 2). These results indicate that overexpression of the 5HT1A receptor did not alter the basic membrane properties of orexin neurons.

Next, I measured membrane potential from orexin neurons in current clamp mode in the presence of TTX (1 μM) in the bath solution. Local application of 5HT (10 μM) significantly hyperpolarized orexin neurons from both control mice and overexpressing mice (Figure 4A). Local application of 5HT (10 μM) induced -13.0 ± 1.6 mV (n=8) hyperpolarization of orexin neurons from control mice and -14.3 ± 1.3 mV (n=14) hyperpolarization of orexin neurons from overexpressing mice. These changes in membrane potential induced by 5HT (10 μM) were not significantly different between

the two mouse groups (p=0.51, Student's t-test). Figure 4B shows that the reversal potential (E_{rev}) induced by 5HT (10 μM) application was -93.6 ± 4.9 mV (n=11), close to theoretical E_{rev} of potassium (-90.8 mV) calculated from the Nernst equation in these recording conditions. These results are consistent with those obtained previously (26), indicating that GIRK channels open downstream of 5HT1A receptor activation even in orexin neurons with overexpressed 5HT1A receptor levels. To confirm that GIRK-induced current is intact in 5HT1A-overexpressing orexin neurons, GIRK channel-induced hyperpolarization by a pathway other than the 5HT1A receptor was tested. Baclofen activates $GABA_B$ receptors that are coupled to the Gi/o subtype of Gα subunit and which activate GIRK channels. $GABA_B$ receptors are expressed in orexin neurons and baclofen-induced hyperpolarization of orexin neurons through activation of GIRK channels has previously been reported (54). The magnitude of baclofen (30 μM)-induced hyperpolarization in 5HT1A-overexpressing orexin neurons from experimental and control mice was -9.2 ± 0.9 mV (n=5) and -9.5 ± 1.1 mV (n=7, p=0.80, Student's t-test), respectively. This result suggests that the intracellular signal transduction pathway to activate GIRK channels is not affected by 5HT1A receptor overexpression in orexin neurons.

The 5HT-induced hyperpolarization was prolonged in orexin neurons in overexpressing mice compared with control mice (Figure 4A merged trace: control (black) and overexpressing mice (red)). To compare the magnitude of the hyperpolarization induced by 5HT application, the area and half-width were analyzed (Figure 4C and Figure 4D, respectively). The area of the hyperpolarizing deflection induced by 5HT application (see inset in Figure 4C) was calculated in units, in which 1 unit was 1 mV x 1 sec. The half-width was calculated as the time to reach 50% of the

peak value induced by 5HT application (see inset in Figure 4D). The area and half-width of 5HT (10 μM)-induced hyperpolarization was increased approximately 3.0-fold and 2.3-fold, respectively, in orexin neurons from overexpressing mice compared with control mice. The areas induced by 5HT (10 μM) in orexin neurons in control and overexpressing mice were 155 ± 23 units (n=8) and 455 ± 43 units (n=10, p=0.00002, ANOVA, vs. control). The half-widths of the hyperpolarization duration induced by 5HT (10 μM) in orexin neurons from control and overexpressing mice were 11.7 ± 1.3 sec (n=8) and 26.3 ± 4.1 sec (n=10, p=0.005, ANOVA, vs. control).

This prolongation of 5HT inhibition was also confirmed using loose cell-attached recording. Orexin neurons from control and overexpressing mice showed spontaneous firing at rates of 2.9 ± 0.2 (n=21) and 3.3 ± 0.2 Hz (n=16), respectively. Although 5HT application inhibited the generation of action potentials in orexin neurons from both control and overexpressing mice, the inhibitory effect was prolonged in orexin neurons from overexpressing mice compared with control mice (Figure 4E and F). Inhibitory duration was measured as the "silent period" induced by 5HT (see inset in Figure 4F). Local application of 3, 10 and 30 μM 5HT prolonged inhibition 2.0-fold (n=10, p=0.002, ANOVA, vs. control), 1.7-fold (n=13, p=0.005, ANOVA, vs. control) and 1.7-fold (n=16, p=0.0003, ANOVA, vs. control), respectively, compared with control (Figure 4F). To confirm that 5HT-induced inhibition of 5HT1A-expressing orexin neurons was a reproducible response, sequential repetitive application of 5HT was tested (Figure 4G). Three sequential 5HT (10 μM) applications induced the same duration of firing inhibition in 5HT1A-overexpressing orexin neurons. When the inhibitory duration of the first application was set as 100%, the second and third applications induced 109.4 ± 8.5% (n=9, p=0.22, ANOVA, vs. 1st) and 94.4 ± 4.8% (n=9, p=0.46, ANOVA, vs. 1st)

inhibition, respectively (Figure 4H). These results indicate that 5HT1A receptor overexpression in orexin neurons significantly enhanced the inhibition produced by 5HT application, that is, the inhibitory serotonergic input to orexin neurons was intensified in orexin neurons of 5HT1A receptor-overexpressing mice.

II-3-5. Effects of enhanced serotonergic inhibition of orexin neurons on sleep/wakefulness regulation

To determine the *in vivo* significance of the inhibitory serotonergic input to orexin neurons, *orexin-tTA; TetO Htr1a* mice were subjected to sleep/wakefulness analyses and littermate *TetO Htr1a* monogenic mice were used as controls. Sleep/wakefulness states were identified as wakefulness, SWS and REM sleep from EEG and EMG recordings. For these experiments, DOX chow was provided and withdrawn according to the protocol presented in Figure 3E. In *TetO Htr1a* monogenic control mice, wakefulness was consolidated in the first half of the dark period (20:00pm-2:00am), with mice maintaining wakefulness bouts as long as 2 h since mice are most active at that time of day (Figure 5A, top). In contrast, during the first half of the light period (8:00am-14:00pm), *TetO Htr1a* mice frequently transitioned between wakefulness and sleep since mice are less active at that time of day (Figure 5A, bottom). Sleep/wakefulness patterns were analyzed in 3 h bins across the 24 h cycle. The total time spent in wakefulness, SWS and REM sleep in the dark (Figure 5B, top) and light (Figure 5B, bottom) periods was analyzed and the frequency of transitions between states was calculated (Figure 5C). In *TetO Htr1a* mice, neither the total time in each state (Figure 5B) nor the transition frequency (Figure 5C) was affected by the presence or absence of DOX in the chow. These results indicated that DOX application had no direct effect on the physiological

regulation of sleep/wakefulness.

In contrast to *TetO Htr1a* mice, *orexin-tTA; TetO Htr1a* mice showed severe fragmentation of wakefulness during the first half of the night in the absence of DOX in the chow ("preDOX", Figure 6A top left). Wakefulness was consolidated at this time of day in the DOX(+) condition ("DOX(+)", Figure 6A top middle). The hypnogram of DOX(+) condition in *orexin-tTA; TetO Htr1a* mice (Figure 6A) was similar to that of *TetO Htr1a* mice (Figure 5A). The mice maintained wakefulness bouts as long as 2 h (Figure 6A top middle) but sleep/wakefulness fragmentation returned when DOX was again removed from the chow for 14 d ("postDOX", Figure 6A top right).

Sleep/wakefulness patterns of *orexin-tTA; TetO Htr1a* mice were analyzed in 3 h bins across the 24 h cycle (Figure 6B and 6C). The total time in wakefulness was increased and total amounts of SWS and REM sleep were decreased during the first 6 h (20:00pm-23:00pm and 23:00pm-2:00am) of the dark period in the presence of DOX (DOX(+)) compared to the absence of DOX (preDOX). The transition frequency significantly decreased in the first 3 h of the dark period (20:00pm-23:00pm) (Figure 6C), consistent with sustained wakefulness bouts (Figure 6B). During the second 3 h (23:00pm-2:00am), there was a tendency toward decreased transition frequency in the presence of DOX. These results indicate that the amount of wakefulness was increased during the first 6 h of the dark period. These effects on sleep/wakefulness were eliminated by removing DOX from chow for 14 d (postDOX condition). No significant differences were observed between preDOX and postDOX during any 3 h epoch during the dark phase. Interestingly, however, the sleep/wakefulness pattern in the *orexin-tTA; TetO Htr1a* mice during the light period was unaffected by the presence or absence of DOX. No significant differences were observed between preDOX, DOX(+) and postDOX during

any time period in the light phase (Figure 6B bottom).

Table 3 summarizes the total time in wakefulness, SWS and REM sleep in the dark and light periods for both mouse strains. In *TetO Htr1a* mice, the time spent in wakefulness, SWS and REM sleep in both the dark and light periods was unaffected by the presence or absence of DOX. However, in *orexin-tTA; TetO Htr1a* mice, ANOVA revealed that the total time in wakefulness was significantly increased and the total time in SWS and REM sleep were significantly decreased during the dark period in DOX(+) condition compared with the preDOX condition. These effects on sleep/wakefulness were eliminated by removing DOX from chow for 14 d (postDOX condition); the total time in wakefulness, SWS and REM sleep were comparable to those in the preDOX condition. The fragmentation of wakefulness in the absence of DOX (preDOX and postDOX) during the first half of the dark phase in conjunction with *Htr1a* mRNA overexpression in the orexin neurons suggests that enhancement of inhibitory serotonergic input to orexin neurons is causally related to the fragmentation of wakefulness during the early dark period.

The mean wakefulness bout duration and mean SWS bout duration were also calculated for the first half of the dark period (6h, 20:00-3:00). The mean wakefulness bout duration in *orexin-tTA; TetO Htr1a* mice was significantly prolonged in the presence of DOX. Mean wakefulness bout durations of *orexin-tTA; TetO Htr1a* mice in the preDOX, DOX(+) and postDOX conditions were 12.3 ± 2.7 min, 25.6 ± 5.2 min (p=0.03 vs. preDOX) and 13.7 ± 5.2 min (p=0.83 vs. preDOX), respectively. In contrast, mean wakefulness bout durations of *TetO Htr1a* mice were not affected by the presence or absence of DOX. Mean wakefulness bout durations of *TetO Htr1a* mice in preDOX, DOX(+) and postDOX conditions were 27.6 ± 8.2 min, 30.7 ± 10.0 min (p=0.80 vs.

preDOX) and 26.2 ± 8.4 (p=0.90 vs. preDOX), respectively. On the other hand, mean SWS bout durations were unaffected by the presence of DOX in either *orexin-tTA; TetO Htr1a* mice or *TetO Htr1a* mice. Mean SWS bout durations of *orexin-tTA; TetO Htr1a* mice in the preDOX, DOX(+) and postDOX conditions were 4.4 ± 0.3 min, 4.2 ± 0.4 min (p=0.55 vs. preDOX) and 4.0 ± 0.3 min (p=0.42 vs. preDOX), respectively. Mean SWS bout durations of *TetO Htr1a* mice from the preDOX, DOX(+) and postDOX conditions were 5.6 ± 0.7 min, 5.4 ± 0.6 min (p=0.86 vs. preDOX) and 4.8 ± 0.5 (p=0.38 vs. preDOX), respectively. These results indicate that 5HT1A receptor overexpression in orexin neurons induced fragmentation of wakefulness.

II-4. Discussion

A combination of electrophysiological and histochemical studies had previously identified a neural circuit between the serotonergic neurons in the raphe nuclei and the orexin neurons in the lateral hypothalamus. However, the function of this circuit in the regulation of sleep/wakefulness is little understood. Here, I generated transgenic mice that enabled reversible control of 5HT1A receptor expression specifically in the orexin neurons and found that this negative feedback circuit likely contributes to stable, sustained periods of wakefulness early in the active (dark) period.

II-4-1. Inhibitory serotonergic input to orexin neurons

Serotonergic neurons in the raphe nuclei are well known to be involved in sleep/wakefulness regulation. However, the effects of 5HT on sleep/wakefulness are complex and how 5HT regulates sleep/wakefulness has been controversial: 5HT promotes wakefulness and inhibits REM sleep in some cases, whereas it increases sleep propensity in other circumstances (42). There are wake active and sleep active serotonergic neurons in DR (55). These conflicting reports of the effect of 5HT on sleep/wakefulness might be explained by the broad innervation of serotonergic neurons. Serotonergic neurons in raphe nucleus innervate cerebral cortex, amygdala, basal forebrain, thalamus, hypothalamus, reaphe nuclei, locus ceruleus, and pontine reticular formation (42). Furthermore, various types of neurons project to DR and release noradrenaline, histamine, GABA, glutamate, acetylcholine, orexin, meranin-concentrating hormone and so on. These neurotransmitters correlated with sleep/wakefulness regulation. Orexin neurons densely innervate serotonergic neurons in the DR nucleus and activate these neurons directly and indirectly through activation of

both orexin 1 and orexin 2 receptors (47, 56). On the other hand, it is previously reported that orexin neurons received dense serotonergic innervation and were strongly inhibited by 5HT through the 5HT1A receptor and subsequent activation of GIRK channels (26, 32). It is currently unclear how this circuit functions to regulate sleep/wakefulness since both orexin neurons and serotonergic neurons in the raphe nuclei are reported as wake active neurons and discharge less or are silent during SWS and REM sleep (37, 43, 55, 57, 58). However, the firing rate of orexin cells is not simply a function of arousal state as they are relatively inactive during quiet wakefulness but discharge in active waking with maximal activity during exploratory behavior (37). Although the effects of 5HT1A overexpression on the firing of orexin neurons is yet to be directly determined, from the results presented here, enhanced 5HT1A-mediated inhibition of these cells apparently reduces wakefulness drive and allows sleep to occur early in the dark period, a time of day when there is normally a low probability of sleep. This resulted in the fragmentation of sleep/wakefulness.

II-4-2. Reversible control of 5HT1A receptor expression in orexin neurons

To reveal the physiological role of the inhibitory serotonergic input to orexin neurons on sleep/wakefulness regulation, 5HT1A receptor expression level in the orexin neurons was reversibly controlled using the Tet-off system. *In situ* hybridization studies confirmed that *Htr1a* mRNA expression level in the orexin neurons of *orexin-tTA; TetO Htr1a* mice was reversibly controlled by adding or removing DOX from the chow. In the absence of DOX in the chow, *Htr1a* mRNA was overexpressed because tTA enhanced transcription of *Htr1a* mRNA in the orexin neurons. 5HT1A receptor overexpression in the orexin neurons returned to basal levels by adding DOX to the chow for 5 d. Although

the TetO sequence was inserted into endogenous 5HT1A receptor promoter region, this insertion does not interfere with the normal 5HT1A receptor expression pattern and DOX does not interfere endogenous 5HT1A receptor promoter activity (53). Thus, *Htr1a* mRNA expression in non-orexin neurons, such as hippocampal neurons, was unaffected by the presence or absence of DOX and histological studies confirmed that *Htr1a* mRNA levels were specifically controlled in the orexin neurons of *orexin-tTA; TetO Htr1a* mice.

Slice patch clamp recording from orexin neurons revealed that *Htr1a* mRNA overexpression prolonged the inhibitory effect of 5HT in orexin neurons approximately 2-fold. This result suggests that the number of 5HT1A receptors in the plasma membrane of orexin neurons was increased by *Htr1a* mRNA overexpression. However, the effect of 5HT1A receptor overexpression on 5HT-induced response was weaker than expected since *in situ* hybridization showed that *Htr1a* mRNA was robustly overexpressed in the absence of DOX. It is possible that 5HT1A receptor protein in the plasma membrane did not increase in parallel with the mRNA increase. Trafficking of GPCRs from the endoplasmic reticulum and Golgi apparatus to the plasma membrane is tightly regulated with multiple steps to ensure correct GPCR targeting (59). Binding to accessory proteins or chaperones is the primary step for trafficking to plasma membrane. These multiple steps might restrict robust expression of GPCRs in the membrane. On the other hand, ligand binding induces internalization of GPCR by β-arrestin binding. Alternatively, a limitation on the number of G proteins and GIRK channels expressed in the orexin neurons might be involved in this mismatch between mRNA expression level and physiological response. The number of open GIRK channels might be limited. Although the induced hyperpolarization was not enhanced in overexpression, continuous stimulation of GIRK channels by the downstream of 5HT1A receptors might be longed

inhibition time of orexin neurons which overexpress 5HT1A receptors.

II-4-3. Physiological significance of inhibitory serotonergic input to the orexin neurons for sleep/wakefulness regulation

Reversible gene expression control using the Tet-off system is a powerful approach for the analysis of the effects of cell type-specific gene expression on physiology or behavior because it enables comparisons to be made before and after gene expression control *within the same animal*. In the present study, I reversibly controlled 5HT1A receptor expression level in the orexin neurons. The pattern and amount of wakefulness in the early dark period was significantly altered by 5HT1A receptor expression level in the orexin neurons as mice showed severe fragmentation of wakefulness when 5HT1A receptor was overexpressed in these cells. These results strongly suggest that enhancement of inhibitory serotonergic input to orexin neurons caused fragmentation of wakefulness. However, sleep/wakefulness architecture in the light period was unaffected by 5HT1A receptor overexpression in the orexin neurons. These results suggest that inhibitory serotonergic input to orexin neurons may function as negative feedback in the early dark period. Since mice are nocturnal, they are highly active during the dark period and many mouse strains are most active shortly after lights off. During this time, inhibitory serotonergic input might keep the activity of orexin neurons in the moderate range as a negative feedback circuit. However, enhancement of inhibitory serotonergic input to orexin neurons by 5HT1A receptor overexpression likely reduces the firing of the orexin neurons that normally provide excitatory input to monoaminergic and cholinergic systems as well as to the serotonergic raphe neurons which believed to promote wakefulness. Fragmentation of wakefulness could thus result

from reduced or unstable excitatory drive onto these arousal systems, resulting in the inability to sustain prolonged bouts of wakefulness during this period.

It has been reported that the activity of serotonergic neurons *in vivo* is highly dependent on the activity of orexin neurons (22). Acute inhibition of orexin neurons using optogenetics induced SWS in conjunction with a decrease in serotonergic neuron activity. Decreased firing of serotonergic neurons in raphe nucleus presumably results in decreased transmitter release at 5HT nerve terminals, including those that synapse on orexin neurons. Most orexin neurons express c-fos in the early dark period (60), suggesting elevated discharge of orexin neurons at this time. Orexin neurons are hypothesized to receive high frequency excitatory inputs that depolarize orexin neuron membrane potential to maintain wakefulness early in the dark phase. Decreased serotonergic inhibition might result in overexcitation of orexin neurons, resulting in increased locomotor activity and sustained wakefulness. Imbalance between excitatory and inhibitory inputs to orexin neurons by 5HT1A receptor overexpression in *orexin-tTA; TetO Htr1a* mice might be the cause of wakefulness fragmentation in the dark period. During the light period, however, serotonergic inhibitory input may be too weak to affect the firing of orexin neurons since they are less active or quiescent during sleep stage. A similar fragmentation of wakefulness was observed in mice with selective loss of $GABA_B$ receptors in orexin neurons (54). This result supports the hypothesis that the balance between excitatory and inhibitory inputs to orexin neurons is important in the physiological regulation of sleep/wakefulness. However, these $GABA_{B1}{}^{flox/flox}$; *orexin-Cre* mice showed fragmentation in the light period as well (54), suggesting inhibitory GABAergic input to orexin neurons functions in both the light and dark periods.

II-4. Figures and Tables

Figure 1

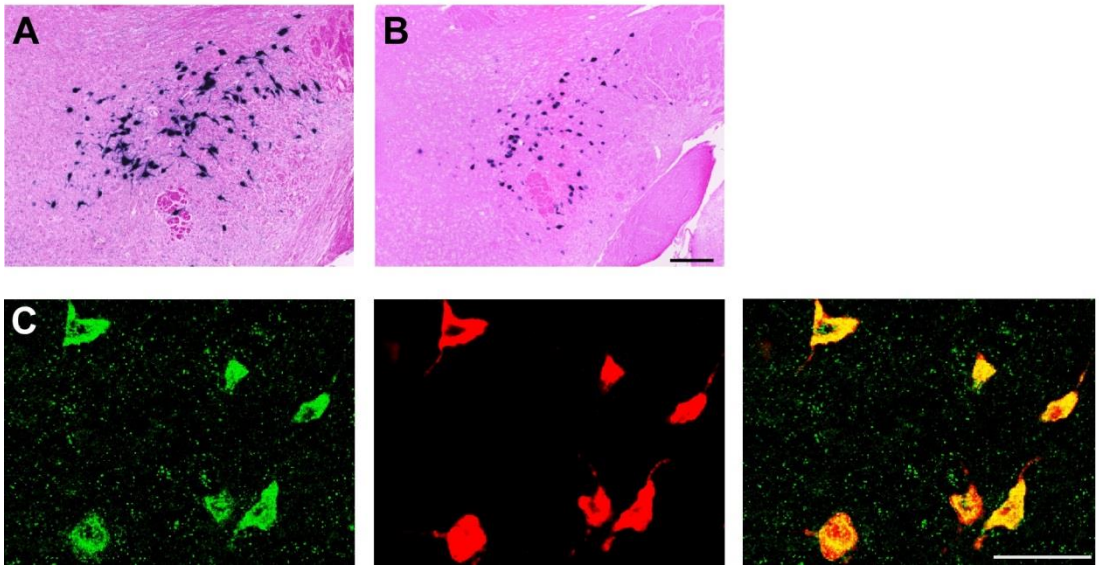

Figure 1. Generation of *orexin-tTA* transgenic mice. *In situ* hybridization revealed that *tTA* mRNA was expressed in the orexin neurons of the *orexin-tTA* mouse brain. *Prepro-orexin* mRNA (**A**) and *tTA* mRNA (**B**) are expressed in the same area within the lateral hypothalamus. The area indicated by white rectangle in (**A**) and (**B**) is magnified in (**C**) and (**D**), respectively. **E**, Double fluorescent *in situ* hybridization. *Prepro-orexin* mRNA (FITC, green, left); *tTA* mRNA (Cy3, red, middle); merged picture (right). Scale bar B, 1 mm; D, 200 μm; E, 50 μm.

Figure 2

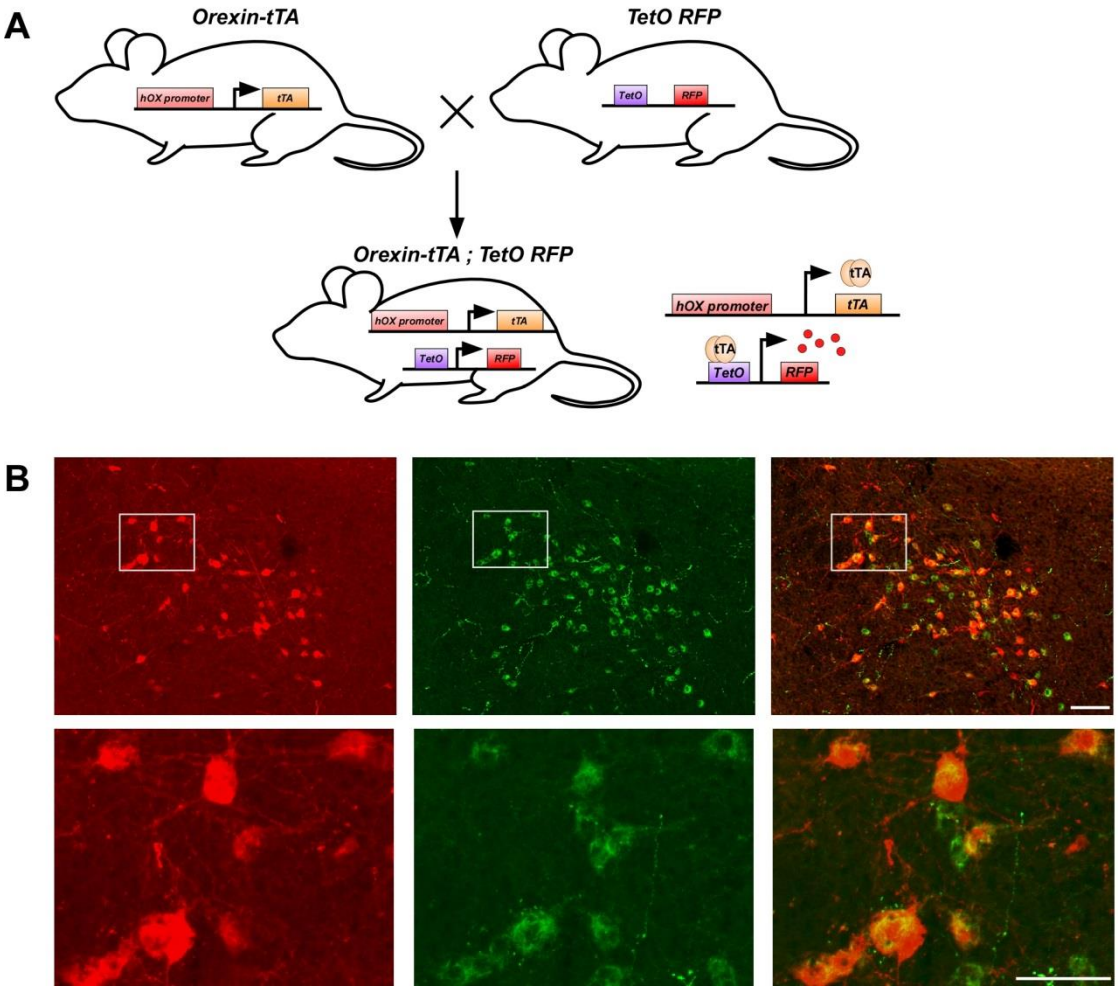

Figure 2. Functional confirmation of tTA-induced gene expression. **A**, Drawing illustrating breeding scheme in which *orexin-tTA* mice were bred with *TetO RFP* mice to generate double transgenic *orexin-tTA; TetO RFP* mice. tTA induced RFP expression in the orexin neurons in *orexin-tTA; TetO RFP* mice. **B**, Immunohistochemical study revealed that RFP was specifically expressed in the orexin neurons. Left to right: RFP-ir (red); orexin-ir (green); merged picture. White square area in the upper panel is enlarged in the bottom panel. *hOX* promoter, human *prepro-orexin* promoter. Scale bars in B: upper panel, 100 μm; lower panel, 50 μm.

Figure 3

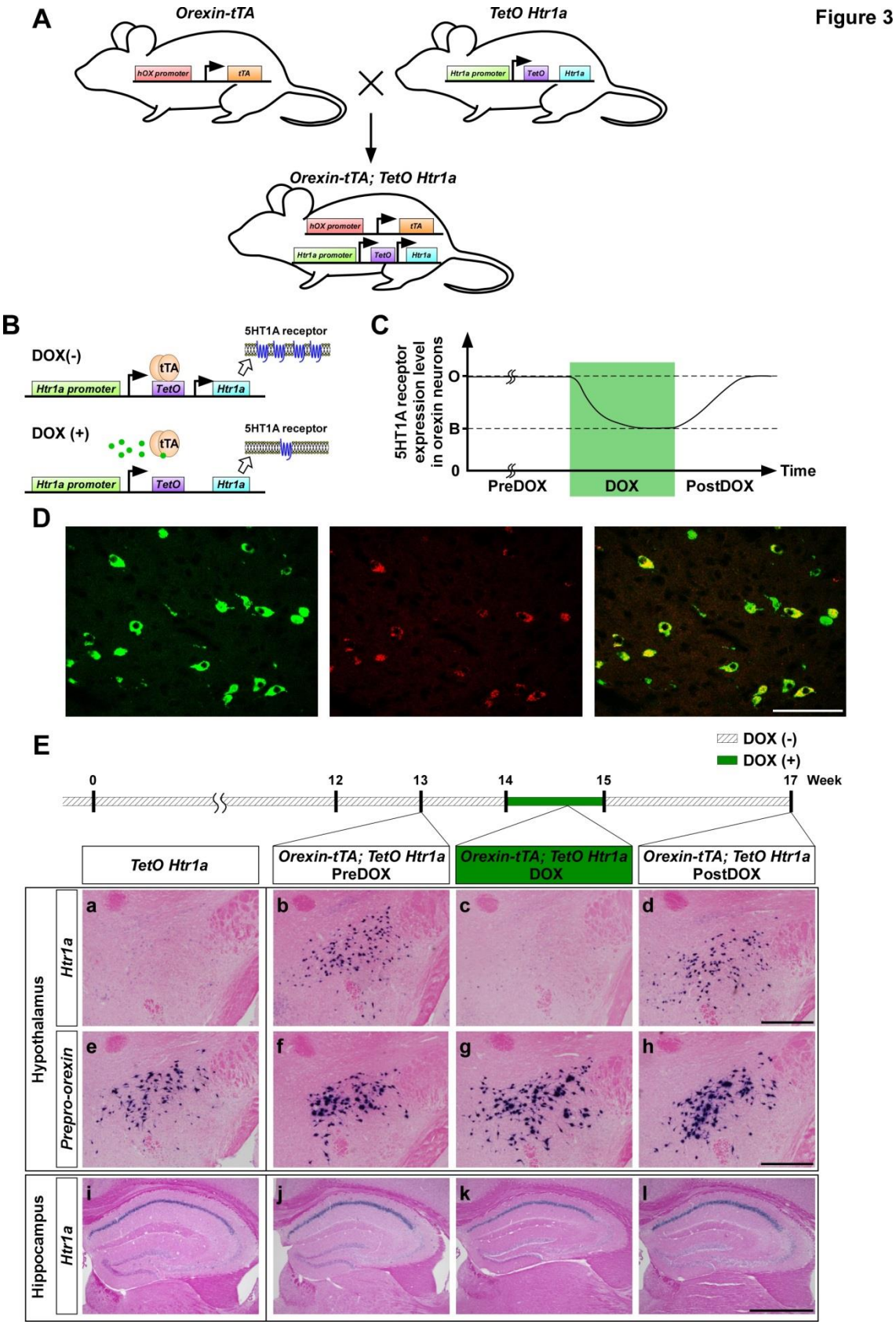
A
Orexin-tTA
TetO Htr1a
hOX promoter
tTA
Htr1a promoter
TetO
Htr1a
Orexin-tTA; TetO Htr1a
B
DOX(-)
5HT1A receptor
DOX (+)
C
5HT1A receptor expression level in orexin neurons
O
B
0
PreDOX
DOX
PostDOX
Time
D
E
DOX (-)
DOX (+)
0
12
13
14
15
17
Week
TetO Htr1a
Orexin-tTA; TetO Htr1a PreDOX
Orexin-tTA; TetO Htr1a DOX
Orexin-tTA; TetO Htr1a PostDOX
Hypothalamus
Htr1a
Prepro-orexin
Hippocampus
a
b
c
d
e
f
g
h
i
j
k
l

Figure 3. Reversible control of *Htr1a* mRNA expression in the orexin neurons. **A**, Drawing illustrating breeding scheme in which *orexin-tTA* mice were bred with *TetO Htr1a* mice to generate double transgenic *orexin-tTA; TetO Htr1a* mice. **B** and **C**, 5HT1A receptor gene expression was reversibly regulated in the orexin neurons using the tTA gene expression system in the presence or absence of DOX. DOX(+) indicates the presence of DOX; DOX(-) indicates the absence of DOX. O, overexpression; B, basal expression. **D**, Double fluorescent *in situ* hybridization revealed that *Htr1a mRNA* was expressed in *prepro-orexin*-expressing neurons in *orexin-tTA; TetO Htr1a* mice. Left to right: *Prepro-orexin* (FITC, green); *Htr1a* (Cy3, red); merged image. **E**, *In situ* hybridization demonstrated reversible control of *Htr1a* mRNA expression in the orexin neurons. The upper and middle panels show *Htr1a* mRNA (a, b, c and d) and *prepro-orexin mRNA* (e, f, g and h) in the hypothalamus. The lower panel shows *Htr1a* mRNA (i, j, k and l) in the hippocampus. *Htr1a* mRNA was overexpressed in the orexin neurons in the absence of DOX (b and d). However, in the presence of DOX for 5 d (c), *Htr1a* mRNA returned to expression levels comparable to those of monogenic *TetO Htr1a* mice (a). Neither *prepro-orexin* nor hippocampal *Htr1a* mRNA expression was altered in the presence or absence of DOX. Scale bars: D, 100 μm; E, 1.0 mm.

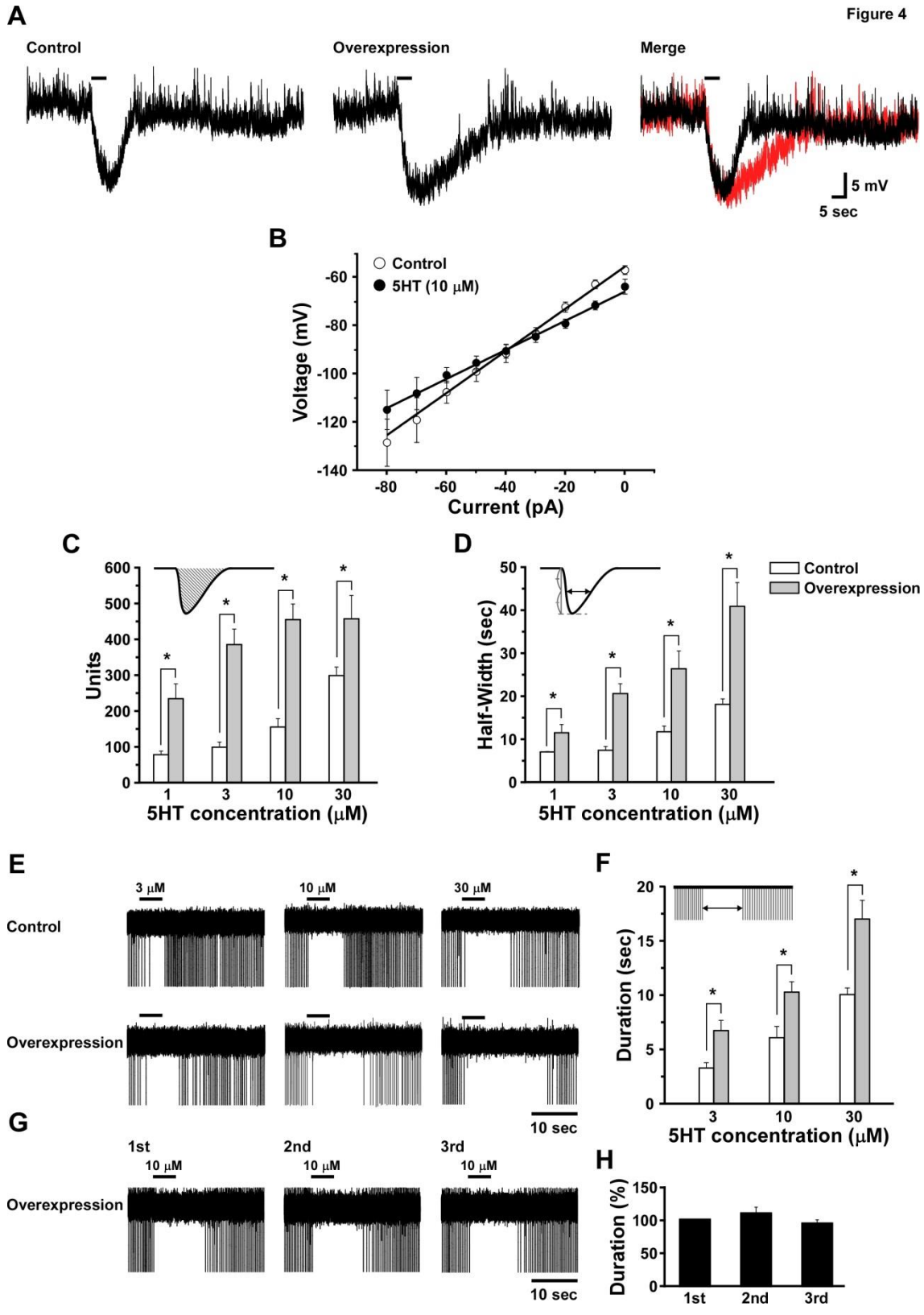
A
Figure 4
Control
Overexpression
Merge
5 mV
5 sec
B
Control
5HT (10 μM)
Voltage (mV)
Current (pA)
C
Units
5HT concentration (μM)
D
Half-Width (sec)
Control
Overexpression
5HT concentration (μM)
E
3 μM
10 μM
30 μM
Control
Overexpression
10 sec
F
Duration (sec)
5HT concentration (μM)
G
1st
2nd
3rd
10 μM
Overexpression
10 sec
H
Duration (%)
1st
2nd
3rd

Figure 4. *Htr1a* overexpression in the orexin neurons prolonged 5HT-induced inhibition of firing. **A**, Under current-clamp mode, local application of 5HT (10 μM) induced a prolonged hyperpolarization of orexin neurons in 5HT1A receptor overexpressing *orexin-EGFP; orexin-tTA*; *TetO Htr1a* mice in the absence of DOX (middle) compared to control *orexin-EGFP; orexin-tTA*; *TetO Htr1a* mice in the presence of DOX (left), as illustrated best in the merged traces (right). In current clamp, the membrane potential was set at -60 mV by current injection before the experiments. **B**, Graph showing current-voltage relationship in the presence (filled circles) or absence (open circles) of 5HT (10 μM) in orexin neurons recorded from overexpressing *orexin-EGFP; orexin-tTA; TetO Htr1a* mice (overexpressing). Membrane potential in response to a series of 100 ms current steps (in 20 pA increments, -80 pA to 0 pA) from -60 mV was plotted (n=11). Estimated reversal potential (E_{rev}) was -93.6 ± 4.9 mV (n=11). **C** and **D**, Bar graphs summarizing the data obtained from recordings such as those illustrated in A. C and D present the area and the half-width induced by 5HT-induced hyperpolarization, respectively, as illustrated by the insets (n=3-16). **E**, Representative traces of loose cell-attached recordings of orexin neurons in hypothalamic slices from *orexin-EGFP; orexin-tTA; TetO Htr1a* mice in the presence of DOX (control, top) and *Orexin-EGFP; orexin-tTA; TetO Htr1a* mice in the absence of DOX (overexpressing, bottom). 5HT was locally applied for 5 sec during the period represented by bars and inhibited the firing of action potentials in the orexin neurons. **F**, Bar graphs comparing the duration of 5HT-induced inhibition illustrated in E (n=10-17). **G**, Representative traces showing loose cell-attached recordings of 5HT1A overexpressing orexin neurons (*orexin-EGFP; orexin-tTA; TetO Htr1a* mice). 5HT (10 μM) was sequentially and repetitively applied for three times. 5HT was locally applied for 5 sec during the period represented by bars and inhibited the firing of action potentials in the orexin neurons. **H**, Bar graph comparing the duration of 5HT-induced inhibition illustrated in E (n=9). Duration of inhibition is represented as percentage of 1st application. *p<0.05 vs. control. Values are mean ± SEM.

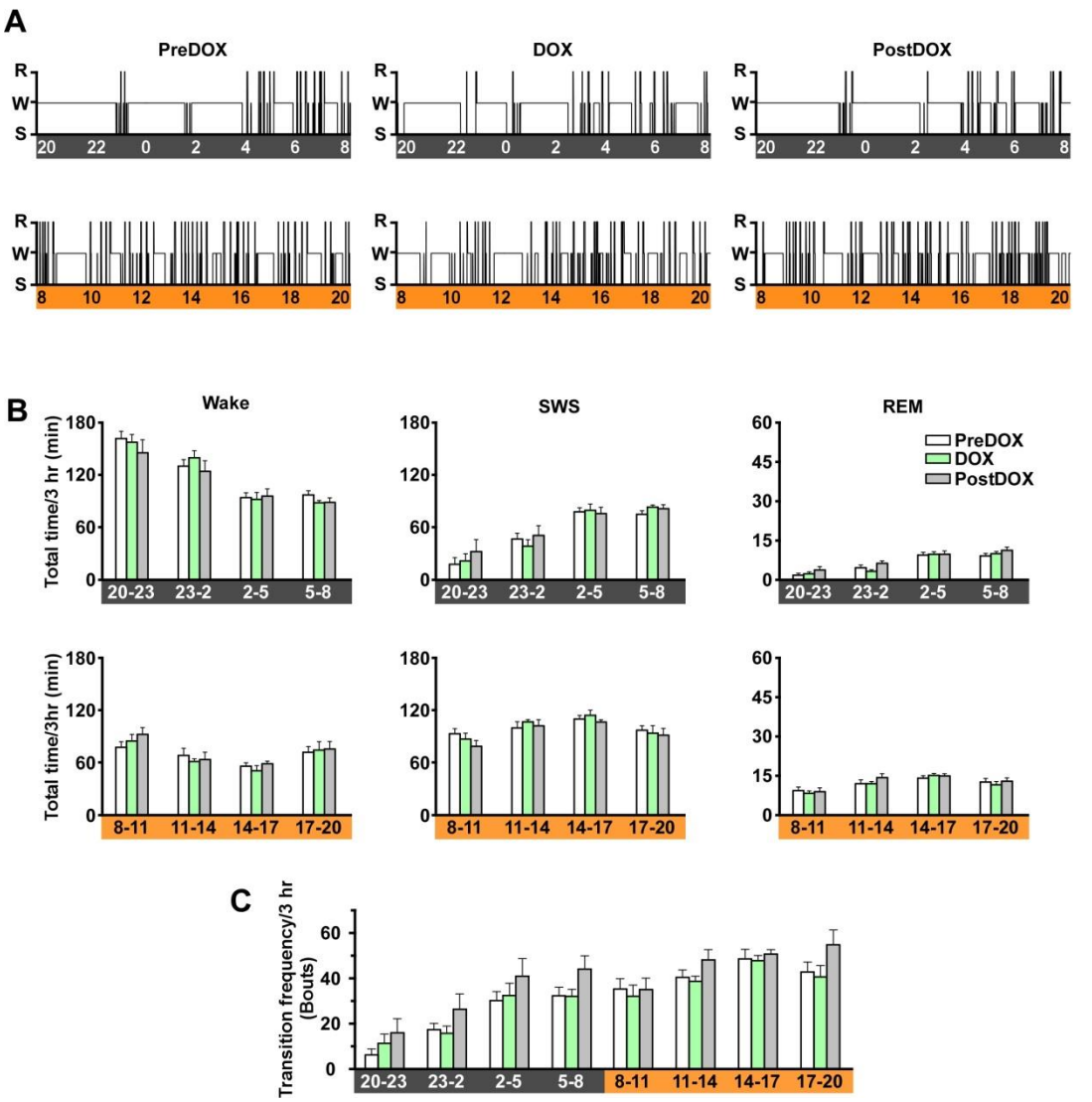

Figure 5. DOX application does not affect sleep/wakefulness pattern in *TetO Htr1a* mice. **A**, hypnograms from *TetO Htr1a* mice recorded in the presence or absence of DOX (100 mg/kg) in chow. The upper panel presents representative hypnograms from the dark period (from 20:00pm to 8:00am). The lower panel presents representative hypnograms from the light period (from 8:00 am to 20:00 pm). PreDOX (left panels) is a recording of 13 week old mouse fed normal chow; DOX(+) (middle panels) is 5 d after DOX chow; postDOX is 14 d after removal of DOX chow. **B,** summarizes the time spent in wakefulness, SWS and REM sleep in each 3 h period throughout the light (bottom) and dark (top) periods. **C**, Bar graphs showing transition frequency in 3 h bins across the 24 h period. Values are mean ± SEM (n=8). W or Wake, wakefulness; S or SWS, slow wave sleep; R or REM, REM sleep.

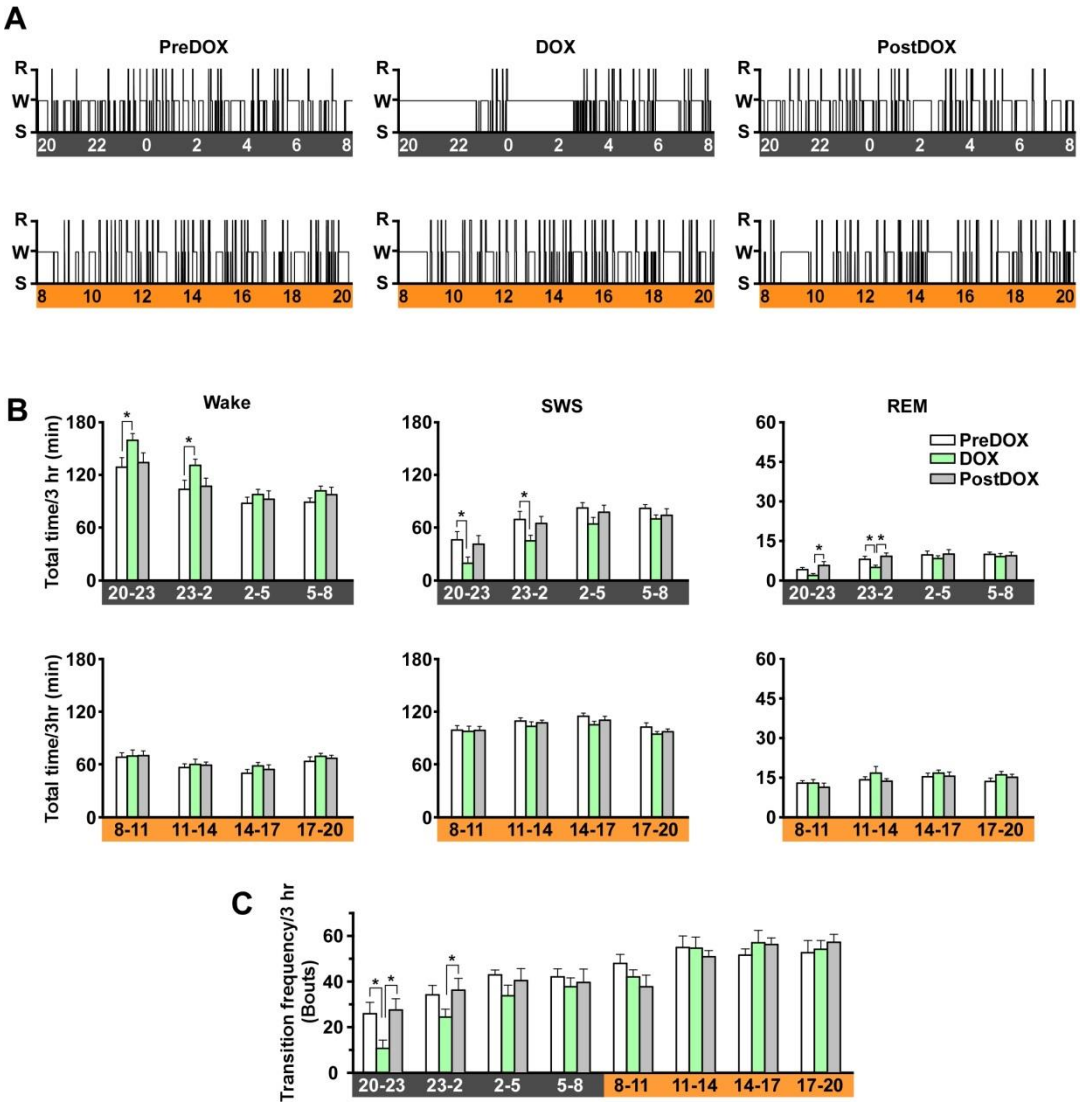

Figure 6. *Htr1a* mRNA overexpression in orexin neurons increases the sleep time during the early dark period but does not affect sleep/wakefulness pattern in the light period. **A,** hypnograms from *orexin-tTA; TetO Htr1a* mice recorded in the presence or absence of DOX in the chow. The upper panel presents representative hypnograms from the dark period (from 20:00 to 8:00). The lower panel presents representative hypnograms from the light period (from 8:00 to 20:00). PreDOX (left panels) is during 5HT1A receptor overexpression; DOX(+) (middle panels) is 5 d after DOX application which reduces 5HT1A receptor overexpression in orexin neurons; postDOX is 14 d after removal of DOX chow. **B** summarizes the time spent in wakefulness, SWS and REM sleep in each 3 h period throughout the light (bottom) and dark (top) periods. **C**, Bar graphs showing transition frequency in 3 h bins across the 24 h period. *p<0.05 vs. DOX (+). Values are mean ± SEM (n=12). W or Wake, wakefulness; S or SWS, slow wave sleep; R or REM, REM sleep.

Table 1. Names and characteristics of transgenic mouse strains used in the present study.

Working Name	**Full name**	**Characteristics and Use in the Present Study**
Orexin-tTA	Orexin-tetracycline-controlled Transcriptional Activator	tTA is driven by human *prepro-orexin* promoter. tTA is exclusively expressed in orexin neurons.
Orexin-EGFP	Orexin-Enhanced Green Fluorescent Protein	EGFP is driven by human *prepro-orexin* promoter. Orexin neurons have green fluorescence and thus could be identified under fluorescence microscope.
TetO Htr1a	Tetracycline Operator 5-Hydroxytryptamine receptor 1a	*TetO* sequence was knocked into the promoter region of the 5HT1A receptor gene allele. This insertion does not affect original promoter activity. *Htr1a* mRNA expression could be upregulated in the presence of tTA.
TetO RFP	Tetracycline Operator Red Fluorescent Protein (mCherry)	RFP reporter mice. RFP is expressed in the presence of tTA.
Orexin-tTA; TetO RFP	Orexin-tetracycline-controlled Transcriptional Activator; Tetracycline Operator Red Fluorescent Protein (mCherry)	Bigenic mice generated by breeding *Orexin-tTA* mice with *TetO RFP* mice. tTA binds to *TetO* and induces RFP expression only in orexin neurons.
Orexin-tTA; TetO Htr1a	Orexin-tetracycline-controlled Transcriptional Activator; Tetracycline Operator 5-Hydroxytryptamine receptor 1a	Bigenic mice generated by breeding *Orexin-tTA* mice with *TetO Htr1a* mice. tTA is exclusively expressed in orexin neurons. tTA binds to *TetO* and induces *htr1a* mRNA overexpression only in orexin neurons in the absence of doxycycline. 5HT1A receptor expression level returns to normal level in the presence of doxycycline (control).
Orexin-tTA; orexin-EGFP; TetO Htr1a	Orexin-tetracycline-controlled Transcriptional Activator; Orexin-Enhanced Green Fluorescent Protein; Tetracycline Operator 5-Hydroxytryptamine receptor 1a	Trigenic mice generated by breeding *Orexin-EGFP* mice with bigenic *Orexin-tTA; TetO Htr1a* mice. Orexin neurons have green fluorescence that could be identified under fluorescence microscope. 5HT1A receptor expression level in orexin neurons could be controlled in the presence or absence of doxycycline.

Table 2. Electrical membrane properties of 5HT1A receptor-overexpressing orexin neurons recorded from mice with and without DOX. AP, action potential. Values are means ± S.E.M.

	Control (DOX(+))	Overexpressing (DOX(-))
Membrane capacitance (pF)	23.4 ± 1.7 (n=13)	26.5 ± 2.6 (n=11)
Resting membrane potential (mV)	-61.1 ± 1.3 (n=13)	-59.0 ± 0.8 (n=15)
Membrane resistance (MΩ)	665.4 ± 36.2 (n=13)	568.4 ± 58.4 (n=8)
Spontaneous firing frequency (Hz)	3.3 ± 0.2 (n=16)	3.1 ± 0.3 (n=15)
AP peak (mV)	21.2 ± 3.7 (n=11)	18.6 ± 0.5 (n=7)
AP amplitude (mV)	63.7 ± 3.7 (n=11)	56.8 ± 0.9 (n=7)
AP half width (msec)	2.91 ± 0.16 (n=11)	2.70 ± 0.00 (n=7)

Table 3. Sleep/wake amounts in *TetO Htr1a* and *orexin-tTA; TetO Htr1a* mice in the presence and absence of DOX.

Dark, Dark period (12 h: 20:00-8:00); Light, Light period (12 h: 8:00-20:00). *, vs. *TetO Htr1a*; #, vs. PreDOX. Wake, wakefulness; SWS, slow wave sleep; REM, REM sleep. Values are means ± S.E.M. (min).

		TetO Htr1a (n=8)			*Orexin-tTA; TetO Htr1a* (n=12)		
		Wake	SWS	REM	Wake	SWS	REM
PreDOX	Dark	476.4 ± 13.5	219.7 ± 11.6	23.7 ± 2.3	410.3 ± 23.1*	275.7 ± 20.1	31.2 ± 2.5*
	Light	278.4 ± 11.4	394.7 ± 11.9	48.3 ± 3.1	245.0 ± 11.7*	418.6 ± 11.0	55.7 ± 2.9
DOX	Dark	475.2 ± 20.0	221.7 ± 18.7	23.2 ± 1.9	482.6 ± 21.4#	190.4 ± 18.5#	22.5 ± 2.2#
	Light	271.4 ± 11.2	400.7 ± 10.3	47.6 ± 2.2	260.9 ± 12.1	397.7 ± 11.2	61.2 ± 4.8
PostDOX	Dark	456.1 ± 32.6	236.7 ± 29.2	27.2 ± 4.0	438.9 ± 27.1	248.1 ± 24.1	32.1 ± 3.3*
	Light	288.8 ± 7.9	381.7 ± 7.9	49.4 ± 2.8	251.9 ± 5.9	412.1 ± 5.3	55.4 ± 3.5

Chapter III: Conditional ablation of orexin neurons: A new mouse model for the study of narcolepsy and orexin system function

Tabuchi S, Tsunematsu T, Black SW, Tominaga M, Maruyama M, Takagi K, Minokoshi Y, Sakurai T, Kilduff TS, Yamanaka A.

The Journal of Neuroscience (2014) 34(19):6495-6509

III-1. Introduction

Narcolepsy is a chronic sleep disorder characterized by excessive daytime sleepiness, fragmentation of sleep/wakefulness, hypnagogic hallucinations, sleep paralysis and cataplexy. In humans, the onset of narcolepsy is typically in adolescence or early adulthood. Since definitive diagnosis may take as long as a decade, it is difficult to study the development of symptomatology after initial onset of the disorder. It is reported that one in six hundred people develop narcolepsy in Japan.

The etiology of narcolepsy is a loss of the hypothalamic neurons that express the orexin neuropeptides (3, 4). Although the cause of orexin neuron loss remains to be determined, genetic linkage of narcolepsy with human leukocyte antigen (HLA)-DQB1*0602 (61), immune system gene polymorphisms (62) suggest an autoimmune mechanism in which the orexin neurons are targeted.

Although narcoleptic dogs, which bear a mutation in the OX2R gene (7), have been extensively used for pharmacological (63) as well genetic studies, the discovery of the orexin neuropeptides opened the door to creation of novel animal models of this disease. *Prepro-orexin* knockout mice were reported to show fragmentation of sleep/wakefulness and behavioral arrests that are similar to cataplexy (5). Although OX1R null mice showed a mild abnormality in sleep/wakefulness behavior, OX2R null mice showed clear narcolepsy-like symptomatology (8) and OX1R and OX2R double null mutant mice showed even more severe symptoms (64, 65). The loss of orexin cells characteristic of human narcolepsy has been modeled in *orexin/ataxin-3* mice in which the neurotoxic polyglutamine repeat of the Ataxin-3 protein is coupled to the *prepro-orexin* promoter (6). Accumulation of polyglutamine causes cell dysfunction and death.

These animal models have helped elucidate the role of orexin neurons in

sleep/wakefulness regulation, metabolism and addiction. However, current animal models lack the orexin peptides, receptors or neurons from birth and thus do not replicate the typical post-pubertal onset of this disorder in humans. Furthermore, current mouse models have limited utility in the development of novel pharmacological treatments for narcolepsy because cataplexy events are relatively infrequent. Accordingly, behavioral (66), dietary (67), and pharmacological (68) approaches have been implemented in attempts to elevate cataplexy levels. Thus, it is necessary to generate a new model with closer fidelity to human narcolepsy. I utilized the Tet-off system in which expression of diphtheria toxin A (DTA) in orexin neurons was controlled by the presence of DOX. I found robust cataplexy as well as disrupted sleep architecture and weight gain in this model. Since the orexin system has been implicated in the control of metabolism and addiction as well as sleep/wakefulness regulation, o*rexin-tTA; TetO DTA* mice are a novel model in which to study these functions, for pharmacological studies of sleep/wakefulness fragmentation or cataplexy, and to understand the process of network reorganization as orexin input is lost.

III-2. Experimental Procedures

III-2-1. Animal usage

All experimental procedures involving animals were approved by the Institutional Animal Care and Use Committee of the National Institutes of Natural Sciences and the Research Institute of Environmental Medicine Nagoya University and were in accordance with NIH guidelines. All efforts were made to minimize animal suffering or discomfort and to reduce the number of animals used.

III-2-2. Animals

Orexin-tTA mice (69), which express tTA exclusively in orexin neurons under control of human *prepro-orexin* promoter (19), were bred with *TetO diphtheria toxin A fragment (DTA)* mice (B6.Cg-Tg(tetO-DTA)1Gfi/J, Jackson Labs) to generate *orexin-tTA; TetO DTA* mice. The transgenic construct to generate *orexin-tTA* transgenic mice was made by substituting the *nLacZ* gene (SalI-BamHI fragment) of the *orexin/nLacZ* transgenic construct (19) with 0.7 kb of the mammalianized *tTA* fragment (70). The transgene was excised and microinjected into pronuclei of fertilized mouse eggs (C57BL/6 mice) to generate transgenic founders. Founders were bred with C57BL/6J mice (Clea-Japan Inc.) to produce stable *orexin-tTA* transgenic lines. A total of 9 *orexin-tTA* transgene-positive founders were obtained. *In situ* hybridization analysis of the N1 generation revealed that lines 29, C5 and G5 showed the highest *tTA* mRNA expression. *TetO DTA* mice express DTA under the control of a tetracycline operator. In these double transgenic mice, DTA expression occurs in the orexin neurons in the absence of DOX. Both *orexin-tTA* mice and *TetO DTA* mice were on the C57BL/6J genetic background.

Doxycycline-containing chow (DOX chow) was made by adding 10% DOX powder (Kyoritsu Seiyaku Corporation) to normal chow (Labo MR Stock) at a final

concentration of 100 mg/kg. Labo MR stock was provided during DOX(-) period. Mating pairs of *orexin-tTA* mice and *TetO DTA* mice were fed with DOX-containing chow (DOX(+) condition) from the day of mating. During the prenatal and early postnatal periods, DOX was supplied via maternal circulation or lactation, respectively. After weaning, *orexin-tTA; TetO DTA* mice were fed with DOX (+) chow until the day of experiment.

III-2-3. Schedules of DOX feeding and behavioral experiments

III-2-3-1. Experimental Protocol 1: Induction of orexin cell loss in *orexin-tTA; TetO DTA mice*

Male and female *orexin-tTA; TetO DTA* mice were maintained from weaning to 10 wk of age on DOX(+) chow. At 10 wk, DOX(+) chow was removed and replaced with Labo MR stock food (DOX(-) condition) for up to 13 wk. At either 0 d (n=5), 1.5 d (n=3), 3.5 d (n=3), 1 wk (n=4), 2 wk (n=3), 4 wk (n=22), or 13 wk (n=4) after DOX removal, mice were perfused and brains were sliced, immunostained for orexin, and cell counts obtained as described below. *Orexin-tTA* (n=7) and *TetO DTA* (n=4) mice, maintained from weaning on DOX(+) chow, were also sacrificed at 10 wk of age as a comparison.

III-2-3-2. Experimental Protocol 2 : Characterization of sleep/wake parameters during orexin cell loss in *orexin-tTA; TetO DTA* mice

For sleep/wake studies, male mice raised on DOX(+) chow were implanted with EEG and EMG electrodes for polysomno-graphic recording at 10 wk of age as described below. At 12 wk, DOX(+) chow was replaced with DOX(-) chow. EEG and EMG recordings occurred approximately weekly from age 12-25 wk (0 to 13 wk after DOX removal). EEG and EMG parameters were compared to *orexin/ataxin-3* mice (6) and to *orexin-tTA; TetO DTA* mice raised from birth on DOX(-) chow (the D(-) group).

III-2-3-3. Experimental Protocol 3: Induction of partial orexin cell loss in *orexin-tTA; TetO DTA* mice

To reduce the number of orexin neurons without elimination of the entire cell population, DOX(+) chow was removed at 10 wk of age and replaced with Labo MR stock food (DOX(-) condition) for 1.5 d or 3.5 d, after which DOX(+) chow was reintroduced (1.5 d+RD; n=3 and 3.5 d+RD; n=3, respectively). Mice were then sacrificed and perfused for immunohistochemical analyses at 14 wk of age. In another variation of the protocol, DOX chow was removed at 12 wk of age and reintroduced at 14 wk (DOX(-)2 wk+RD; n=6); mice were then sacrificed at 25 wk of age.

III-2-3-4. Experimental Protocol 4: Partial orexin cell loss and cataplexy assessment

To maintain the number of orexin neurons at 5% of the control number, DOX(+) chow was removed at 12 wk of age and replaced with Labo MR stock food (DOX(-) condition) for 2 wk, after which DOX(+) chow was reintroduced for 13 wk until mice were 25 wk old. Cataplexy bouts after DOX(-) were monitored.

III-2-3-5. Experimental Protocol 5: Food-elicited cataplexy test

In attempt to increase cataplexy above basal levels, chocolate 1.8 ± 0.5 g (milk chocolate, Meiji Co., Ltd., Tokyo, Japan) was made available along with DOX(-) chow at light offset (20:00) to mice at 4 wk and 15 wk after removal of DOX from the diet. Cataplexy levels were compared to those observed on the day prior to chocolate availability.

III-2-3-6. Experimental Protocol 6 - Body weight, food and water consumption and activity measures

Male *orexin-tTA; TetO DTA* mice, *orexin-tTA* mice and *TetO DTA* mice were maintained from weaning to 10 wk of age on DOX(+) chow. At 10 wk, DOX(+) chow

was removed and replaced with Labo MR stock food (DOX(-) condition) for up to 4 wk. Daily measurements of body weight, food and water consumption were initiated 3 d before the DOX(-) condition was imposed; measurements occurred at 8:00am each day. Spontaneous activity was continuously monitored by a weight sensor (Actracer-2000, Arco System, Chiba, Japan) positioned under the cage. Blood samples (200 μl) were taken from the tail vein before DOX(-) at 10 wk and after 4 wk DOX(-). Blood glucose levels were measured by a glucose sensor (G sensor, Glucocard DIA meter, Arkley, Kyoto, Japan) on 5 μl serum samples. Serum levels of insulin (ELISA kit, Morinaga Institute of Biological Science, Inc., Yokohama, Japan), leptin (ELISA kit, Morinaga Institute of Biological Science) and free fatty acids (Free fatty acid C kit, Wako) were determined; insulin and leptin concentrations were determined as the mean value of triplet measurements.

III-2-4. Immunohistochemical studies

Male and female mice were deeply anesthetized with pentobarbital (50 mg/kg, i.p.) and perfused sequentially with 15 ml of chilled saline and 15 ml of chilled 10% formalin solution (Wako). Brains were isolated and immersed in formalin solution for 24 h at 4°C, followed by a 30% sucrose solution at 4°C for at least 2 d. Brains were quickly frozen in embedding solution (Sakura Finetek Co., Ltd.). Coronal sections containing the lateral hypothalamic area, dorsal raphe, and locus coeruleus were cut on a cryostat (CM3050 S, Leica) at a thickness of 40 μm. Sections were incubated for 40 min in phosphate buffer containing 0.3% H_2O_2 to inactivate endogenous peroxidase. After washing three times in phosphate-buffered saline containing 0.25% Triton X-100 and 1% bovine serum albumin fraction V (PBS-BX), sections were incubated in PBS-BX for 24 h at 4°C with goat anti-orexin IgG antibody (Santa Cruz, CA), guinea pig anti-HTT IgG

antibody (Frontier Institute), rabbit anti-TH IgG antibody (Millipore, MA), rabbit anti-MCH IgG antibody (Sigma), or rabbit anti-IbaI IgG antibody (Wako). After several washes in PBS-BX, sections were incubated overnight with biotinylated horse anti-goat IgG antibody (Vector Laboratories), biotinylated goat anti-guinea pig IgG antibody (Vector Laboratories), or biotinylated goat anti-rabbit IgG antibody (Vector Laboratories) in PBS-BX for 1 h at RT. Sections were then washed with PBS-BX and reacted with avidin-biotin peroxidase complex (Vector Laboratories) diluted in PBS-BX for 1 h at RT. Bound peroxidase was visualized by DAB (Merck, NJ) with 0.0015% H_2O_2, resulting in a golden-brown reaction product. For double staining, bound peroxidase was visualized by 0.01 M imidazole acetate buffer containing 0.05% 3,3-diaminobenzidine tetrahydrochloride (Dako, Carpinteria, CA), 0.0015% H_2O_2 and 2.5% nickel ammonium sulfate (Wako), resulting in a black reaction product. For orexin and NeuN doublestaining, sections were incubated with mouse anti-NeuN IgG antibody (Millipore) and goat anti-orexin IgG antibody (Santa Cruz) for 24 h at 4°C. These sections were incubated with CF488-labeled donkey anti-mouse IgG (Biotium, CA) and CF 647-labeled donkey anti-goat IgG (Biotium) for 1 h at RT. Antisera concentrations are listed in Table 1. Sections were mounted and examined with a microscope (BZ-9000, Keyence). To confirm the specificity of antisera, incubations without primary antibody were conducted as a negative control in each experiment and the expected absence of signal was confirmed (data not shown). Approximately 10 slices from a 1 in 4 series were selected for counting of orexin and MCH neurons. NeuN-ir cells and orexin-ir cells were counted in a region (counting box width 363 μm, height 273 μm) within the lateral hypothalamic area. The size and area of orexin neurons, axon fibers and IbaI-ir cell were automatically calculated using image analysis software (Hybrid cell count, Keyence).

III-2-5. EEG/EMG surgery, recording and analyses

Male mice were anesthetized with pentobarbital (50 mg/kg, i.p.) and implanted with EEG and EMG electrodes for polysomnographic recording at 10 wk of age. Mice were then housed separately for at least 7 d recovery before recording. Continuous EEG and EMG recordings were conducted through a slip ring (Air Precision) designed so that the movement of the mouse was unrestricted. EEG and EMG signals were amplified (AB-610J, Nihon Koden), filtered (EEG 1.5-30 Hz; EMG 15-300 Hz), digitized at a sampling rate of 128 Hz, and recorded using SleepSign version 3 (Kissei Comtec). The animal's behavior was monitored through a CCD video camera and recorded on a computer synchronized with EEG and EMG recording using the SleepSign video option system (Kissei Comtec). During the dark period, activity was monitored by infrared sensor. EEG/EMG records were automatically scored in 4 s epochs and classified as wakefulness, SWS, or REM sleep by SleepSign software according to standard criteria (14, 51). Vigilance state classifications assigned by SleepSign were examined visually and corrected. The same individual, blinded to genotype and experimental condition, scored all EEG/EMG recordings.

Spectral analysis of the EEG was performed by fast FFT (sampled at 128 Hz). This analysis yielded power spectra profiles over a 0-40 Hz window with a 1 Hz resolution for the delta (1-5 Hz), theta (6-10 Hz), alpha (10-13 Hz), and beta (13-25 Hz) bandwidths. An average EEG spectral profile was calculated from EEG power densities in each frequency bin and expressed as average power values for the delta, theta, alpha, and beta bandwidths for each state.

Cataplexy was scored according to the consensus definition of cataplexy (71) based on four criteria: an abrupt episode of EMG atonia lasting ≥10 s, immobility during

the episode, predominance of theta activity during the episode, and more than 40 s of wakefulness preceding the episode. In some very rare cases, mice briefly came out of cataplexy only to have another attack within 10-30 sec; such a sequence was scored as two bouts of cataplexy.

III-2-6. Statistical analyses

Data were analyzed by one-way ANOVA followed by Fisher's protected least significant difference test and t-test using OriginPro 8.2 software (OriginLab). Probability (*p*)-values less than 0.05 were considered statistically significant.

III-3. Results

III-3-1. Control of orexin neurons using the Tet-off system

To produce orexin neuron-specific degeneration in adulthood, DTA was expressed in orexin neurons using the Tet-off system (Figure 1A). *Orexin-tTA* mice (69, 72), in which tTA is exclusively expressed in orexin neurons under control of human *prepro-orexin* promoter, were bred with *TetO DTA* mice to generate *orexin-tTA; TetO DTA* mice. In these double transgenic mice, tTA induces DTA expression by binding to the TetO sequence. Expression of DTA, which induces cell death by inhibiting protein synthesis (73), was controlled by the presence or absence of DOX in the diet since tTA loses its ability to bind to the TetO sequence in the presence of DOX. Thus, tTA-induced DTA expression was initiated by replacing DOX(+) chow with DOX(-) chow.

To determine whether orexin cell death could be controlled by DOX in *orexin-tTA; TetO DTA* mice, in Experimental Protocol 1, the number of orexin neurons was counted after DOX removal from the diet as illustrated in Figure 1B. At 10 wk of age on DOX(+) chow, the number of orexin neurons in *orexin-tTA; TetO DTA* mice was 891 ± 54 (n=5), which was comparable to monogenic littermate *TetO DTA* (897 ± 32; n=4) or *orexin-tTA* (889 ± 54; n=7) control mice. Throughout the experiments, the number of neurons reported is a sum of the neurons counted in every 4th brain section (brains were sliced into 40 μm sections). Neither the shape nor the size of orexin neurons was altered at this age. The area of orexin neurons in control (*TetO DTA*), 0 wk, 1 wk, 2 wk and 4wk was 185 ± 21 μm^2, 155 ± 14 μm^2, 170 ± 16 μm^2, 163 ± 25 μm^2 and 196 ± 26 μm^2, respectively (n=13-73, $p>0.3$, ANOVA, not significantly difference). These results indicated that Tet-off system worked in the presence of DOX without leakage of DTA expression in orexin neurons until at least 10 wk of age. After replacing DOX(+) chow

with DOX(-) chow, the number of orexin neurons dramatically decreased in *orexin-tTA; TetO DTA* mice (Figure 1Cb-e, 1Cg-j and Figure 2A). The number of orexin neurons after 1.5 d (36 h), 3.5 d, 1 wk, 2 wk, 4 wk and 13 wk DOX(-) decreased to 572 ± 68 (64.2%, n=5), 323 ± 3, (36.2%, n=6), 127 ± 26 (14.3%, n=4), 47 ± 7 (5.2%, n=3), 25 ± 2 (2.8%, n=22) and 7 ± 1 (0.8%, n=4), respectively. *Post hoc* tests revealed significant reductions in all groups relative to 0 wk. Figure 2B presents the rostrocaudal pattern of orexin neuron ablation after DOX removal. Orexin neurons are distributed approximately -1.0 mm to bregma -2.0 mm from bregma, with the peak population occurring at bregma -1.3 mm. The number of orexin neurons rostral-caudally decreased uniformly after DOX removal. However, the number of orexin neurons in the lateral hypothalamus decreased faster than the medial population (Figure 2C).

Orexin neurons densely innervate monoaminergic nuclei, such as the noradrenergic LC and serotonergic DR nucleus, which play an important role in the regulation of sleep/wakefulness. In conjunction with loss of orexin cell bodies in the hypothalamus, orexin neuron nerve endings in terminal fields in the LC and DR decreased as well. By 4 wk after removal of DOX, orexin nerve endings almost completely disappeared from these projection sites (LC: Figure 1Cl-o, l'-o'; midline pontine central gray: Figure 1Cl*-o*; DR: Figure 1Cq-t, q'-t', q*-t*). Although orexin nerve endings gradually decreased after removal of DOX, the number of noradrenergic neurons and serotonergic neurons was not altered in either of these nuclei.

To confirm whether DTA-induced cell death induction was restricted to the orexin neurons, melanin-concentrating hormone (MCH) neurons were stained and counted (Figure 3A). MCH neurons are distributed in the lateral hypothalamic area but do not colocalize with orexin (74). The number of MCH neurons was unaffected by DOX

removal for 4 wk in *orexin-tTA; TetO DTA* mice (Figure 3B). Even though MCH neurons are located near the orexin neurons, no signs of unhealthiness such as shrinkage of MCH cell bodies or unclear edges of MCH neurons were observed. To determine whether any other neurons located near orexin cells were affected, sections of the tuberal hypothalamus were stained with an anti-NeuN antibody. NeuN-ir cells and orexin-ir cells were counted (counting box width 363 μm X height 273 μm) in the area where orexin neurons are densely distributed. The number of non-orexin neurons (NeuN-ir cells – orexin-ir cells) in *TetO DTA* mice and *orexin-tTA; TetO DTA* mice at DOX(-) 6 wk was 67 ± 8 (NeuN-ir cells: 79 ± 8; orexin-ir cells: 12 ± 0.1, n=3) and 65 ± 7 (NeuN-ir cells: 65 ± 9; orexin-ir cells: 0.2 ± 0.1) (n=4, p=0.848, Student's t-test), respectively. These results confirmed that the Tet-off system functioned correctly in the transgenic mice and that orexin cell bodies and nerve terminals were specifically ablated after removing DOX from the chow.

To determine the effect of orexin neuron cell death on other cells in the surrounding hypothalamus, immunostaining with IbaI, a marker for microglial cells which act as scavengers in the brain (75-77), was conducted. Double staining with anti-orexin and anti-IbaI antisera was performed at 0, 1, 2 and 4 wk after removal of DOX (Figure 4). IbaI-microglial cell number increased in the lateral hypothalamic area by 2 wk in the DOX(-) condition, suggesting that microglial cells were activated to remove dead cell bodies by phagocytosis. The area of IbaI-ir cell in the hypothalamic area in *orexin-tTA; TetO DTA* mice at 0, 1, 2 and 4 wk was 775 ± 146 μm^2, 1047 ± 105 μm^2, 3133 ± 613 μm^2 and 1250 ± 154 μm^2, respectively (n=3). However, that in the ventromedial hypothalamic area in *orexin-tTA; TetO DTA* mice at 0, 1, 2 and 4 wk was unchanged (638 ± 84 μm^2, 563 ± 69 μm^2, 626 ± 118 μm^2 and 641 ± 57 μm^2, respectively (n=3)). Microglial

cell activation was restricted to the local area where the orexin neurons were distributed; microglial cells in other hypothalamic regions such as the ventral medial hypothalamus were unaffected by DOX removal. Activated microglial cells returned to normal shape and number by 4 wk after DOX removal.

III-3-2. Alteration of sleep/wakefulness patterns in conjunction with ablation of orexin neurons

Orexin-tTA; TetO DTA mice allowed us to study the relationship between the number of orexin neurons and sleep/wakefulness regulation before and after DOX removal as illustrated in Experimental Protocol 2 (Figure 5A). EEG and EMG electrodes were implanted at 10 wk of age and mice were habituated for at least 1 wk after surgery. At 12 wk of age, DOX(-) chow was supplied for 13 wk. Control recordings were conducted the day prior to replacing DOX(+) chow with DOX(-) chow. *Orexin/ataxin-3* mice, in which orexin neurons degenerate due to expression of the ataxin-3 protein under control of *prepro-orexin* promoter (6), were used as a comparison. To determine the effect of orexin neuron degeneration during early postnatal development, *orexin-tTA; TetO DTA* mice fed DOX(-) chow from birth were also studied (D(-) condition; Figure 5A). Although the D(-) condition is similar to *orexin/ataxin-3* mice, degeneration may be faster and more severe in D(-) group. When sacrificed at 12 wk of age, the number of remaining orexin neurons of D(-) group and *orexin/ataxin-3* mice was 2 ± 1 (n=8) and 39 ± 6 (n=5), respectively (Figure 5B).

Sleep/wakefulness states were determined as wakefulness, SWS, and REM sleep from EEG and EMG recordings. Figure 5C shows representative hypnograms from *orexin-tTA; TetO DTA* mice during ablation of orexin neurons (control, 1, 2, 4, and 13 wk)

and *orexin/ataxin-3* mice. At 1 wk DOX(-), fragmentation of wakefulness was particularly observed in the early dark period that progressed in conjunction with ablation of orexin neurons. Cataplexy was observed as early as 2 wk after DOX removal. At 13 wk DOX(-), sleep/wakefulness fragmentation and cataplexy bout frequency was greatly increased. In contrast, *orexin/ataxin-3* mice exhibited a mild phenotype when compared to *orexin-tTA; TetO DTA* mice.

The time spent in each state was compared to the control (0 wk) period (Figure 5D). During the dark period, the total time spent in wakefulness was significantly reduced from 3 to 10 wk after DOX removal. Interestingly, however, the amount of wakefulness recovered by 11 wk DOX(-). On the other hand, the total time spent in SWS did not significantly change except during the dark period at 4 wk after DOX removal. The total time spent in REM sleep significantly decreased during the light period after 2 wk and there was a trend toward reduced REM sleep during the dark period as well. The time spent in cataplexy significantly increased after 3 wk DOX(-) during both the dark and the light periods, which may be related to the reduced time in wakefulness and REM sleep after 3 wk DOX(-). The transition frequency between sleep/wakefulness states significantly increased during the dark period between 1-13 wk compared to control (Figure 6A) but not in the light period. Transition frequency during the dark period was further analyzed in detail (Figure 6B). Transition frequency to each state was counted during ablation of orexin neurons. At DOX(-) 1w, transition frequency from wakefulness to SWS was significantly increased. Transition frequency between wakefulness and SWS was dramatically increased until DOX(-) 4w. The increase in cataplexy frequency was followed by a decrease in transitions to REM sleep. *Orexin-ataxin3* mice showed severe sleep/wakefulness fragmentation with fewer transitions to cataplexy compared to *orexin-*

tTA; TetO DTA mice. Although the distribution of EEG power within each state was unaffected by orexin neuron loss (Figure 7A), spectral power in most bandwidths significantly increased after DOX removal (Figure 7B).

III-3-3. Cataplexy in *orexin-tTA; TetO DTA* mice vs. *orexin/ataxin-3* mice

In humans, narcolepsy is diagnosed with and without cataplexy; about half of narcoleptic patients report cataplexy. Although symptoms in narcoleptic patients without cataplexy are milder than in narcolepsy with cataplexy (78), the cause of this difference is incompletely understood. Consequently, cataplexy-like behavioral arrests in *orexin-tTA; TetO DTA* mice during ablation of orexin neurons were analyzed in detail. First, we determined the proportion of orexin neurons that were lost prior to cataplexy being observed. Cataplexy was initially observed at 2 wk DOX(-) in both the dark (3.0 ± 0.9 bouts) and light (0.6 ± 0.3 bouts) periods (Figure 8A), by which time about 95% of the orexin neurons were lost (Figure 2A). Cataplexy bout frequency dramatically increased from 2 wk to 11 wk DOX(-) in both the dark and light periods (Figure 8A). During this period, the proportion of orexin neurons decreased from 5% to 1% (Figure 2A). At 11 wk DOX(-), the number of cataplexy bouts in the dark period and the light period was 56.2 ± 7.7 bouts (n=5, $p< 0.001$ vs. 2 wk, ANOVA) and 15.0 ± 2.2 bouts (n=5, $p<0.001$ vs. 2 wk, ANOVA), respectively. On the other hand, the number of cataplexy bouts in the D(-) group was much lower than *orexin-tTA; TetO DTA* mice at 13 wk DOX(-) even though the number of remaining orexin neurons was much less than that of 13 wk DOX(-) (Figure 5B). During the dark period, the number of cataplexy bouts in the D(-) group and in *orexin/ataxin-3* mice was 17.6 ± 2.6 bouts (n=8, $p<0.001$ vs 13 wk, ANOVA) and 6.7 ± 2.6 bouts (n=5, $p<0.001$ vs 13 wk, ANOVA), respectively. During the light period, the

number of cataplexy bouts in the D(-) group and *orexin/ataxin-3* mice was 6.1 ± 1.4 bouts (n=8, p=0.005 vs. 13 wk, ANOVA) and 0.5 ± 0.4 bouts (n=5, p<0.001 vs 13 wk, ANOVA), respectively.

The mean cataplexy bout duration did not change in either the dark or the light periods as cataplexy frequency increased (Figure 8B). During the dark period, the mean cataplexy duration at 2 wk, 9 wk and 13 wk was 64.0 ± 10.7 sec (30 bouts), 78.0 ± 4.8 sec (188 bouts, p=0.27 vs. 2 wk, ANOVA) and 58.8 ± 3.4 sec (265 bouts, p=0.68 vs. 2 wk, ANOVA). During the light period, the mean cataplexy duration at 2 wk, 9 wk and 13 wk was 114.0 ± 21.3 sec (6 bouts), 85.1 ± 9.3 sec (57 bouts, p=0.32, vs. 2 wk, ANOVA) and 73.5 ± 7.0 sec (69 bouts, p=0.16, vs 2 wk, ANOVA). The mean duration of D(-) group and *orexin/ataxin-3* mice was significantly longer when compared with 13 wk in either the dark or the light periods. In the dark period, the mean duration of D(-) group and *orexin/ataxin-3* mice was 100.1 ± 3.5 sec (463 bouts, p<0.001, vs. 13 wk, ANOVA) and 101.1 ± 6.7 sec (100 bouts, p<0.001 vs. 13 wk, ANOVA), respectively. In the light period, mean cataplexy duration of D(-) group and *orexin/ataxin-3* mice was 99.8 ± 5.9 sec (167 bouts, p=0.007 vs. 13 wk, ANOVA) and 101.1 ± 40.6 sec (7 bouts, p=0.30 vs. 13 wk, ANOVA), respectively.

To determine whether the characteristics of cataplexy changed as the orexin neurons degenerated, the EEG spectrum was compared between the initial occurrence of cataplexy and subsequent weeks. Figure 8C and D shows that the EEG power spectrum and the average power of each bandwidth did not change during cataplexy between the dark and light periods nor over the course of weeks 2-4 DOX(-) when the number of orexin neurons declined from ~5% to ~3% of control values (Figure 2A).

Figure 9 presents the diurnal distribution of cataplexy bouts as the orexin neurons

degenerated. Cataplexy bout frequency was greater during the dark (active) period and highest during the first half of the dark period. Bout frequency tended to increase during the last two hours of light period. Similar trends were observed in D(-) and *orexin/ataxin-3* mice, although cataplexy rarely occurred during the light period in *orexin/ataxin-3* mice.

These results indicate that cataplexy appeared when ~95% of orexin neurons were lost. Ablation of orexin neurons in adulthood induced much more severe cataplexy episodes than ablation from birth, suggesting compensation during postnatal development. Although cataplexy bout frequency dramatically increased with age, the electrophysiological properties of cataplexy were unaltered. Lastly, cataplexy bout occurrence was not uniform throughout the day but rather was related to circadian time.

III-3-4. Partial ablation of orexin neurons

The Tet-off system enables reversible control of gene expression in the presence or absence of DOX. In theory, this feature would enable partial ablation of orexin neurons by restoration of DOX (RD) after mice were subjected to the DOX(-) condition for a period of time. Experimental Protocol 3 (Figure 10A) determined whether this occurred in *orexin-tTA; TetO DTA* mice. After being raised from birth in the presence of DOX(+) chow, mice were fed with DOX(-) chow for 1.5 or 3.5 d at 10 wk of age and then either sacrificed (1.5 d-RD and 3.5 d-RD groups; n=3 each) or fed DOX(+) chow for 4 wk until age 14 wk (1.5 d+RD and 3.5 d+RD groups; n=3 each) and then sacrificed. Figure 10B shows that the number and shape of orexin neurons in 3.5 d+RD were comparable to those of 3.5 d-RD. Figure 10C and D shows that the number of orexin neurons remaining 4 wk after DOX restoration was comparable to the DOX(-) group sacrificed prior to DOX(+) restoration at 10 wk of age. The number of orexin neurons in the 1.5 d+RD and

3.5 d+RD groups was 597 ± 52 (p=0.599 vs. 1.5 d, ANOVA) and 328 ± 31 (p=0.817 vs. 3.5 d, ANOVA), respectively, indicating that ablation of orexin neurons was arrested by DOX restoration and that the magnitude of ablation was dependent on the duration of DOX removal. Analysis of the remaining orexin neurons revealed that the distribution of these cells in the DOX restoration groups coincided with that of the corresponding DOX(-) groups (Figure 10D), indicating the absence of an orexin neuron subpopulation that was differentially sensitive to DTA. These results confirmed that the number of remaining orexin neurons could be controlled by varying the DOX(-) period and subsequent restoration of DOX.

III-3-5. Partial ablation of orexin neurons and cataplexy bout frequency

As indicated above and in Figure 8, cataplexy bout frequency at 11 wk was approximately 30-fold greater than the values observed after 2 wk of DOX(-). This increase might be caused by further reduction of the number of orexin neurons from 5% to 1% (Figure 2A). Alternatively, the 95% decrease in the number of orexin neurons induced by 2 wk of DOX(-) might be sufficient to not only trigger cataplexy, but also to cause the increase in cataplexy bout frequency over time. To distinguish between these possibilities, the number of orexin neurons was maintained ~5% using the experimental protocol illustrated in Figure 11A and cataplexy bout frequency was monitored. Mice were fed DOX(+) chow from birth to 12 wk of age, DOX(-) chow for 2 wk (which induced 95% loss of orexin neurons, see Figure 2A), and then DOX(+) chow was restored for 11 wk (2 wk+RD group; n=6) to arrest further degeneration. Cataplexy bout frequency was monitored for 11 wk after DOX restoration and compared to the cataplexy frequency of mice in which DOX was permanently removed from the diet at 12 wk of age (DOX(-)

group). For both groups, the cataplexy bout frequency at 2 wk DOX(-) was used as a reference value. Figure 11B shows that cataplexy bout frequency did not increase if the number of orexin neurons was maintained at 5% in the 2 wk+RD group in contrast to the cataplexy increase that occurred in the DOX(-) group. The cataplexy bout increment in the 2 wk+RD group at 11 wk after DOX restoration was -0.33 ± 4.35 (n=6).

At the end of the experiment, the number of remaining orexin neurons in the 2 wk+RD group was counted (Figure 11C) and found to be 44 ± 3 (n=6). As reported in Figure 2A, at 2 wk DOX(-), the number of remaining orexin neurons was 47 ± 7 (n=3; p=0.598, unpaired t test). Furthermore, from medial to lateral analyses showed a similar bias in the ablation of orexin neurons both in 2 wk-RD and 2 wk+RD (Figure 11D). Since cataplexy continued to increase in the DOX(-) group but not in the 2 wk+RD group (Figure 11B), these results indicate that the dramatic increase in cataplexy bout frequency in the DOX(-) group results from the decrease in the number of orexin neurons from 5% to 1%.

III-3-6. Food-elicited cataplexy test

The food-elicited cataplexy test was established to quantify cataplexy intensity in canine narcolepsy models (79). It has previously been reported that palatable food significantly increases cataplexy bout frequency in narcoleptic mice (67, 80). To determine whether *orexin-tTA; TetO DTA* mice showed a response similar to that which occurs in other mouse narcolepsy models, *orexin-tTA; TetO DTA* mice were fed 1.8 ± 0.5 g chocolate in addition to DOX(-) chow at the beginning of the dark period at 4 wk and 15 wk of DOX(-). Mice fed with chocolate at 4 wk DOX(-) (4 wk+chocolate) showed a 3.6-fold increase in cataplexy bouts in the dark period compared with 4 wk (Figure 12A).

In the 15 wk+chocolate group, cataplexy bouts increased 1.6-fold in the dark period compared with 15 wk (Figure 12A). However, no significant differences were observed during the light period in either group. The distribution of cataplexy bouts across the day is shown in Figure 12B. Cataplexy bouts gradually increased after mice had chocolate. The effect of chocolate lasted for 12-13 h. These results confirmed that palatable food increased cataplexy in *orexin-tTA; TetO DTA* mice as occurs in other mouse narcolepsy models.

III-3-7. Metabolic measurements in *orexin-tTA; TetO DTA* mice

Since the activity of orexin neurons is modulated by metabolic factors such as glucose, leptin and ghrelin (20), orexin neurons are thought to be involved in energy and fluid homeostasis as well as sleep/wakefulness regulation. In addition, *orexin/ataxin-3* mice become obese despite eating less food than wild type mice (81). Narcoleptic patients also show metabolic abnormalities including a higher body mass index (BMI) than normal subjects (82, 83). Consequently, *orexin-tTA; TetO DTA* mice were subjected to measurement of body weight, food and water consumption and spontaneous activity during ablation of orexin neurons. Monogenic *orexin-tTA* or *TetO DTA* littermate mice were used as controls. The body weight of *orexin-tTA; TetO DTA* mice began to increase shortly after DOX removal and was significantly higher by 2 wk after DOX removal (Figure 13A). Body weight of *orexin-tTA; TetO DTA* mice at 4 wk after DOX removal was 30.1 ± 1.1 g (n=9) vs. 26.2 ± 1.0 g (n=9) for age-matched control mice (p=0.01, unpaired t-test). The incremental increase of body weight became significant by 5 d after DOX removal (Figure 13B) despite the fact that food consumption was unaltered (Figure 13C). On the other hand, water intake significantly decreased in *orexin-tTA; TetO DTA*

mice by 4 d after DOX removal (Figure 13D). These results suggest that the increase in body weight was not caused by overeating or overdrinking.

To further study the mechanism of weight gain in *orexin-tTA; TetO DTA* mice, bloodborne metabolic markers were measured in the same individuals before and after DOX removal (Table 2). Insulin and leptin concentrations increased significantly in *orexin-tTA; TetO DTA* mice at 4 wk after DOX removal compared to age-matched control mice. However, there were no significant changes in the levels of glucose or free fatty acids. Spontaneous activity was also analyzed to reveal the cause of the body weight increase. In control mice, there was no difference in the level of spontaneous activity in either the light period or the dark period after DOX removal (Figure 13E). In contrast, *orexin-tTA; TetO DTA* mice became hypoactive after DOX removal with a decrease in spontaneous activity evident in the light period by 1 wk after DOX removal (Figure 13F). Spontaneous activity in the dark period significantly decreased by 3 wk after DOX removal.

III-4. Discussion

In the present study, a novel mouse model of narcolepsy, *orexin-tTA; TetO DTA* mice, were generated and analyzed the relationship between the number of orexin neurons and symptoms of narcolepsy. The timing of orexin neurons degeneration was controlled using the Tet-off system. By replacing DOX(+) chow with DOX(-) chow, orexin neurons were ablated within a couple of weeks. The specificity of orexin neuron ablation was confirmed since the co-extensive MCH neurons as well as non-orexin-ir/NeuN-ir cells were intact; consequently, DTA expressed in the orexin neurons apparently did not affect neurons in the surrounding hypothalamus. This conclusion is consistent with the fact that DTA does not induce cell death when applied extracellularly in the absence of diphtheria toxin B fragment, which helps DTA to enter the cytoplasm (84).

Although it has been reported that regulation of gene expression of Tet system can be problematic, I conclude that leakage of DTA in the presence of DOX was not observed in this application of the Tet-off system because the number of orexin neurons in the presence of DOX was comparable to that of control mice. To exclude the possibility of DTA expression before DOX removal, high concentrations of DOX were added in the chow. In the absence of DOX, DTA expression was strongly induced in orexin neurons as the number of orexin neurons was reduced to 64.2% only 1.5 d after removal of DOX. Neuronal loss was more rapid in the lateral part of the orexin population than in the medial portion. This difference might be because tTA expression level differed among orexin neurons. Alternatively, sensitivity to DTA might be differ between the medial and lateral orexin neuron populations. The properties of remaining cells might be different from other cells. This is another interest to approach to the further understanding of narcolepsy and the role of orexin neurons not only in the regulation of sleep/wakefulness but others

such as anxiety or addiction. DTA expression was reversibly regulated by DOX since restoration of DOX terminated DTA expression, which enabled control of the number of remaining orexin neurons. These results indicate that the Tet-off system in *orexin-tTA; TetO DTA* mice enabled control of both the timing of cell death as well as the number of orexin neurons. These features will allow investigators to produce models for different types of narcolepsy, such narcolepsy with and without cataplexy.

III-4-1. Relationship between number of orexin neurons and narcolepsy symptoms

Using *orexin-tTA; TetO DTA* mice, it became possible to study the progression of narcoleptic symptoms during ablation of orexin neurons by comparing behavior and physiology before, during and after ablation of orexin neurons within the same individual animal. The first symptom observed was fragmentation of sleep/wakefulness. This symptom was especially prominent in the early dark period at one week after DOX(-) by which time ~86% of orexin neurons had been ablated. Although Mice show multiphasic sleep, humans show monophasic sleep. Thus observed fragmentation of sleep/wakefulness is equivalent to excessive day time sleepiness in human. The first cataplexy bout was observed 2 wk after DOX(-) when ~95% of orexin neurons had been ablated. Although 95% orexin neurons loss was necessary to trigger cataplexy, further orexin neurons loss exacerbated sleep/wakefulness fragmentation and dramatically increased cataplexy bout frequency. These observations indicate that a small difference in the number of remaining orexin neurons produced a large difference in symptomatology. Conversely, these results imply that a small increase in the number of orexin neurons, the efficacy of orexin neuron function, or orexin concentration in the CSF might prevent the most severe symptoms of narcolepsy. Low levels of orexin restoration

might prevent fragmentation of sleep/wakefulness, in particular.

Narcolepsy is divided into two types based on the presence or absence of cataplexy. These distinct symptomatologies might be caused by a small difference in the number of orexin neurons remaining, a difference of the pattern of degeneration of orexin neurons, or differential efficacy of neurotransmission of the remaining orexin cells. In humans, excessive sleepiness (fragmentation of sleep/wakefulness) is usually the first symptom of narcolepsy and cataplexy develops after the onset of sleepiness (85). Thus, *orexin-tTA; TetO DTA* mice reproduce the order of symptom appearance in narcoleptic patients. Recently, it is reported that restoration of orexin receptors in DR improved cataplexy attacks (86). The difference in symptoms of patients might be due to the projection area of degenerated orexin neurons. *Orexin-tTA; TetO DTA* mice showed a greater number of cataplexy bouts compared to *orexin/ataxin-3* mice or to the D(-) group in which orexin neuron cell death was initiated early in the postnatal period. Although the number of orexin neurons remaining in D(-) group was smaller than DOX(-) 13 wk, these mice showed milder sleep/wakefulness fragmentation and fewer cataplexy bouts. These results strongly indicate that functional compensation occurred when orexin neurons were ablated during early postnatal development since orexin neurons develop their processes after birth (87).

In this study, the number of cataplexy bouts reached a plateau after 11 wk DOX(-). In humans, the number of sleep onset REM periods (SOREMPs) and cataplexy frequency are reported to decrease with age (88). The decrease in cataplexy in narcoleptic patients is attributed to avoidance of emotional situations that trigger cataplexy. The saturation of cataplexy bout frequency observed in *orexin-tTA; TetO DTA* mice after 11 wk DOX(-) might reflect functional adaptation of the underlying neural circuitry to loss of orexin

innervation. Conversely, the increase in cataplexy frequency subsequent to orexin neuron degeneration may reflect functional reorganization of the deafferented projection sites of the orexin neurons. However, when provided with a novel and palatable food, the number of cataplexy bouts increased in *orexin-tTA; TetO DTA* mice even 15 wk after DOX removal, indicating the efficacy of emotional stimuli to increase cataplexy above the plateau level. Notably, the EEG spectral features of cataplexy (89) are stable across all weeks of DOX(-) and between dark and light periods, and appear consistent with the EEG power density observed during cataplexy in mice that lack orexin peptides. Furthermore, EEG spectral power during wake, SWS and REM sleep gradually increased as the orexin neurons degenerated. This observation suggests that synchronization of cortical neurons may be enhanced by orexin neuron loss.

I observed cataplexy bouts throughout 24 h period. The frequency of cataplexy bouts in the dark period was greater than in the light period since mice are nocturnal and are primarily active during the dark and spend most of the light period asleep. However, rodents have a multiphasic sleep/wakefulness rhythm and, thus, cataplexy attacks also occurred during waking in the light period. Cataplexy attacks during light period might be equivalent to sleep paralysis in human. Mice tended to have many attacks during early half of dark period and at the end of light period, which seems to be correlated with the arousal rhythm.

III-4-2. Orexin neurons and metabolism.

I observed a significant increase in body weight in *orexin-tTA; TetO DTA* mice subsequent to ablation of orexin neurons without any accompanying signs of overfeeding or overdrinking. Ablation of orexin neurons also induced hypoactivity. These results are

in good agreement with the observation that narcoleptic patients show mild obesity without increasing caloric intake and that the activity level of narcoleptics is lower than that of control subjects (90). Ablation of orexin neurons might affect bloodborne metabolic parameters as well. Insulin and leptin concentrations were higher than control mice, although free fatty acid and glucose concentrations were unaffected, suggesting that the physiological role of orexin neurons in energy homeostasis is not simple. The increased serum leptin concentration could be a result of the weight gain. The altered metabolism may be due, at least in part, to disruption of the circadian timekeeping system. The decrease in water intake is in agreement with previous reports that orexin is involved in fluid, as well as energy, homeostasis (33, 91).

III-4-3. Utility of *orexin-tTA; TetO DTA* mice

In the present study, it became possible to control the number of orexin neurons and found that it was possible to create mice that varied in symptom severity from presymptomatic to severe narcolepsy simply by changing the duration of the DOX(-) period. Several drugs are in clinical use to treat various symptoms of narcolepsy (92-94). Since symptomatology varies among narcoleptic patients, *orexin-tTA; TetO DTA* mice could be a useful tool for discovery of new drugs that target symptoms associated with this disorder (95). It is commonly believed that symptom progression in human narcoleptics stops at some point and become stable. However, longitudinal studies of symptom dynamics in individual patients has not been possible to date, in part, because most narcoleptics are medicated to prevent symptoms. Using *orexin-tTA; TetO DTA* mice, it is possible to determine the effect of aging on narcoleptic symptoms, which may reveal novel aspects of orexin deficiency with aging. These mice will also be valuable to study

the process of network reorganization in terminal fields such as the LC and DR as orexin input is lost. The number of histaminergic neurons has recently been reported to significantly increase in human narcoleptic patients (96, 97). Orexin neurons release glutamate (36, 98), dynorphin (99) and neurotensin (100) as well as orexin. In *prepro-orexin* or orexin receptor gene knockout mice, these other neurotransmitters are still released.

Although the present study primarily focused on narcolepsy, orexin neurons are involved in many physiological functions, such as addiction, reward, and the stress response. *Orexin-tTA; TetO DTA* mice will likely be valuable to study the regulatory mechanisms underlying these physiological functions in the future.

III-5. Figures and Tables

Figure 1

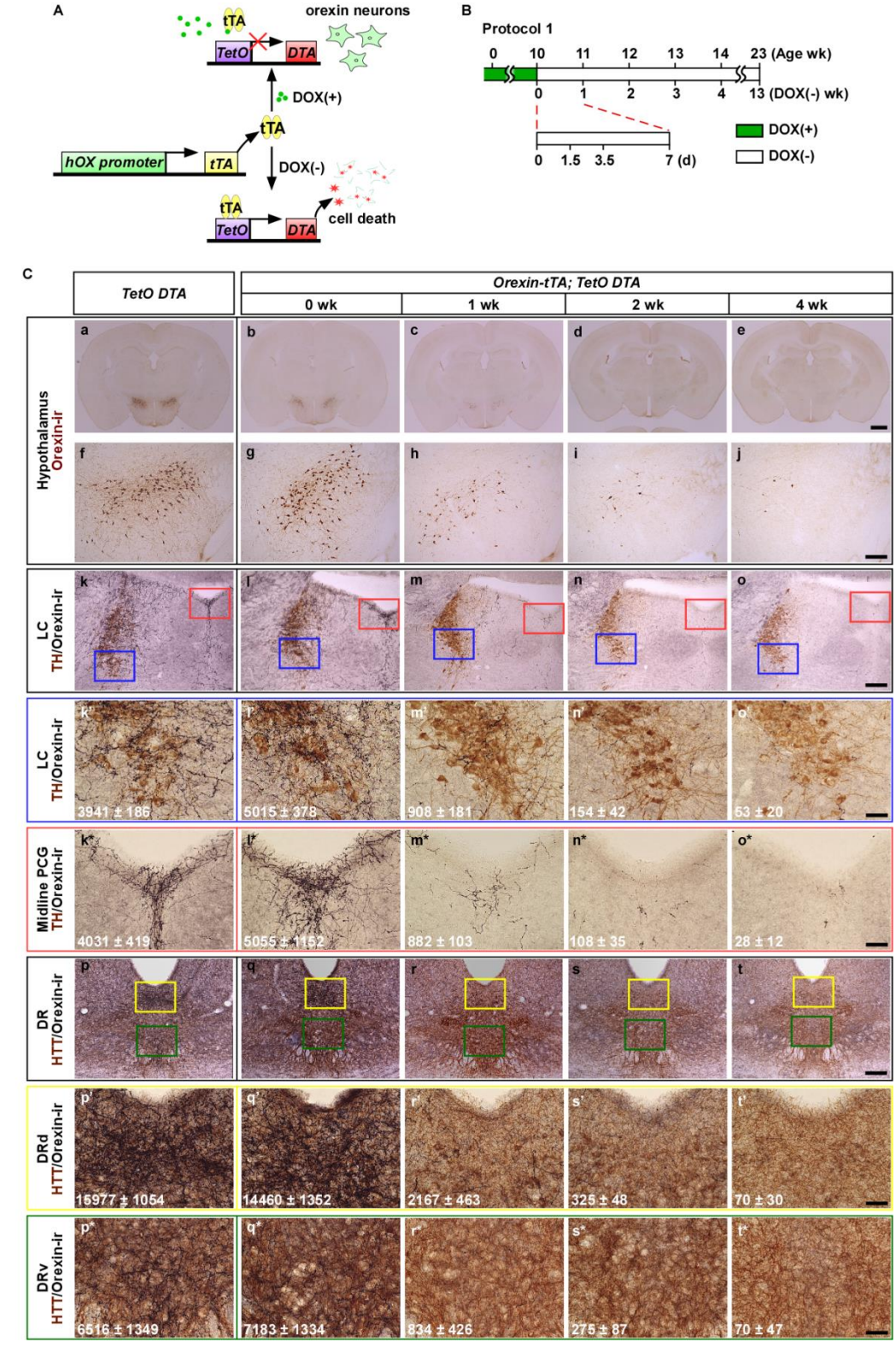

Figure 1. Induction of orexin neuron-specific cell death using the tet-off system. (A) In the presence of DOX, DTA expression is suppressed in *orexin-tTA; TetO DTA* mice and orexin neurons are normal. In the absence of DOX, DTA is expressed and orexin cell death results. (B) Schematic illustrating Experimental Protocol 1. Green bar indicates that mice were fed chow containing DOX until 10 weeks of age (DOX(+) condition); open bar indicates when mice were fed chow without DOX (DOX(-) condition), which induces DTA expression. (C) Immunostaining of orexin neurons and projections to terminal fields. Orexin neurons stained in brown (a-j) and terminals in black (k-t). The upper panels show orexin-ir neurons in the hypothalamus (a-j) under different conditions. The lower panels show orexin projection fields in the LC (k-o, k'-o' and k*-o*) and DR (p-t, p'-t' and p*-t*) in the corresponding conditions. Noradrenergic neurons in the LC were stained with anti-tyrosine hydroxylase (TH) in brown (k-o, k'-o' and k*-o*). Higher magnification of LC (blue rectangle in k-o) is shown in k'-o'. Red rectangle in k-o show the midline pontine central gray (PCG); a higher magnification of this area is shown in k*-o*. Serotonergic neurons in the DR were stained with anti-5-hydroxytryptamine transporter (HTT) in brown (p-t, p'-t' and p*-t*). Yellow and green rectangles show the dorsal part of the DR (DRd) and the ventral DR (DRv), respectively. Higher magnification of these areas are shown in p'-t' and p*-t*, respectively. Numbers in k'-t' and k*-t* indicates the area of orexin-ir fibers in the region (counting box width 363 μm x height 273 μm) measured by image analysis software. Area (μm^2) is mean ± SEM (n=3-5). 0 wk, 1 wk, 2 wk and 4 wk indicate the number of weeks that *orexin-tTA; TetO DTA* mice were in the DOX(-) condition before perfusion, as indicated in B. Littermate monogenic *TetO DTA* mice were used as controls. Scale bars in C: a-e, 1 mm; f-t, 200 μm; k'-t' and k*-t*, 50 μm.

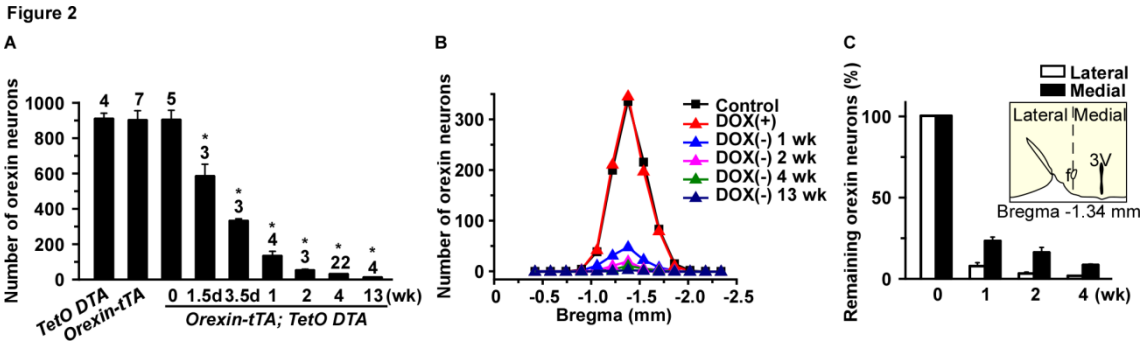

Figure 2. Transition of the number of orexin-ir cell bodies. (A) Bar graph showing the number of orexin-ir cell bodies in the hypothalamus at various time points after removal of DOX from the diet. Number on the top of bar indicates number of mice in each experiment. (B) Number of orexin-ir cell bodies in coronal sections at multiple anterior-posterior levels relative to bregma. (C) Number of orexin-ir neurons in the lateral part and the medial part of the lateral hypothalamus after DOX removal. Inset shows that the fornix was used to delineate the lateral and medial orexin populations. *p<0.05 vs. *TetO DTA*. Values are mean ± SEM.

Figure 3

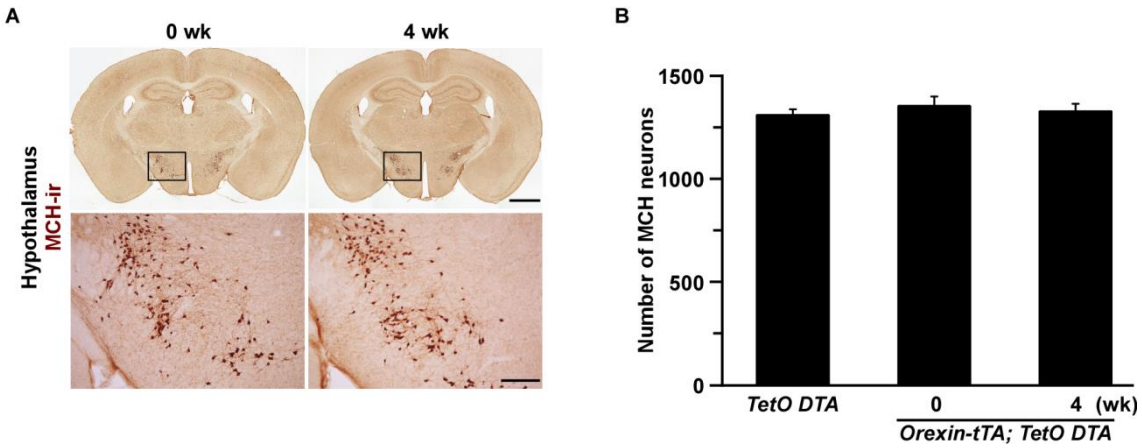

Figure 3. MCH neurons were intact after ablation of orexin neurons in *orexin-tTA; TetO DTA* mice. **(A)** MCH neurons (brown) were stained with anti-MCH antibody. Bottom panels are higher magnification of the region indicated by the square in the top panel. Scale bars: top, 1 mm; bottom, 200 μm. **(B)** Number of MCH-ir cell bodies in the hypothalamus of *orexin-tTA; TetO DTA* mice after 4 wk DOX(-) vs. 0 wk DOX(-) or controls. Values are mean ± SEM (n=3-4).

Figure 4

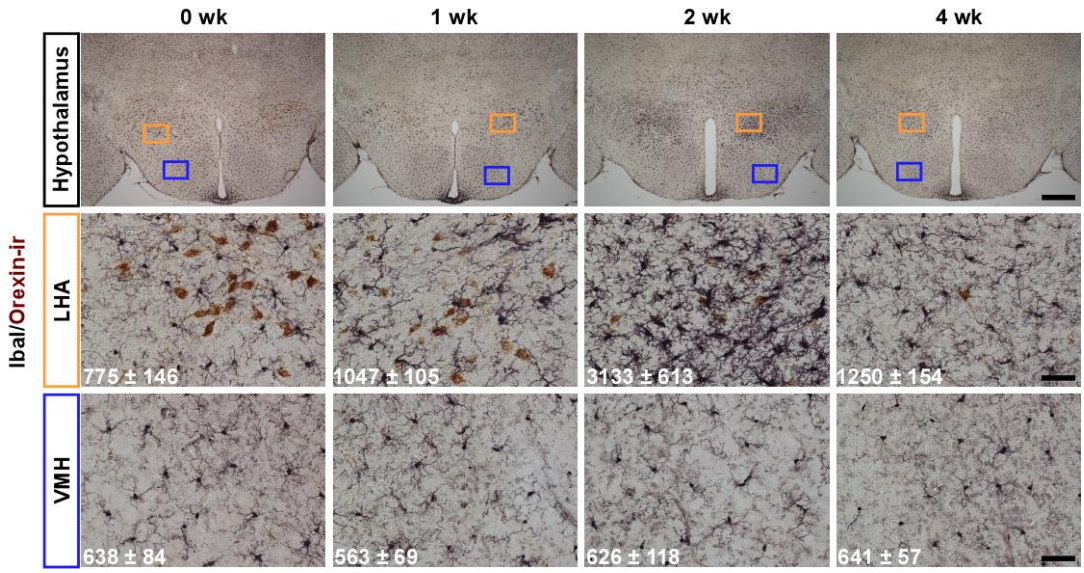

Figure 4. Immunohistochemistry indicating activation of microglia cells in hypothalamus after DOX removal from diet (0, 1, 2 and 4 wk after DOX(-)). Orexin neurons (brown) were stained with anti-orexin antibody. Microglia cells (black) were stained with anti-IbaI antibody. Orange and blue rectangles in the top panels are shown in middle (orange, LHA, lateral hypothalamic area) and lower panels (blue, VMH, ventromedial hypothalamus). The numbers in each panel indicates the area of IbaI-ir cell in the region measured by image analysis software. Area (μm^2) is mean ± SEM (n=3). Scale bars: top row = 500 μm, middle row = 50 μm, and bottom row = 50 μm.

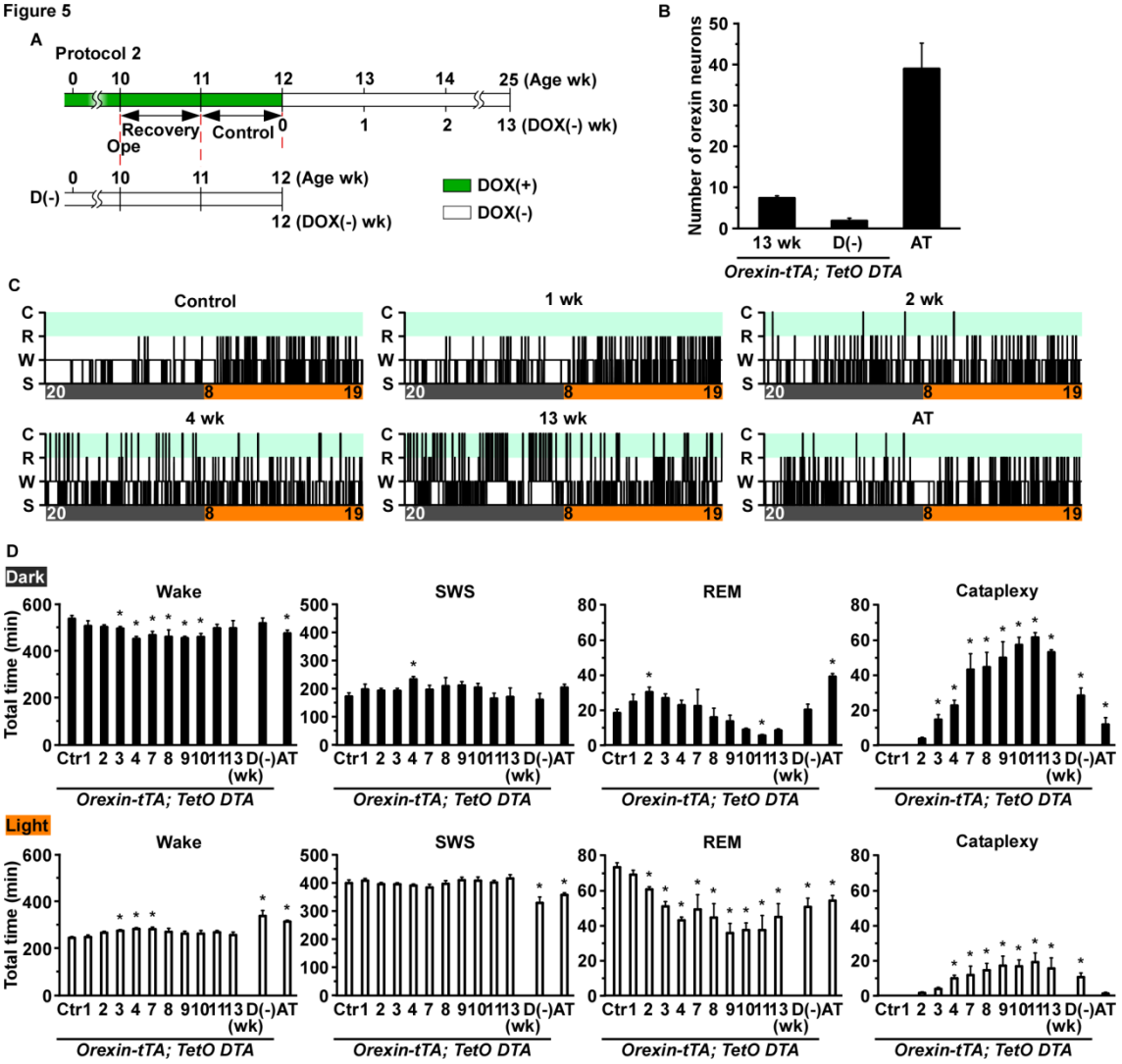

Figure 5. Analysis of sleep and wakefulness in *orexin-tTA; TetO DTA* mice. **(A)** Schematic illustrating Experimental Protocol 2. EEG and EMG electrodes were implanted at 10 wk of age. Control recordings for *orexin-tTA; TetO DTA* mice occurred between 11 and 12 wk of age. At 12 wk of age, DOX was removed from the chow for the subsequent 13 wk. In contrast, *orexin-tTA; TetO DTA* D(-) mice were raised from birth without DOX in the chow. In this strain (referred to as D(-) mice), EEG and EMG were recorded between 11-12 wk as a comparison. Green bar, DOX(+) condition; open bar DOX(-) condition. **(B)** Number of orexin-ir cell bodies counted at the end of experiments. **(C)** Example hypnograms from *orexin-tTA; TetO DTA* mice (control and 1, 2, 4 and 13 wk in DOX(-) condition) and *orexin/ataxin-3* (AT) mice. Clock time and light-dark period is indicated bottom of hypnogram (light on 8:00-20:00; light off 20:00-8:00). **(D)** Time spent in wakefulness, SWS, REM sleep, and cataplexy in the dark (top) and light

(bottom) periods. In *orexin-tTA; TetO DTA* mice, 24 h recordings occurred at 1, 2, 3, 4, 7, 8, 9, 10, 11 and 13 weeks after DOX removal from the diet. *p<0.05 vs. control. Values are mean ± SEM (n=5-10). D(-), *orexin-tTA; TetO DTA* mice raised from birth in DOX(-) condition; Ctr, Control; AT, *orexin/ataxin-3* mice; Wake or W, wakefulness; SWS or S, slow wave sleep; REM or R, REM sleep; C, cataplexy.

Figure 6

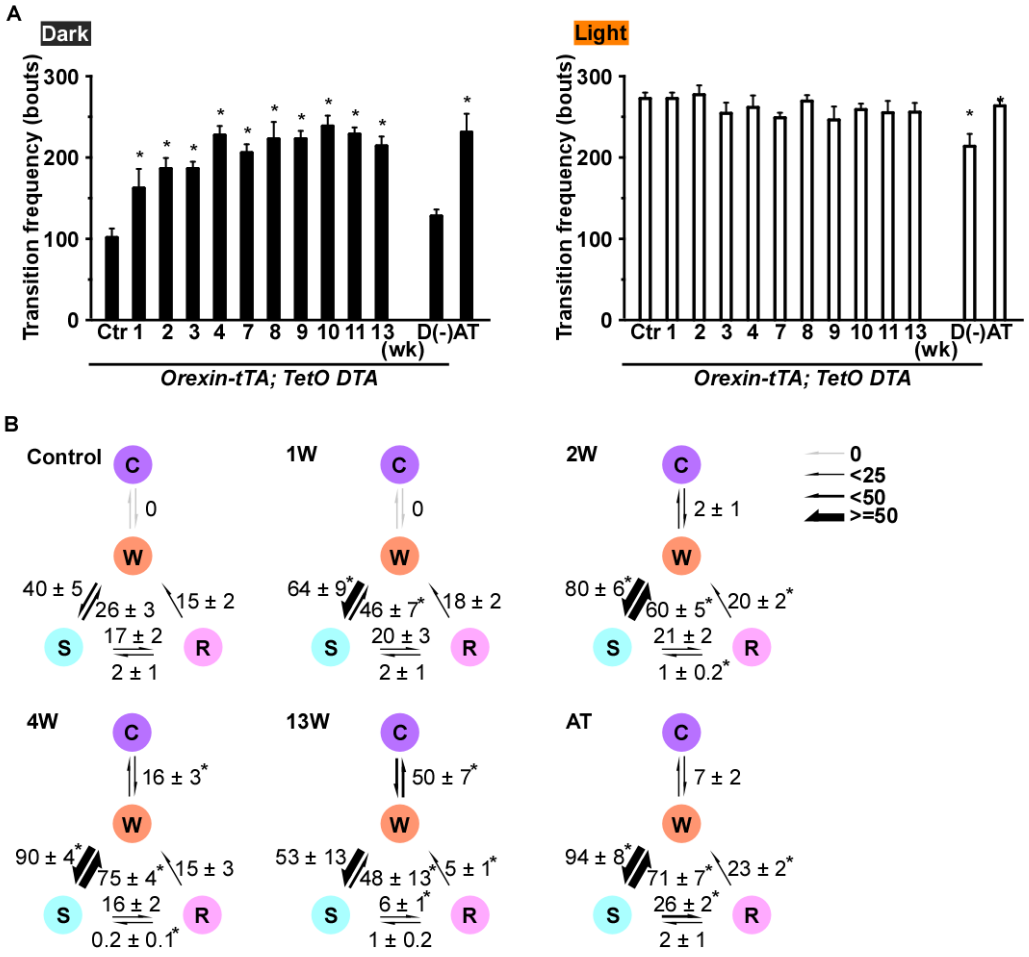

Figure 6. The frequency of stage transitions. **(A)** The frequency of transitions between all states across the 24 h in the control condition and 1, 2, 3, 4, 7, 8, 9, 10, 11 and 13 wk after DOX removal in *orexin-tTA; TetO DTA* mice, in D(-) mice, and in AT mice during the dark (left) and light (right) periods. **(B)** The frequency of transitions between each stage during the dark period in the control condition and 1, 2, 4 and 13 wk after DOX removal in *orexin-tTA; TetO DTA* mice, and in AT mice. The numbers indicate the frequency of transitions between each stage. *p<0.05 vs. control. Values are mean ± SEM (n=5-10). D(-), *orexin-tTA; TetO DTA* mice raised from birth in DOX(-) condition; Ctr, Control; AT, *orexin/ataxin-3* mice; W, wakefulness; S, slow wave sleep; R, REM sleep; C, cataplexy.

Figure 7

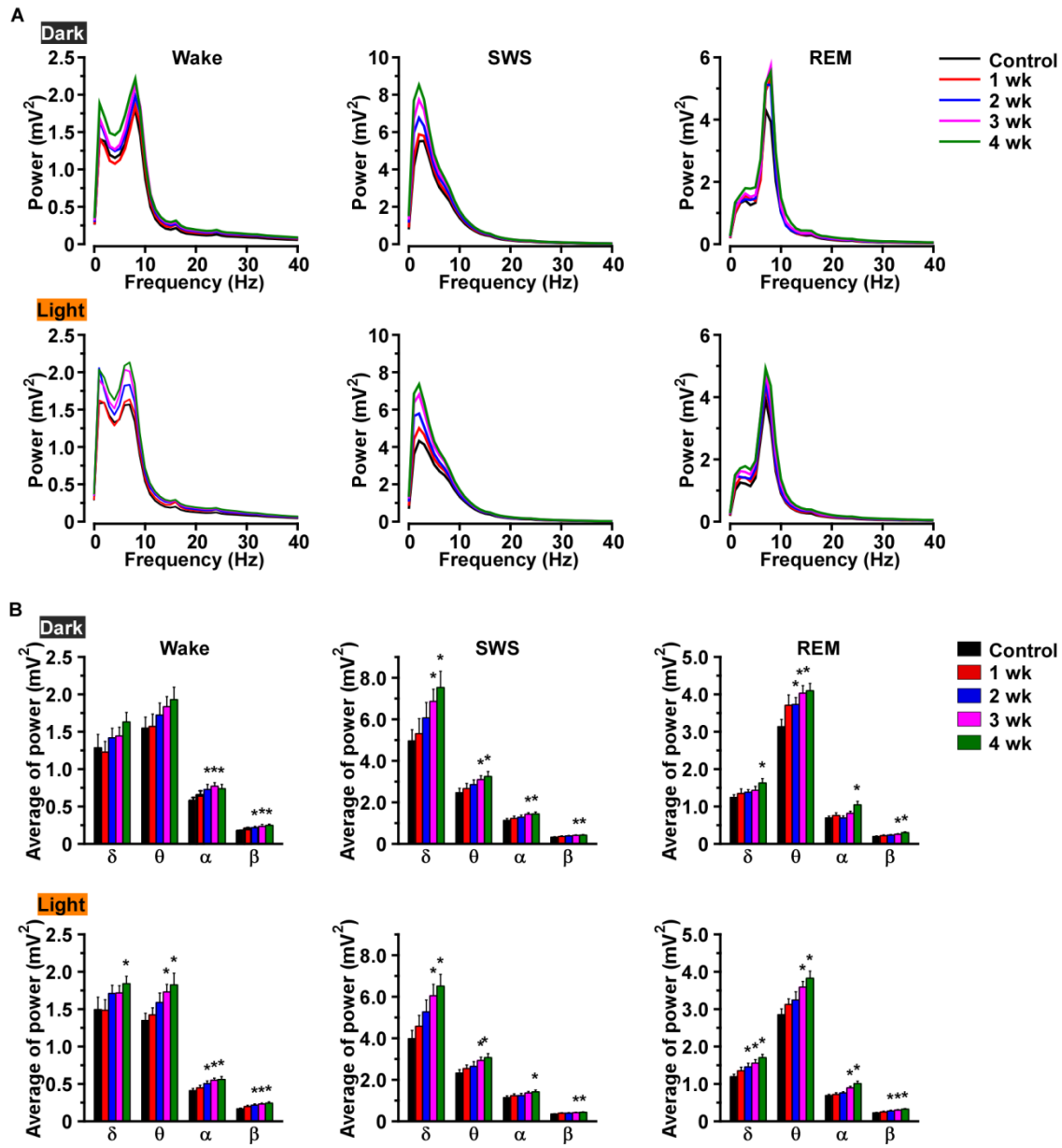

Figure 7. EEG power spectra during wakefulness, SWS and REM sleep in *orexin-tTA; TetO DTA* mice during the first 4 weeks after DOX removal. **(A)** Average EEG power spectra during wakefulness (left), SWS (middle) and REM sleep (right) in the dark (top) and light (bottom) periods (n=8). **(B)** Average power in the delta, theta, alpha and beta bands in each stage of sleep and wakefulness (n=8). *p<0.05 vs. control. Values are mean ± SEM. Control, EEG recordings conducted before DOX(-). EEG recordings were conducted for 4 wk after removal of DOX.

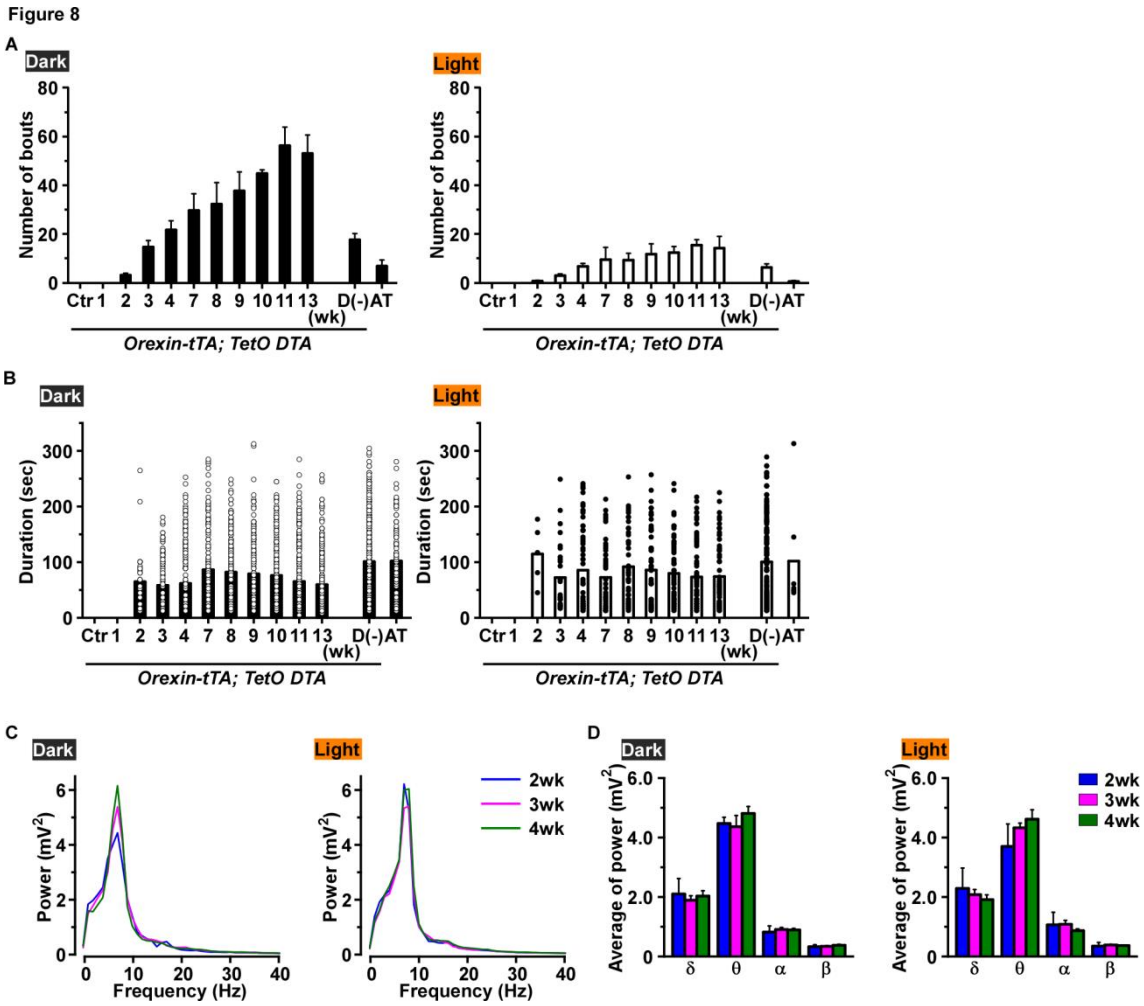

Figure 8. (A) Cataplexy bout frequency in the dark (left) and light (right) periods as orexin neurodegeneration progresses in *orexin-tTA; TetO DTA* mice (n=5-10). D(-) and AT mice plotted as a comparison. **(B)** Durations of individual cataplexy bouts plotted as circles in the dark (left) and light (right) periods (n=5-10). **(C)** EEG power spectra during cataplexy in *orexin-tTA; TetO DTA* mice during the dark (left) and light (right) periods (n=8). **(D)** The average power of the delta (δ), theta (θ), alpha (α) and beta (β) bands during cataplexy in the dark (left) and light (right) periods (n=8). Values are mean ± SEM.

Figure 9

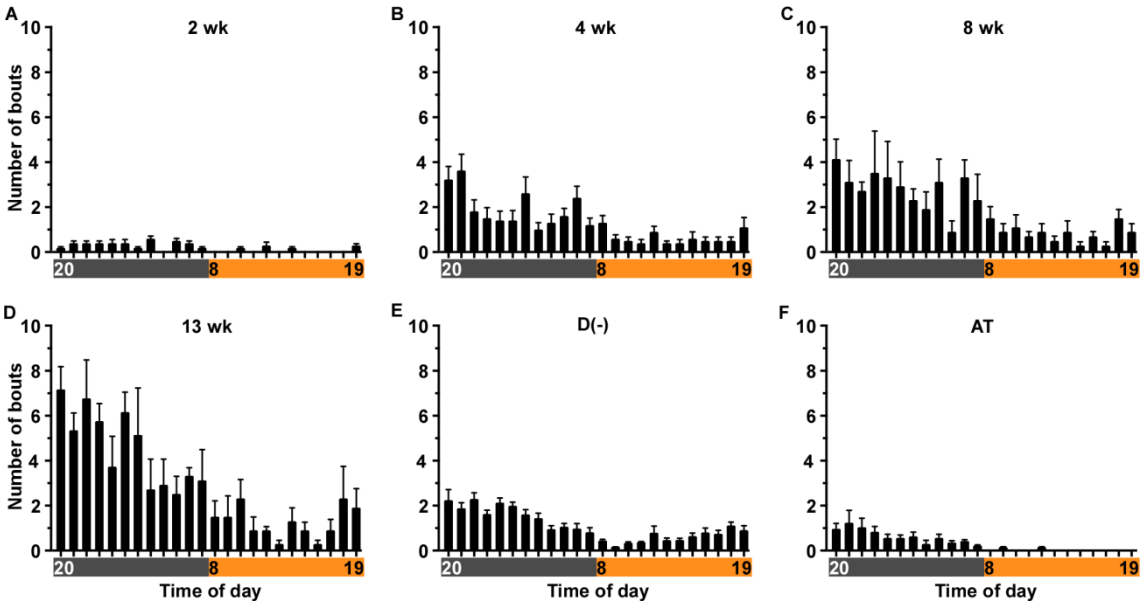

Figure 9. Hourly distribution of cataplexy bouts across the 24 h period in *orexin-tTA; TetO DTA* mice at 4 time points after DOX removal, **(A)**; 2 wk, **(B)**; 4wk, **(C)**; 8 wk, **(D)**; 13 wk. **(E)**; D(-) and **(F)**; AT mice plotted as a comparison. Horizontal axis indicates clock time. Gray and orange bars indicate dark and light periods, respectively. Values are mean ± SEM (n=5-10).

Figure 10

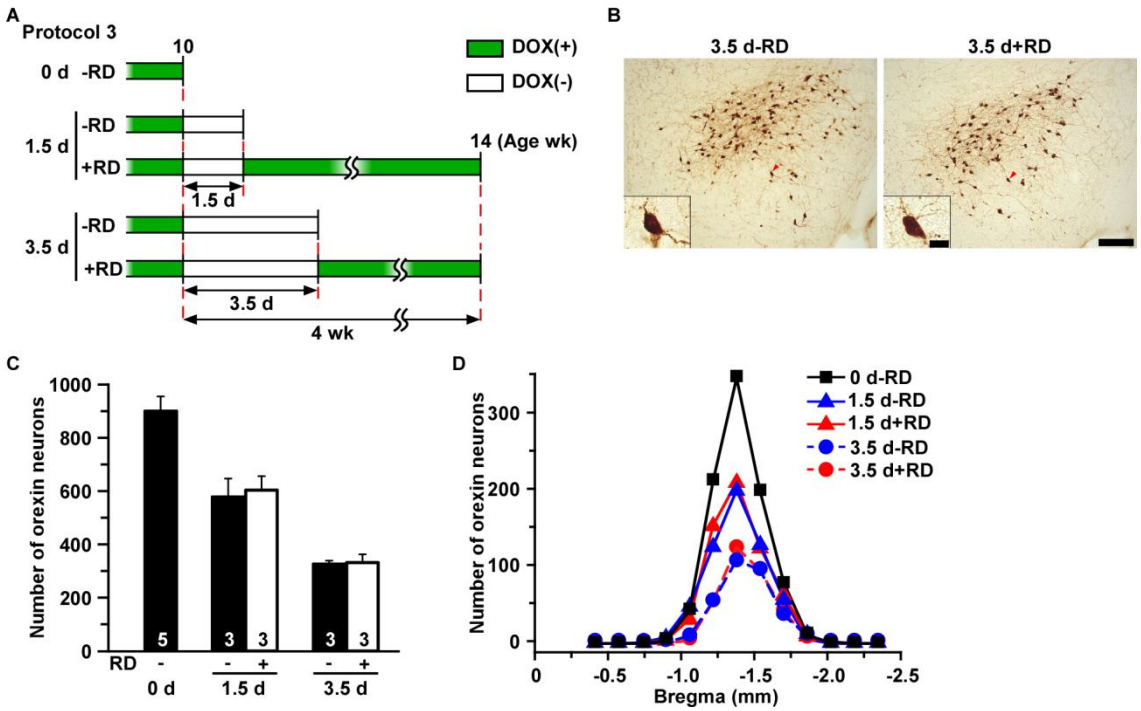

Figure 10. Partial lesion of orexin neurons induced by manipulation of DOX chow availability. **(A)** Schematic illustrating DOX chow availability in different experimental groups in Experimental Protocol 3. Green bar, DOX(+); open bar DOX(-). RD, restoration of DOX. **(B)** Immunostaining of orexin neurons. Inset is higher magnification of single neurons indicated by the red arrowhead. **(C)** Bar graph showing the number of orexin-ir cell bodies in the hypothalamus in different conditions indicated in A (n=3-7). **(D)** Distribution of orexin-ir cell bodies in coronal sections at multiple anterior-posterior levels relative to bregma (n=3-7). Scale bars in B; 200 μm and 20 μm (inset).

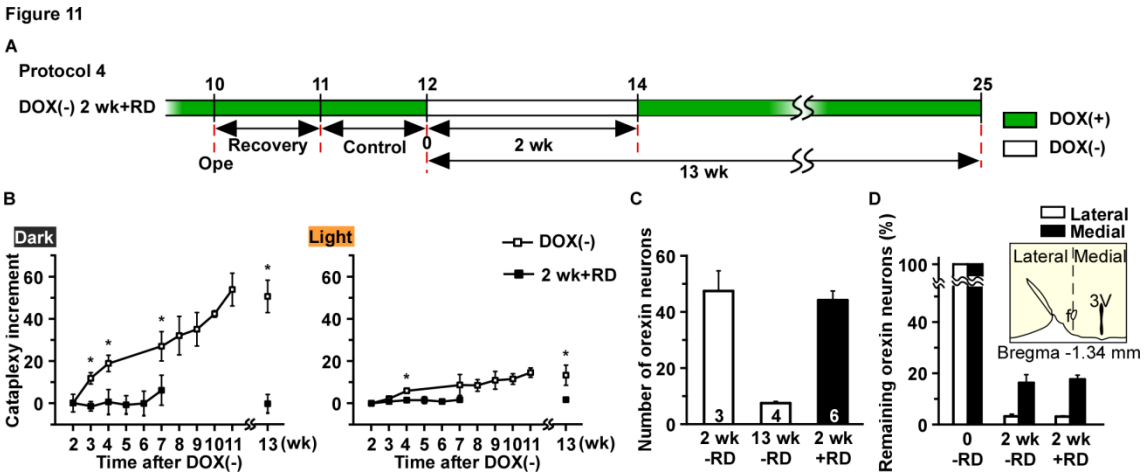

Figure 11. (A) Schematic illustrating design of DOX(-) 2 wk+RD trial in Experimental Protocol 4. DOX was removed from diet at 12 wk of age for 2 wk followed by DOX replacement for 10 wk. Green bar, DOX(+); open bar DOX(-) conditions. **(B)** Increment in the number of cataplexy bouts during the dark (left) and light (right) periods (n=6) relative to the number of bouts at 2 wk of DOX(-). Horizontal axis indicates time after DOX(-). **(C)** The number of orexin-ir cell bodies at the end of the DOX(-) 2 wk+RD trial, with DOX(-) for 2 wk and 13 wk plotted as a comparison. **(D)** Number of orexin-ir cells distributed in the lateral and the medial portions of the hypothalamus using the fornix to delineate the border. *p<0.05 vs. 2 wk+RD. Values are mean ± SEM.

Figure 12

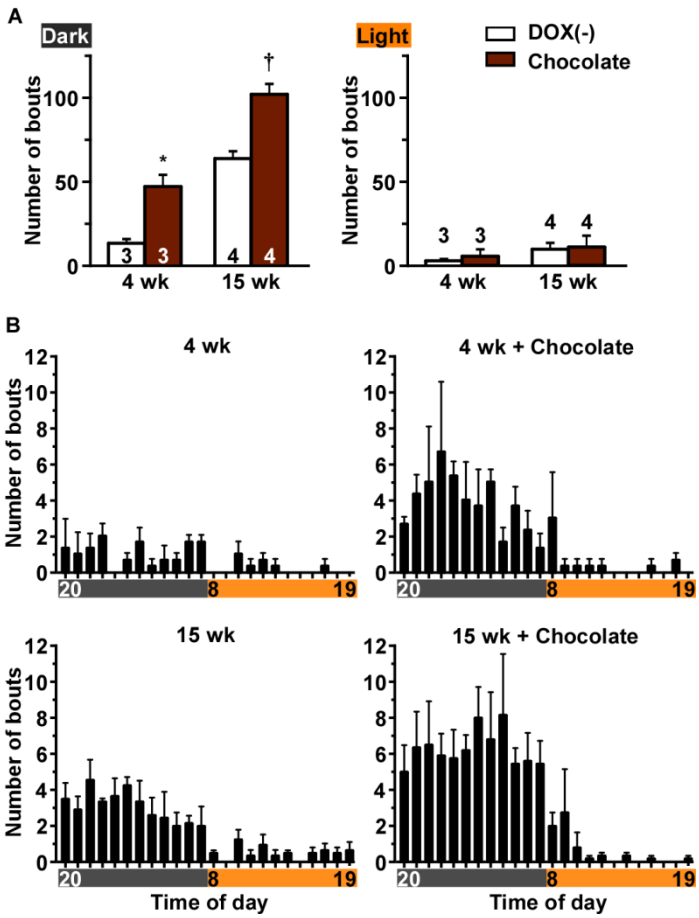

Figure 12. Palatable food induces cataplexy in *orexin-tTA; TetO DTA* mice. In Experimental Protocol 5, chocolate (1.8 g) was made available at beginning of the dark period. *Orexin-tTA; TetO DTA* mice DOX (-) for 4 wk and 15 wk were subjects for this experiment. **(A)** Number of cataplexy bouts induced by chocolate in the dark (left) and the light (right) periods. **(B)** Hourly distribution of cataplexy bouts across the 24 h period in *orexin-tTA; TetO DTA* mice in the presence or absence of chocolate. *p<0.05 vs. DOX(-) 4 wk. †p<0.05 vs.DOX(-) 15 wk. Values are mean ± SEM.

Figure 13

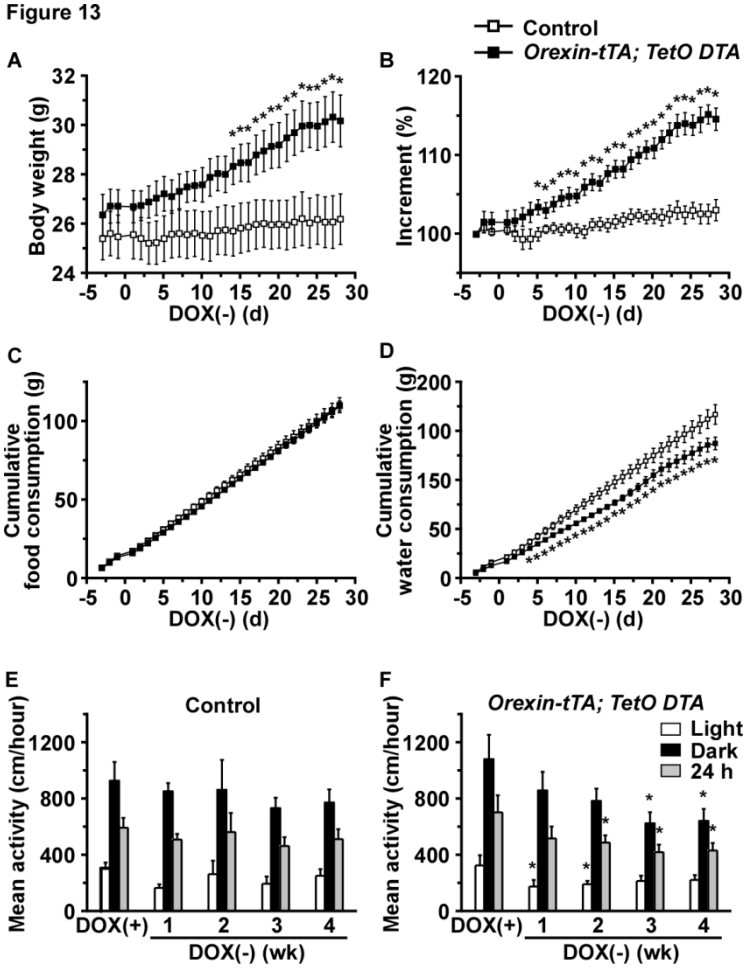

Figure 13. Abnormalities of energy and fluid homeostasis and spontaneous activity in *orexin-tTA; TetO DTA* mice. **(A)** Body weight of *orexin-tTA; TetO DTA* mice for 4 wk after DOX removal from the diet; both *orexin-tTA* and *TetO DTA* littermates were used as controls. **p*<0.05 vs. control (n=9). **(B)** Increment of body weight in *orexin-tTA; TetO DTA* vs. control mice. Body weight on Day -3 is set as 100% (n=9). **p*<0.05 vs. control. **(C)** Cumulative food consumption in *orexin-tTA; TetO DTA* vs. control mice for 4 wk after DOX removal (n=9). **(D)** Cumulative water consumption in *orexin-tTA; TetO DTA* and control mice for 4 wk after DOX removal (n=9). **(E)** Mean activity of control mice during light and dark periods and the 24 h average for 4 weeks after DOX removal (n=9). **(F)** Mean activity of *orexin-tTA; TetO DTA* mice during light and dark periods and the 24 h average for 4 weeks after DOX removal (n=9). **p*<0.05 vs. DOX(+). Values are mean ± SEM.

3. Overall Discussion

I examined orexin neurons which modulate the function of sleep/wakefulness regulating circuits to reveal its detail function on sleep/wakefulness regulation. First, I focused on local networks of orexin neurons and revealed that orexin neurons form a positive feedback circuit among orexin neurons (101). Second, the negative feedback circuit between orexin neurons and one of wake promoting neurons, serotonergic neurons, were studied. Using the gene expression system, a Tet-off system, the 5HT1A receptor expression level in orexin neurons was reversibly controlled. Sleep/wakefulness pattern analyses revealed that the negative feedback circuit between orexin neurons and serotonergic neurosn mainly function during the early dark period which is the first half of active period(69). Using the same gene expression system, the timing of orexin neuron ablation was controlled to study the relationship between the number of orexin neurons and narcolepsy symptoms. This revealed that more than 86% of orexin neuron ablation is required to express the symptoms of narcolepsy (102).

The activity of orexin neurons shows a circadian rhythm. The firing rate of orexin neurons depends on behavioral state in rat (37, 57). Orexin neurons fire in high frequenxy during exploratory behaviors. Grooming and eating is the secondary active behavior. During quiet wake its firing rate become one-eighth of that during exploratory behaviors. From these observations the wake state might be divided into several stages not only an active wake and a quiet wake. Orexin neurons are activated by cholinergic neurons in basal forebrain (103) and activate wake promorting neurons in brainstem and TMN (104). Orexin neurons autoactivate via OX2R by orexins and were indirectly activated by nearby glutamatergic neurons via OX2R. This positive feedback circuit raises the activity level of orexin neurons and might play an important role for

maintenance of wakefulness. Although orexin neurons activate wake promoting neurons, orexin neurons receive inhibitory inputs from wake promoting neurons such as serotonergic neurons except TMN. This negative feedback circuit seems to have discrepancy. The combination of this positive feedback circuit and negative feedback circuit might explain the part of mechanism for stabilization of wakefulness. Hyper activation of orexin neurons may cause cell death. Furthermore, it could affect mental status since orexins involved in anxiety, panic attack (105), addiction and reward seeking (106). Thus it is necessary to regulate the activation level of orexin neurons in a moderate range by inhibitory inputs from wake promoting neurons. Getting another perspective on these circuits, to keep wake promoting neurons acitivity orexin neruons might own the positive feedback circuit. In either case, these feedback circuits are required for wakefulness. The variability of activation level of orexin neurons may contribute to the induction of various levels of wakefulness such as an active wake or a quiet wake.

More than 86% of deficiency of orexin neurons cause narcolepsy, namely only 15% of oexin neurons are necessary and sufficient to keep the normal sleep/wakefulness pattern. This observation suggests that our brain system may be prepared for unforeseeable circumstances such as neurodegenerations triggered by autoimmunity. Wakefulness as with sleep is essential for creatures. Thus, to keep the orexin system in the functionable level is imperative.

Scientists have tried to restore orexins in the appropriate brain region to rescue the narcoleptic animals (107). However, it is still unknown how the orexin neruons recognized as antigen. If the antigen is orexin peptide itself, the restoration of orexins into the brain has no meaning. Meanwhile, to investigate the best symptomatic therapy is also required. The new narcolepsy model mice, *orexin-tTA; TetO DTA* mice, will contribute

greatly to drug development in near future.

4. Acknowledgements

I would like to great thank Professor A. Yamanaka for leading me to study sciences and also for his advices and mentorship. I also would like to great thank Professor M Tominaga for grateful advices and contiuous encouragement as my supervisor. I would like to thank Professor TS Kilduff (SRI International) for his kind advices. I could join sleep science field and enjoy science thanks to Dr. T Tsunemasu who were always by my side. I would like to thank Professor KF Tanaka (Keio University), Associate Professor Y Fukazawa (Nagoya University), Dr. SW Black (SRI International), C. Saito and K. Nishimura for technical supports and continuous encouragement, and all mice which used for experiment for cost of precious life.

I also would like to thank all my laboratory members in NIPS and RIEM for their advice and encouragement.

This study was supported by the Japan Society for Promotion of Science postdoctoral fellowship.

I would like to great thank my friends who encouraged me a lot. And also Girl Scouting and *Chado* always let me regain my smile.

Finally, I give a special thanks to my parents, my sister, my grandfather, my grandmather’s heartwarming smile and significant other.

5. Reference

1. Li Y, Gao XB, Sakurai T, & van den Pol AN (2002) Hypocretin/Orexin excites hypocretin neurons via a local glutamate neuron-A potential mechanism for orchestrating the hypothalamic arousal system. *Neuron* 36(6):1169-1181.
2. Saper CB, Fuller PM, Pedersen NP, Lu J, & Scammell TE (2010) Sleep state switching. *Neuron* 68(6):1023-1042.
3. Sakurai T*, et al.* (1998) Orexins and orexin receptors: a family of hypothalamic neuropeptides and G protein-coupled receptors that regulate feeding behavior. *Cell* 92(4):573-585.
4. de Lecea L*, et al.* (1998) The hypocretins: hypothalamus-specific peptides with neuroexcitatory activity. *Proc Natl Acad Sci U S A* 95(1):322-327.
5. Chemelli RM*, et al.* (1999) Narcolepsy in orexin knockout mice: molecular genetics of sleep regulation. *Cell* 98(4):437-451.
6. Hara J*, et al.* (2001) Genetic ablation of orexin neurons in mice results in narcolepsy, hypophagia, and obesity. *Neuron* 30(2):345-354.
7. Lin L*, et al.* (1999) The sleep disorder canine narcolepsy is caused by a mutation in the hypocretin (orexin) receptor 2 gene. *Cell* 98(3):365-376.
8. Willie JT*, et al.* (2003) Distinct narcolepsy syndromes in Orexin receptor-2 and Orexin null mice: molecular genetic dissection of Non-REM and REM sleep regulatory processes. *Neuron* 38(5):715-730.
9. Marcus JN*, et al.* (2001) Differential expression of orexin receptors 1 and 2 in the rat brain. *J Comp Neurol* 435(1):6-25.
10. Lin JS, Sakai K, & Jouvet M (1988) Evidence for histaminergic arousal mechanisms in the hypothalamus of cat. *Neuropharmacology* 27(2):111-122.
11. Monti JM (1993) Involvement of histamine in the control of the waking state. *Life Sci* 53(17):1331-1338.
12. Steininger TL, Alam MN, Gong H, Szymusiak R, & McGinty D (1999) Sleep-waking discharge of neurons in the posterior lateral hypothalamus of the albino rat. *Brain Res* 840(1-2):138-147.
13. Eriksson KS, Sergeeva O, Brown RE, & Haas HL (2001) Orexin/hypocretin excites the histaminergic neurons of the tuberomammillary nucleus. *J Neurosci* 21(23):9273-9279.
14. Yamanaka A*, et al.* (2002) Orexins activate histaminergic neurons via the orexin 2 receptor. *Biochem Biophys Res Commun* 290(4):1237-1245.
15. Bayer L*, et al.* (2001) Orexins (hypocretins) directly excite tuberomammillary neurons. *Eur J Neurosci* 14(9):1571-1575.

16. Huang ZL, *et al.* (2001) Arousal effect of orexin A depends on activation of the histaminergic system. *Proc Natl Acad Sci U S A* 98(17):9965-9970.
17. Hondo M, *et al.* (2009) Histamine-1 receptor is not required as a downstream effector of orexin-2 receptor in maintenance of basal sleep/wake states. *Acta Physiol (Oxf)*.
18. Anaclet C, *et al.* (2009) Orexin/hypocretin and histamine: distinct roles in the control of wakefulness demonstrated using knock-out mouse models. *J Neurosci* 29(46):14423-14438.
19. Sakurai T, *et al.* (1999) Structure and function of human prepro-orexin gene. *J Biol Chem* 274(25):17771-17776.
20. Yamanaka A, *et al.* (2003) Hypothalamic orexin neurons regulate arousal according to energy balance in mice. *Neuron* 38(5):701-713.
21. Yamanaka A, Muraki Y, Tsujino N, Goto K, & Sakurai T (2003) Regulation of orexin neurons by the monoaminergic and cholinergic systems. *Biochem Biophys Res Commun* 303(1):120-129.
22. Tsunematsu T, *et al.* (2011) Acute optogenetic silencing of orexin/hypocretin neurons induces slow-wave sleep in mice. *J Neurosci* 31(29):10529-10539.
23. Nambu T, *et al.* (1999) Distribution of orexin neurons in the adult rat brain. *Brain Res* 827(1-2):243-260.
24. Fiala JC (2005) Reconstruct: a free editor for serial section microscopy. *Journal of microscopy* 218(Pt 1):52-61.
25. Asahi S, *et al.* (2003) Development of an orexin-2 receptor selective agonist, [Ala(11), D-Leu(15)]orexin-B. *Bioorganic & medicinal chemistry letters* 13(1):111-113.
26. Muraki Y, *et al.* (2004) Serotonergic regulation of the orexin/hypocretin neurons through the 5-HT1A receptor. *J Neurosci* 24(32):7159-7166.
27. Spassova MA, *et al.* (2004) Calcium entry mediated by SOCs and TRP channels: variations and enigma. *Biochimica et biophysica acta* 1742(1-3):9-20.
28. Takai Y, Sugawara R, Ohinata H, & Takai A (2004) Two types of non-selective cation channel opened by muscarinic stimulation with carbachol in bovine ciliary muscle cells. *The Journal of physiology* 559(Pt 3):899-922.
29. Lintschinger B, *et al.* (2000) Coassembly of Trp1 and Trp3 proteins generates diacylglycerol- and Ca2+-sensitive cation channels. *J Biol Chem* 275(36):27799-27805.
30. Gerashchenko D, Salin-Pascual R, & Shiromani PJ (2001) Effects of hypocretin-saporin injections into the medial septum on sleep and hippocampal theta. *Brain Res* 913(1):106-115.
31. Zhu Y, *et al.* (2003) Orexin receptor type-1 couples exclusively to pertussis toxin-insensitive G-proteins, while orexin receptor type-2 couples to both pertussis toxin-

sensitive and -insensitive G-proteins. *J Pharmacol Sci* 92(3):259-266.

32. Tsujino N*, et al.* (2005) Cholecystokinin activates orexin/hypocretin neurons through the cholecystokinin A receptor. *J Neurosci* 25(32):7459-7469.
33. Tsunematsu T*, et al.* (2008) Vasopressin increases locomotion through a V1a receptor in orexin/hypocretin neurons: implications for water homeostasis. *J Neurosci* 28(1):228-238.
34. Burdakov D, Liss B, & Ashcroft FM (2003) Orexin excites GABAergic neurons of the arcuate nucleus by activating the sodium--calcium exchanger. *J Neurosci* 23(12):4951-4957.
35. Williams RH*, et al.* (2014) Optogenetic-mediated release of histamine reveals distal and autoregulatory mechanisms for controlling arousal. *J Neurosci* 34(17):6023-6029.
36. Torrealba F, Yanagisawa M, & Saper CB (2003) Colocalization of orexin a and glutamate immunoreactivity in axon terminals in the tuberomammillary nucleus in rats. *Neuroscience* 119(4):1033-1044.
37. Mileykovskiy BY, Kiyashchenko LI, & Siegel JM (2005) Behavioral correlates of activity in identified hypocretin/orexin neurons. *Neuron* 46(5):787-798.
38. Eriksson KS, Sergeeva OA, Selbach O, & Haas HL (2004) Orexin (hypocretin)/dynorphin neurons control GABAergic inputs to tuberomammillary neurons. *Eur J Neurosci* 19(5):1278-1284.
39. Korotkova TM, Eriksson KS, Haas HL, & Brown RE (2002) Selective excitation of GABAergic neurons in the substantia nigra of the rat by orexin/hypocretin in vitro. *Regul Pept* 104(1-3):83-89.
40. Schone C, Apergis-Schoute J, Sakurai T, Adamantidis A, & Burdakov D (2014) Coreleased orexin and glutamate evoke nonredundant spike outputs and computations in histamine neurons. *Cell Rep* 7(3):697-704.
41. Jouvet M (1999) Sleep and serotonin: an unfinished story. *Neuropsychopharmacology : official publication of the American College of Neuropsychopharmacology* 21(2 Suppl):24S-27S.
42. Monti JM (2011) Serotonin control of sleep-wake behavior. *Sleep medicine reviews* 15(4):269-281.
43. McGinty DJ & Harper RM (1976) Dorsal raphe neurons: depression of firing during sleep in cats. *Brain Res* 101(3):569-575.
44. Morairty SR, Hedley L, Flores J, Martin R, & Kilduff TS (2008) Selective 5HT2A and 5HT6 receptor antagonists promote sleep in rats. *Sleep* 31(1):34-44.
45. Chou TC*, et al.* (2002) Afferents to the ventrolateral preoptic nucleus. *J Neurosci* 22(3):977-990.

46. Brown RE, Sergeeva O, Eriksson KS, & Haas HL (2001) Orexin A excites serotonergic neurons in the dorsal raphe nucleus of the rat. *Neuropharmacology* 40(3):457-459.
47. Brown RE, Sergeeva OA, Eriksson KS, & Haas HL (2002) Convergent excitation of dorsal raphe serotonin neurons by multiple arousal systems (orexin/hypocretin, histamine and noradrenaline). *J Neurosci* 22(20):8850-8859.
48. Inamura N*, et al.* (2012) Gene induction in mature oligodendrocytes with a PLP-tTA mouse line. *Genesis* 50(5):424-428.
49. Richardson-Jones JW*, et al.* (2010) 5-HT1A autoreceptor levels determine vulnerability to stress and response to antidepressants. *Neuron* 65(1):40-52.
50. Ma J, Matsumoto M, Tanaka KF, Takebayashi H, & Ikenaka K (2006) An animal model for late onset chronic demyelination disease caused by failed terminal differentiation of oligodendrocytes. *Neuron glia biology* 2(2):81-91.
51. Tobler I, Deboer T, & Fischer M (1997) Sleep and sleep regulation in normal and prion protein-deficient mice. *J Neurosci* 17(5):1869-1879.
52. Isomoto S, Kondo C, & Kurachi Y (1997) Inwardly rectifying potassium channels: their molecular heterogeneity and function. *Jpn J Physiol* 47(1):11-39.
53. Audero E*, et al.* (2008) Sporadic Autonomic Dysregulation and Death Associated with Excessive Serotonin Autoinhibition. *Science* 321(5885):130-133.
54. Matsuki T*, et al.* (2009) Selective loss of GABA(B) receptors in orexin-producing neurons results in disrupted sleep/wakefulness architecture. *Proceedings of the National Academy of Sciences of the United States of America* 106(11):4459-4464.
55. Sakai K (2011) Sleep-waking discharge profiles of dorsal raphe nucleus neurons in mice. *Neuroscience* 197:200-224.
56. Liu RJ, van den Pol AN, & Aghajanian GK (2002) Hypocretins (orexins) regulate serotonin neurons in the dorsal raphe nucleus by excitatory direct and inhibitory indirect actions. *J Neurosci* 22(21):9453-9464.
57. Lee MG, Hassani OK, & Jones BE (2005) Discharge of identified orexin/hypocretin neurons across the sleep-waking cycle. *J Neurosci* 25(28):6716-6720.
58. Takahashi K, Lin JS, & Sakai K (2008) Neuronal activity of orexin and non-orexin waking-active neurons during wake-sleep states in the mouse. *Neuroscience* 153(3):860-870.
59. Jean-Alphonse F & Hanyaloglu AC (2011) Regulation of GPCR signal networks via membrane trafficking. *Mol Cell Endocrinol* 331(2):205-214.
60. Estabrooke IV*, et al.* (2001) Fos expression in orexin neurons varies with behavioral state. *J Neurosci* 21(5):1656-1662.
61. Mignot E, Hayduk R, Black J, Grumet FC, & Guilleminault C (1997) HLA

DQB1*0602 is associated with cataplexy in 509 narcoleptic patients. *Sleep* 20(11):1012-1020.

62. Mahlios J, De la Herran-Arita AK, & Mignot E (2013) The autoimmune basis of narcolepsy. *Current opinion in neurobiology*.
63. Nishino S & Mignot E (1997) Pharmacological aspects of human and canine narcolepsy. *Prog Neurobiol* 52(1):27-78.
64. Kisanuki Y*, et al.* (2001) Behavioral and polysomnographic characterization of orexin-1 receptor and orexin-2 receptor double knockout mice. *Sleep* 24:A22.
65. Kalogiannis M*, et al.* (2011) Cholinergic modulation of narcoleptic attacks in double orexin receptor knockout mice. *PloS one* 6(4):e18697.
66. Espana RA, McCormack SL, Mochizuki T, & Scammell TE (2007) Running promotes wakefulness and increases cataplexy in orexin knockout mice. *Sleep* 30(11):1417-1425.
67. Oishi Y*, et al.* (2013) Role of the medial prefrontal cortex in cataplexy. *J Neurosci* 33(23):9743-9751.
68. Black SW*, et al.* (2013) Almorexant promotes sleep and exacerbates cataplexy in a murine model of narcolepsy. *Sleep* 36(3):325-336.
69. Tabuchi S*, et al.* (2013) Influence of inhibitory serotonergic inputs to orexin/hypocretin neurons on the diurnal rhythm of sleep and wakefulness. *Sleep* 36(9):1391-1404.
70. Inamura N*, et al.* (2011) Gene induction in mature oligodendrocytes with a PLP-tTA mouse line. *Genesis*.
71. Scammell TE, Willie JT, Guilleminault C, & Siegel JM (2009) A consensus definition of cataplexy in mouse models of narcolepsy. *Sleep* 32(1):111-116.
72. Tsunematsu T, Tanaka KF, Yamanaka A, & Koizumi A (2013) Ectopic expression of melanopsin in orexin/hypocretin neurons enables control of wakefulness of mice in vivo by blue light. *Neurosci Res* 75(1):23-28.
73. Lee P*, et al.* (1998) Conditional lineage ablation to model human diseases. *Proc Natl Acad Sci U S A* 95(19):11371-11376.
74. Brischoux F, Fellmann D, & Risold PY (2001) Ontogenetic development of the diencephalic MCH neurons: a hypothalamic 'MCH area' hypothesis. *Eur J Neurosci* 13(9):1733-1744.
75. Hanisch UK & Kettenmann H (2007) Microglia: active sensor and versatile effector cells in the normal and pathologic brain. *Nat Neurosci* 10(11):1387-1394.
76. Graeber MB*, et al.* (1998) The microglia/macrophage response in the neonatal rat facial nucleus following axotomy. *Brain Res* 813(2):241-253.

77. Ohsawa K, Imai Y, Kanazawa H, Sasaki Y, & Kohsaka S (2000) Involvement of Iba1 in membrane ruffling and phagocytosis of macrophages/microglia. *J Cell Sci* 113 (Pt 17):3073-3084.

78. Sasai T, Inoue Y, Komada Y, Sugiura T, & Matsushima E (2009) Comparison of clinical characteristics among narcolepsy with and without cataplexy and idiopathic hypersomnia without long sleep time, focusing on HLA-DRB1(*)1501/DQB1(*)0602 finding. *Sleep Med* 10(9):961-966.

79. Babcock DA, Narver EL, Dement WC, & Mitler MM (1976) Effects of Imipramine, Chlorimipramine, and Fluoxetine on Cataplexy in Dogs. *Pharmacol Biochem Be* 5(6):599-602.

80. Clark EL, Baumann CR, Cano G, Scammell TE, & Mochizuki T (2009) Feeding-elicited cataplexy in orexin knockout mice. *Neuroscience* 161(4):970-977.

81. Hara J, Yanagisawa M, & Sakurai T (2005) Difference in obesity phenotype between orexin-knockout mice and orexin neuron-deficient mice with same genetic background and environmental conditions. *Neurosci Lett* 380(3):239-242.

82. Honda Y, Doi Y, Ninomiya R, & Ninomiya C (1986) Increased frequency of non-insulin-dependent diabetes mellitus among narcoleptic patients. *Sleep* 9(1 Pt 2):254-259.

83. Schuld A, Hebebrand J, Geller F, & Pollmacher T (2000) Increased body-mass index in patients with narcolepsy. *Lancet* 355(9211):1274-1275.

84. Murphy JR (2011) Mechanism of diphtheria toxin catalytic domain delivery to the eukaryotic cell cytosol and the cellular factors that directly participate in the process. *Toxins (Basel)* 3(3):294-308.

85. Okun ML, Lin L, Pelin Z, Hong S, & Mignot E (2002) Clinical aspects of narcolepsy-cataplexy across ethnic groups. *Sleep* 25(1):27-35.

86. Hasegawa E, Yanagisawa M, Sakurai T, & Mieda M (2014) Orexin neurons suppress narcolepsy via 2 distinct efferent pathways. *The Journal of clinical investigation* 124(2):604-616.

87. Steininger TL, Kilduff TS, Behan M, Benca RM, & Landry CF (2004) Comparison of hypocretin/orexin and melanin-concentrating hormone neurons and axonal projections in the embryonic and postnatal rat brain. *Journal of chemical neuroanatomy* 27(3):165-181.

88. Dauvilliers Y*, et al.* (2004) Effect of age on MSLT results in patients with narcolepsy-cataplexy. *Neurology* 62(1):46-50.

89. Vassalli A*, et al.* (2013) Electroencephalogram paroxysmal theta characterizes cataplexy in mice and children. *Brain : a journal of neurology* 136(Pt 5):1592-1608.

90. Middelkoop HA, *et al.* (1995) Circadian distribution of motor activity and immobility in narcolepsy: assessment with continuous motor activity monitoring. *Psychophysiology* 32(3):286-291.
91. Kunii K, *et al.* (1999) Orexins/hypocretins regulate drinking behaviour. *Brain Res* 842(1):256-261.
92. Hirai N & Nishino S (2011) Recent advances in the treatment of narcolepsy. *Curr Treat Options Neurol* 13(5):437-457.
93. Morgenthaler TI, *et al.* (2007) Practice parameters for the treatment of narcolepsy and other hypersomnias of central origin. *Sleep* 30(12):1705-1711.
94. Aran A, *et al.* (2010) Clinical and therapeutic aspects of childhood narcolepsy-cataplexy: a retrospective study of 51 children. *Sleep* 33(11):1457-1464.
95. Black SW, *et al.* (2014) GABAB agonism promotes sleep and reduces cataplexy in murine narcolepsy. *J Neurosci* 34(19):6485-6494.
96. John J, *et al.* (2013) Greatly increased numbers of histamine cells in human narcolepsy with cataplexy. *Annals of neurology* 74(6):786-793.
97. Valko PO, *et al.* (2013) Increase of histaminergic tuberomammillary neurons in narcolepsy. *Annals of neurology* 74(6):794-804.
98. Rosin DL, Weston MC, Sevigny CP, Stornetta RL, & Guyenet PG (2003) Hypothalamic orexin (hypocretin) neurons express vesicular glutamate transporters VGLUT1 or VGLUT2. *J Comp Neurol* 465(4):593-603.
99. Chou TC, *et al.* (2001) Orexin (hypocretin) neurons contain dynorphin. *J Neurosci* 21(19):RC168.
100. Furutani N, *et al.* (2013) Neurotensin co-expressed in orexin-producing neurons in the lateral hypothalamus plays an important role in regulation of sleep/wakefulness states. *PloS one* 8(4):e62391.
101. Yamanaka A, Tabuchi S, Tsunematsu T, Fukazawa Y, & Tominaga M (2010) Orexin directly excites orexin neurons through orexin 2 receptor. *J Neurosci* 30(38):12642-12652.
102. Tabuchi S, *et al.* (2014) Conditional ablation of orexin/hypocretin neurons: a new mouse model for the study of narcolepsy and orexin system function. *J Neurosci* 34(19):6495-6509.
103. Brown RE, Basheer R, McKenna JT, Strecker RE, & McCarley RW (2012) Control of sleep and wakefulness. *Physiological reviews* 92(3):1087-1187.
104. de Lecea L & Huerta R (2014) Hypocretin (orexin) regulation of sleep-to-wake transitions. *Frontiers in pharmacology* 5:16.
105. Johnson PL, Molosh A, Fitz SD, Truitt WA, & Shekhar A (2012) Orexin, stress, and

anxiety/panic states. *Progress in brain research* 198:133-161.

106. Sharf R, Sarhan M, & Dileone RJ (2010) Role of orexin/hypocretin in dependence and addiction. *Brain Res* 1314:130-138.

107. Kantor S*, et al.* (2013) Orexin gene therapy restores the timing and maintenance of wakefulness in narcoleptic mice. *Sleep* 36(8):1129-1138.